Development and Demonstration of Thin Waveguide Ultrasonic Thermometer

A Dissertation

Presented in Partial Fulfillment of the Requirements for the

Degree of Doctor of Philosophy

with a

Major in Mechanical Engineering

in the

College of Graduate Studies

University of Idaho

by

Joshua Earl Daw

May 2015

Major Professor: John Crepeau, Ph.D.

Committee Members: Vivek Utgikar, Ph.D.; Ali Siahpush, Ph.D.; Joy Rempe, Ph.D.

Department Administrator: John Crepeau, Ph.D.

Authorization to Submit
Dissertation

This dissertation of Joshua E. Daw, submitted for the degree of Doctor of Philosophy with a major in Mechanical Engineering and titled "Development and Demonstration of Thin Waveguide Ultrasonic Thermometer," has been reviewed in final form, as indicated by the signatures and dates given below. Permission is now granted to submit copies to the College of Graduate Studies for approval.

Major Professor   _____Date_____
                                      John C. Crepeau, Ph.D.

Committee
Members   _____Date_____
                                        Vivek Utgikar, Ph.D.

                   _____Date_____
                                        Ali Siahpush, Ph.D.

                   _____Date_____
                                        Joy Rempe, Ph.D.

Department
Chair   _____Date_____
                                       John C. Crepeau, Ph.D.

Abstract

The objective of this research is to enable deployment of Ultrasonic Thermometers (UTs) in irradiations of ceramic and metallic fuels. Research was broken into two main areas; out-of-core development and testing of the UT and its components in a laboratory environment and in-core assessment of the radiation tolerance of the magnetostrictive transducers used to generate and sense the acoustic signals.

Significant progress was made toward the deployment of UTs. Appropriate sensor materials were identified. For applications below 1000 °C stainless steel was identified. For temperatures between 1000 and 2500 °C, a variety of molybdenum doped with tungsten and potassium silicate was selected. A new, high frequency coil was developed and used to improve spatial resolution of reflectors by allowing minimization of reflector spacing. This effect is enhanced by the use of a new method of damping developed to remove "back end" reflections, eliminating interference caused by them and simplifying signal processing. A signal processing method was also identified and tested, which changed the difficult identification of Gaussian sinusoids into simple peak detection.

An irradiation test capsule design was developed that includes both piezoelectric and magnetostrictive materials, transducers, and sensors. It is the first to include both piezoelectric and magnetostrictive materials, and is scheduled to surpass other ultrasonic transducer irradiations in terms of total fluence. As part of this research, a new design of magnetostrictive transducers was developed, fabricated, evaluated in a laboratory setting, and included in this irradiation test. The irradiation test was initiated to identify transducer materials that can survive in a high radiation environment. The included transducers were operated online during irradiation; and the test capsule was heavily instrumented with real time sensors,

resulting in a high degree of confidence in the results. The results shows ultrasonic transducers based on magnetostrictive materials, such as Remendur and Galfenol, to be highly resistant to degradation caused by neutron and gamma radiation.

Acknowledgements

I would like to thank Professor John C. Crepeau, Ph.D., P.E., Chairman of the Department of Mechanical Engineering of the University of Idaho for all the advice afforded during this effort, as well as for the opportunity to be a part of this project. As the Major Professor, Dr. Crepeau provided invaluable direction and insight, without which this dissertation could not have been completed.

I would also like to thank the other members of my committee, Professors Vivek Utgikar, Ph.D., P.E., and Ali Siahpush, Ph.D., for their time and advice throughout the course of this research.

I would also like to thank Joy L. Rempe, Ph.D. Joy acted as my mentor and provided direct oversight and daily guidance, personally initiating this effort and driving it forward while allowing me the freedom to guide it and be creative in pursuing my research goals.

Special thanks goes to S. Curtis Wilkins. Curt has long been involved in the development of specialized high temperature instrumentation. Specifically, Curt had very rare personal experience working in the early research in this field; and I have benefited greatly from his experience, expertise, and friendship.

I would especially like to thank my family. My parents have supported me through this long journey despite mistakes that I have made that may have otherwise kept me from having the educational and professional opportunities that I have been afforded. My siblings have found success in their lives that drive me to try and make them as proud of me as I am of them. My grandparents, though no longer with us, always made a point of letting me know how proud they were of me, something that will always keep me moving forward.

Dedication

I would like to dedicate this work to my grandmother, Verda Daw. Grandma Daw passed away during the writing of this dissertation and she has been in my thoughts throughout this time.

Contents

List of Figures

List of Tables

List of Abbreviations

AC	Alternating Current
ANL	Argonne National Laboratory
ATR	Advanced Test Reactor
CEA	Commissariat à l'Énergie Atomique et aux Energies Alternatives
DC	Direct Current
DOE	Department of Energy
DSC	Differential Scanning Calorimeter
EMAT	ElectroMagnetic Acoustic Transducer
HFIR	High Flux Isotope Reactor
HTGR	High Temperature Gas Reactor
HTIR-TC	High Temperature Irradiation Resistant Thermocouple
HTTL	High Temperature Test Laboratory
IEEE	Institute of Electrical and Electronics Engineers
INL	Idaho National Laboratory
ITS 90	International Temperature Standard-1990
JNPT	Johnson Noise Power Thermometry
LOFT	Loss of Fluids Test
LWR	Light Water Reactor
MIT	Massachusetts Institute of Technology
MITR	Massachusetts Institute of Technology Research Reactor
MTR	Material Testing Reactor
NEET	Nuclear Energy Enabling Technologies

NIST	National Institute of Standards and Testing
NSUF	National Scientific User Facility
ORNL	Oak Ridge National Laboratory
PBF	Power Burst Facility
PIE	Post Irradiation Examination
PNNL	Pacific Northwest National Laboratory
PRT	Platinum Resistance Thermometer
PSU	Pennsylvania State University
RF	Radio Frequency
RSS	Root Sum Square
RTD	Resistance Temperature Device
SFR	Sodium Fast Reactor
SNR	Signal to Noise Ratio
SPGD	Self Powered Gamma Detector
SPND	Self Powered Neutron Detector
TC	Thermocouple
ULTRA	Ultrasonic Transducer Irradiation Test
UT	Ultrasonic Thermometer

List of Symbols

A_G	DC gain accuracy, %
A_L	Inductive element cross sectional area, m^2
A_R	Resistive element cross sectional area, m^2
A_t	Time measurement accuracy, ppm
A_{Therm}	Accuracy of thermometer, %
$\dfrac{d}{dt}$	Time derivative operator
c_L	Longitudinal wave velocity, m/s
c_P	Phase velocity, m/s
c_T	Transverse wave velocity, m/s
d_L	Diameter of induction coil, m
d_R	Diameter of wire, m
E	Young's modulus, N/m^2
E_v	Applied voltage, V
G	Shear modulus, N/m^2
i	Current, A
J_0	Zeroth order Bessel function of the first kind
J_1	First order Bessel function of the first kind
k	Acoustic wavenumber, 1/m
K	Bulk modulus, N/m^2
l	Initial length, m
L	Sensor length, m
Δl	Change in length, m

$L(0,1)$	First order longitudinal wave mode
L_i	Inductance, H
l_L	Inductor length, m
l_R	Length of wire included in the coil, m
M	Available oscilloscope bit size, bits
n	Number of wire turns per unit length, 1/m
N	Number of wire turns of inductor
r	Waveguide radius, m
R	System bandwidth ratio
$Range$	Oscilloscope voltage input range, V
R_{DC}	DC resistance, Ohms
R_r	Resolution of ruler, mm
R_{Therm}	Resolution of thermometer, ^oC
s_{noise}	Noise variance, V
s_{signal}	Signal variance, V
t	Time, s
Δt	Change in time, s
$T(0,1)$	First order transverse wave mode
$\overline{T}_{TypeS}$	Average absolute temperature reported by Type S thermocouple, K
$\overline{T}_{Therm}$	Average recorded absolute thermometer temperature, K
x_i	Directional unit vector
u	Displacement, m
$u\%$	Total percent uncertainty, %

$u_{Oscope}\%$	Percent uncertainty due to oscilloscope, %
$u_{P\text{-}R}\%$	Percent uncertainty due to pulser/receiver system bandwidth, %
$u_r\%$	Percent uncertainty due to sensor length measurement, %
$u_{SNR}\%$	Percent uncertainty due to signal to noise ratio, %
$u_{Therm}\%$	Percent uncertainty of thermometer, %
$u_{TypeS}\%$	Percent uncertainty of the Type S thermocouple signal, %
α	Pocchammer-Chree equation placeholder variable
β	Pocchammer-Chree equation placeholder variable
δ	Kroneker delta
ε	Material elastic strain, m/m
ε_{TypeS}	Measurement error due to thermocouple, ^oC
λ	Lame's first constant, N/m^2
μ	Lame's second constant (Shear modulus), N/m^2
μ_0	Permeability of free space, $\dfrac{V \cdot s}{A \cdot m}$
μ_r	Relative material permeability
∇	Three dimensional differential operator
ρ	Material mass density, kg/m^3
ρ_w	Electrical resistivity, Ω*m
σ	Stress tensor, N/m^2
τ	Time constant of inductor, s
ω	Angular frequency, rad/s
i	Subscript indicating index number of 1, 2, or 3
$large$	Subscript indicating large diameter inductor

small   Subscript indicating small diameter inductor

Chapter 1: Introduction

New nuclear fuel, cladding, and structural materials offer the potential for safer and more economic energy from existing and advanced nuclear reactor designs. However, insufficient data are available to characterize these materials in high temperature, radiation conditions. To evaluate candidate material performance, robust instrumentation is needed that can survive these conditions. Furthermore, the nuclear industry increasingly relies on computer models to predict the behavior of components and systems in both normal and off-normal conditions. Current measurement techniques cannot resolve physical phenomena with sufficient resolution to match the level of detail current models are capable of achieving. The results of these simulations must be validated by experimental data in order to be used to acquire regulator approval. New sensors and measurement techniques are needed to provide this validation. Irradiation testing of new, high performance fuels and materials for advanced reactor designs will require sensors capable of operation in conditions unsuitable for other, commonly used temperature sensors. These conditions may include high temperatures of over 2000 $^{\circ}$C in gases, or exposure to corrosive environments such as liquid metals or molten salts.

1.1 Objective

The objective of this research is to enable deployment of Ultrasonic Thermometers (UTs) in irradiations tests of ceramic and metallic fuels, primarily for fuel rod centerline temperature measurements at the Idaho National Laboratory (INL) Advanced Test Reactor (ATR). Test conditions within the ATR can be severe, including thermal neutron fluxes of up to 1.0×10^{15} n/cm^{2}s and fast neutron fluxes up to 0.5×10^{14} n/cm^{2}s. Research was broken into two main areas; out-of-core development and testing of the UT and its components in a laboratory environment and in-core assessment of the radiation tolerance of the

magnetostrictive transducers used to generate and sense the acoustic signals. A UT is a sensor that uses the measurement of the propagation velocity of high frequency sound waves to infer the average temperature of the material through which the waves are travelling. Typically, a thin metallic rod is used as the sensor. This rod may be divided into multiple segments and used to acquire a measurement of the temperature profile along the length of the rod. A typical UT system is shown in Figure 1-1.
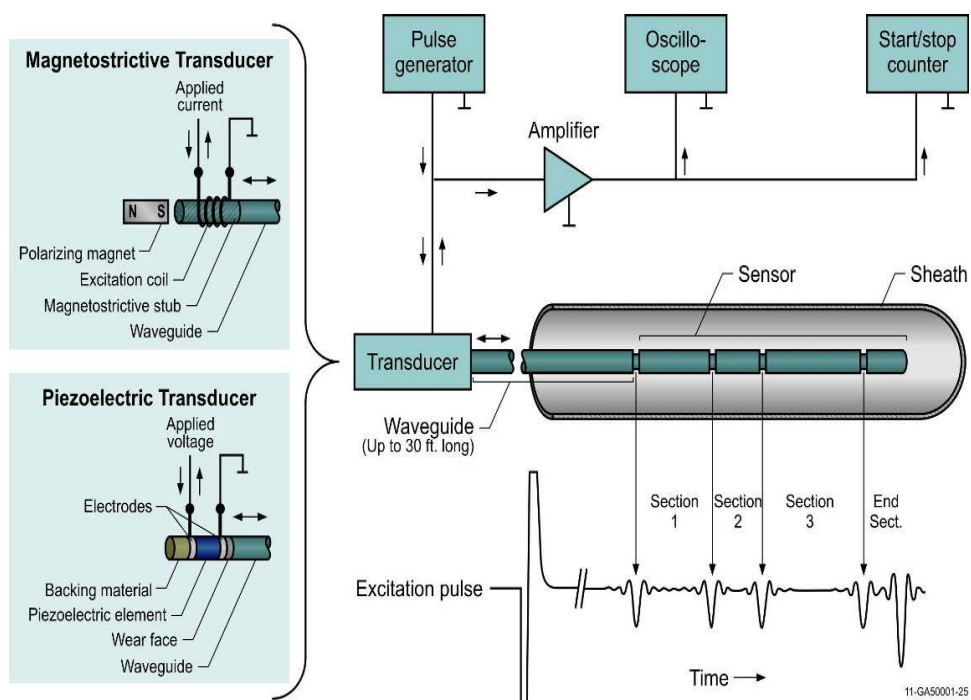
Figure 1-1. Typical ultrasonic thermometry system [Daw, 2012].

1.2 Dissertation Organization

Chapter 2 provides a survey of available literature; a review of in-core temperature measurements and prior work performed in pursuit of a functional UT system. Chapter 3 presents the theory of operation of a UT. Chapter 4 describes the initial design and testing of the prototype UT components for this research. Chapter 5 summarizes the work performed to demonstrate the survival of magnetostrictive transducers in an in-core environment. Chapter 6

provides a brief summary of the work described in this dissertation and suggests possible

follow-on work that may build on the results of this research.

Chapter 2: Literature Review

This chapter contains background information gathered from existing literature regarding general temperature measurements for in-core experiments, previous research toward ultrasonic thermometry, and the issues associated with deployment of ultrasonic transducers in a radiation environment.

2.1 General Temperature Measurements for Irradiation Environments

Both Priest [Priest, 2004] and Swenson [Swenson, 2004] present an excellent introduction to the subject of thermometry and modern temperature sensors. Priest defines the major temperature scales, both relative (Fahrenheit and Celsius) and absolute (Rankine and Kelvin) and describes the relationships between them as well as relative ranges of temperatures with respect to common phenomena. The basis of the 1990 iteration of the International Temperature Scale (ITS 90) is also described, being a range of temperatures between 0.65 K and above. The scale is divided into many sections, the endpoints of which are defined by natural fixed temperature points such as triple points and melting points of several materials. Intermediate temperatures are determined by interpolative measurement devices such as helium gas thermometers, platinum resistance thermometers (PRTs), and optical pyrometers. The operating principles behind these devices as well as thermocouples, thermistors, noise thermometers and magnetic thermometers are described, as are some of the advantages and failings of each.

The paper by Swenson covers much of the same information as Priest's, but in more detail. This paper focuses on cryogenic applications and is applicable only in terms of description of some of the failings of certain devices. Of those devices described only thermocouples, PRTs, thermistors, and radiation thermometers are identified as being useful at

high temperatures. Radiation thermometers, such as the optical thermometer, measure temperature based on emitted light intensity at certain wavelengths. This technique can be used at very high temperatures and does not require direct contact, but does require a line of sight for use. Thermistors are small and sensitive, responding to temperature changes as a change in the resistance of a semiconductor, but are described as having an upper temperature limit of about 700 ^{o}C. PRTs are described as being very stable with smooth temperature response. Also platinum is very insensitive to oxidation. PRTs consist of a small platinum wire or film whose resistance, which is temperature dependant, is measured accurately. In wire wound PRTs, the wire is coiled around a ceramic insulator of cylindric shape (the film deposited in a zigzag pattern on an insulating wafer) to increase its length and, correspondingly, its sensitivity. The useful range of these devices is described as being bounded by an upper limit of approximately 1200 ^{o}C.

Thermocouples work on the principle of the Seebeck effect, which states that a thermal gradient over the length of two wires of dissimilar metals, connected at one end, causes a voltage differential between the wires. The strength of this type of device is that any two metals, or doped semiconductors, may form a thermocouple. This leads to a wide range of possible thermocouple types, each of which will have different characteristics. By selecting wires with specific properties, a thermocouple may be created for specific needs, such as temperature range, lifetime, or work environment. Bliss [Bliss, 1965] describe, in great detail, the process used for creating swaged (metal sheathed) thermocouples. Minimization of contaminants and high purity of components was described as being essential to stable performance.

A.W. Fenton postulates that the operating principle governing thermocouples has been

widely misrepresented in the literature [Fenton, 1980]. Typically, thermocouples are described as reacting to a temperature difference between two junctions connecting wires of dissimilar materials. A voltage is generated which is dependant on the magnitude of the temperature differential and the wire compositions. Fenton states that a temperature gradient between the two ends of a wire causes electrons at the hot end to vibrate with more energy than those at the cold end. This causes a flow of electrons toward the cold end and a charge build-up. The charge magnitude is determined by the magnitude of the temperature gradient and by inherent material properties. This charge differential causes a voltage to exist between the wire ends. This voltage cannot be measured by itself. By connecting two wires, the difference in the induced voltages may be measured. If the wires are of the same material, the difference will be zero; but if different materials are used, the voltage will be non-zero. Further, Fenton states that a thermocouple that has decalibrated due to signal drift can only be recalibrated if material changes are slow and irreversible in nature, and the temperature gradient encountered by the thermocouple will always be the same for a specified temperature difference. The importance of this concept has to do with the problems of decalibration inherent in current high temperature in-core instrumentation for test reactors. Decalibration in a reactor environment comes about not only from temperature effects, but also due to material transmutation caused by neutron radiation. To correct for this combined decalibration, both the temperature and radiation gradients must be consistent and known. In many material test reactors, the radiation and temperature conditions are likely to change between tests or even during the course of a single test. This makes it impossible to implement a practical method of compensating for decalibration of TCs for in-core testing.

An assessment of the state of the art was made in 2005 at Idaho National Laboratory in

an attempt to identify an ideal temperature measurement technology for deployment in a Gas Test Loop (GTL) at the Advanced Test Reactor (ATR) [Wilkins, 2005]. The assessment included a comparison of high-temperature measurement sensors for near-term development and deployment. The technologies compared were thermocouples, resistance temperature devices, ultrasonic thermometers, Johnson noise power thermometers, and several optical methods. Thermocouples constructed from doped molybdenum and a niobium alloy were selected, with W-Re alloy thermocouples as a backup. These doped molybdenum/niobium alloy based thermocouples were eventually developed as the High Temperature Irradiation Resistant ThermoCouple (HTIR-TC). Ultrasonic thermometers operating in pulse-echo mode were disregarded due to complex signal processing and the lack of an ideal material. It was concluded that most of the interesting high temperature metals suffer excessive transmutation effects, while molybdenum and niobium were thought to have insufficient temperature sensitivity. Conversations with the report author reveal that molybdenum had likely been discounted prematurely, based on insufficient prior testing. The resonant method (first developed by Bell) was deemed too under-developed for application as little high temperature work outside of that done by Bell could be found. Optical methods were disregarded due to lack of radiation hardness of sensors (pyrometers, infrared detectors), lack of line of sight, and darkening of optical fibers. Resistance Temperature Devices (RTDs) were deemed to be limited to temperatures below 660 °C (platinum) or 1200 °C (tungsten, very uncommonly used due to brittleness). Johnson Noise Power thermometers (JNPTs) discounted for several reasons; signal processing is as complicated and expensive as for UTs, and electrical shunting problems (as in TCs).

The Idaho National Laboratory (INL) developed High Temperature Irradiation

Resistant-ThermoCouple (HTIR-TC) [(Rempe, 2006), (Daw, 2008-1), (Daw, 2008-2), (Rempe, 2009)] significantly reduces the problems associated with the use of thermocouples in an in-core application. The HTIR-TC is constructed with thermoelements that have low thermal neutron capture cross sections (a niobium alloy and a doped variant of molybdenum), which reduce transmutation caused decalibration to an insignificant level. The HTIR-TC is also capable of higher temperature operation than type-K or type-N thermocouples, having been demonstrated in laboratory testing to 1800 ^{o}C. However, some limitations still exist with this sensor. Of primary concern is the degradation of electrical resistivity of the insulating material (hafnium oxide) at temperatures above 1800 ^{o}C. This is a problem with any temperature measurement system that uses electrical measurements within the heated region (i.e., PRT's, TC's). As the electrical resistance between the thermoelements is reduced, shunting between the thermoelements can occur. This is an error known as a virtual junction. Signal errors caused by this effect are difficult to recognize and impossible to correct.

Table 2-1 summarizes commonly used sensors and developmental technologies for in-core temperature measurement.

Table 2-1. Summary of previously used temperature measurement systems for in-core use.

Sensor	Temperature Range	Comments
Type K and Type N Thermocouple	up to approximately 1100 $^{\circ}$C	Decalibration at temperatures over approximately 1100 $^{\circ}$C due to cross contamination from thermo-elements and sheath.
Tungsten/Rhenium Thermocouple	up to approximately 2400 $^{\circ}$C	Decalibration due to thermal neutron induced transmutation of tungsten to rhenium and rhenium to osmium. Degradation of electrical insulation at high temperatures.
Platinum/Rhodium Thermocouple	up to approximately 1800 $^{\circ}$C	Decalibration due to thermal neutron induced transmutation of rhodium to palladium. Degradation of electrical insulation at high temperatures.
Platinum Resistance Thermometer	up to approximately 660 $^{\circ}$C	Degradation of electrical insulation at high temperatures. Embrittlement of platinum.
HTIR-TC	demonstrated to approximately 1800 $^{\circ}$C	Degradation of electrical insulation at high temperatures. Small scale production.
JNPT	demonstrated to approximately 1500 $^{\circ}$C	Degradation of electrical insulation at high temperatures. Complicated and expensive signal processing.
Fiber Optics	direct measurement to approximately 800 $^{\circ}$C	Darkening and embrittlement of fibers with radiation exposure. Low upper limit on temperature.
Optical Pyrometry	approximately 600 to 3000 $^{\circ}$C	Requires line of sight or optical delivery method. Sensitive to emissivity changes.
Ultrasonic Thermometer	demonstrated to approximately 3000 $^{\circ}$C	Complicated and expensive signal processing.

2.2 Prior Ultrasonic Thermometer Research

The earliest practical research into ultrasonic thermometry is typically credited to Bell [Bell, 1968]. Bell's work dealt with resonant temperature sensors. The resonant ultrasonic thermometer uses a metallic lead-in connected to a (typically) metallic resonator comprised of one of many various geometries. Conceptually, the thermometer is operated by driving the resonator into resonance (resonant frequency being dependent on temperature) using either a continuous wave or a short tonal pulse. Bell proposed a self-calibration method via a fixed-point melting cell in the coupler between the lead-in and resonator (the change from solid to liquid creating a strong, detectable change in coupling). Overall, the setup is basically identical to the subsequently developed pulse-echo time domain reflectometry thermometer, with a lead in waveguide and an isolated sensor segment. However, the resonant method requires a larger sensor size (i.e., more mass, leading to slower response time) for most configurations and only single sensor segment.

The greatest body of work regarding ultrasonic thermometry seemingly belongs to Lynnworth and his collaborators. Giving credit to Bell and his earlier work for inspiration, Lynnworth et. al [Lynnworth, 1967] developed a time of flight based multi-point ultrasonic thermometer for use in monitoring temperatures in nuclear thermal rockets (both in the reactor and the exhaust flow). Lynnworth's system worked on the pulse-echo concept, in which a single transducer (magnetostrictive, in this case) produces and senses the acoustic signal. After comparing with tungsten, niobium, molybdenum, tantalum, platinum, graphite, and tungsten-rhenium alloy waveguides, Lynnworth selected rhenium as the ideal candidate due to its high melting temperature and excellent temperature sensitivity in the range of interest. Sensors constructed with rhenium were tested to its melting point (3180 °C) in a vacuum and

to the eutectic temperature in graphite. In both cases the system performed well. Samples of rhenium were irradiated to 8.7×10^{19} n/cm^2 thermal and 2.6×10^{19} n/cm^2 fast (Energy > 1.0 MeV). After irradiation, their ultrasonic velocities were compared to unirradiated samples. The differences were found to be negligible, leading to the belief that rhenium sensors were tolerant to neutron irradiation. However, these samples were annealed prior to the out-of-core comparison test, and the results are not typical. Irradiated wires initially differed from non-irradiated by approximately 10%, but recovered during annealing to over 1949 °C. As the thermometers were developed for use in a hydrogen fueled rocket, they were tested in hydrogen to 2374 °C, with a goal of measuring up to 2500 °C with 28 °C accuracy in the core. The designed sensor was 0.5 mm in diameter and 50 mm long. Measurement uncertainties were estimated to be within 2% up to 840 °C, 1% to 1400 °C, and less than 1% to 1950 °C. Kinks and welds were both tested as reflectors. Molybdenum was found to be a poor candidate in graphite due to carbide formation (which were caused embrittlement and spurious signal artifacts). Results for materials other than molybdenum and rhenium were not reported.

Lynnworth's work in the space application of ultrasonic thermometry also included measurement of temperature in gases, using the gas to propagate the ultrasonic waves [Lynnworth, 1967]. Space exploration was described as the primary driver for the development of high temperature measurements. An important expansion on his previous work was the use of momentary contact between a transducer and the material (i.e., the gas) to be interrogated ultrasonically to avoid reaching curie temperature of transducer. Some methods of measuring material properties at high temperature were also described, such as elastic moduli and Poisson's ratio in solids (both bulk solids and thin wires).

Lynnworth also began to explore the use of UTs for nuclear reactors [Lynnworth, 1968-1]. Based on prior work, rhenium was again selected as the sensor material of interest. New testing indicated negligible radiation effects up to a fast fluence of $2.6\times10^{\wedge19}$n/cm^2 (Energy > 1.0 MeV) and thermal fluence of $8.7\times10^{\wedge19}$n/cm^2. Pulse echo tests were performed to 3060 °C with good results. Development of a UT system for fast breeder reactors is summarized, but is further described in other reports. Lynnworth also describes the development of a dual element Cu-Al ultrasonic sensor for measuring fluence. The Young's modulus of copper is very sensitive to fast neutron damage, while that of aluminum is significantly less so. The accumulated fluence can therefore be estimated by a comparative measurement of the change in sound velocity in the materials (with appropriate temperature compensation).

A conference proceeding [Lynnworth, 1968-2] gives a background description of ultrasonic thermometry methods, including normalized delay time plots for various materials (with respect to temperature), as shown in Figure 2-1.The normalized delay time illustrated in the plot indicates the fractional change in travel time for an acoustic pulse. It is the reciprocal to the fractional change in acoustic velocity experienced as the temperature of a material is changed and acts as a general calibration curve for a specified material. Also included is a description of some other measurement techniques for use at high temperatures (thickness, flaw detection, flow rate).
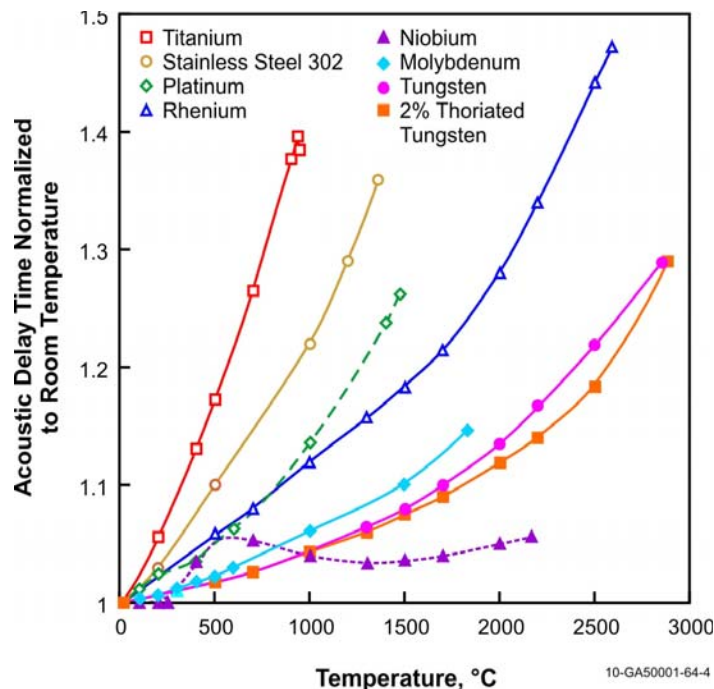
Figure 2-1. Acoustic velocity measured for various metallic samples [Lynnworth, 1968-2].

Lynnworth expands the applications possible for ultrasonic thermometry with a description of measurement methods with emphasis on relative temperature and spatial scales [Lynnworth, 1969]. Methods of measuring temperatures from nearly absolute zero to 16,650 °C are described. Some of the improvements Lynnworth expected (over other thermometry methods) include an estimated temperature resolution of 1 mK, spatial resolutions from the size of a thermocouple junction to tens of miles, and millisecond response times.

Lynnworth [Lynnworth, 1970] summarizes progress to date with a description of multiple methods of time of flight thermometry (thin wire, bulk, surface) for solids, liquids, and gases. A description of various methods of creating reflectors on a waveguide is also given. A new method is described, which allows tracking of a solidification/liquifaction front

in a melting or freezing liquid metal.

The major work in developing an ultrasonic thermometry system for nuclear reactors was focused on liquid metal fast breeder reactor applications [Papadakis, 1972]. The first test phase involved testing to 2750 °C in a furnace. In the second phase, irradiation effects were characterized. Magnetostrictive transducers were tested for 600 hours at temperatures above 500 °C in the Bulk Shielding Reactor at Oak Ridge National Laboratory (ORNL). No significant degradation was reported. Measurement effects caused by decalibration of rhenium sensors due to transmutation was tested out-of-core by use of rods with built in osmium impurities of 5, 10, and 15% in rhenium (as rhenium transmutes to osmium). The results of these tests were proposed to be used to re-calibrate sensors used in-core. During phase 3 of the ORNL study, a complete ultrasonic thermometry system was evaluated. First, a 1.5 mm rhenium probe sheathed in a tungsten-rhenium tube was furnace tested to 2200 °C. A similar probe was cycled to 2650 °C. "Sticking" was observed during this test. Sticking occurs when a sensor waveguide forms weak diffusion bonds with its surroundings, typically a protective sheath. These bonds represent extraneous acoustic discontinuities and cause signal artifacts that can interfere with, or obscure, desired signal features. Results of these tests yielded information on acoustic velocity and attenuation in a rhenium sensor; and practical experience with measuring a temperature profile. A temperature resolution of approximately 2 °C was claimed. In anticipation of use within liquid sodium, an unsheathed sensor was tested in liquid water to a depth of 6 m without problems (room temperature water and hot liquid sodium (550 °C [Lineberry, 2002]) have similar viscosities). Liquid sodium temperature was shown to be measurable without vessel penetration using an ultrasonic transducer coupled to a vessel wall. A rhenium sensor was selected for additional tests to 2400

°C. Furnace testing was conducted to 2110 °C, at which point the test furnace failed. Sticking was again observed at higher temperatures. Thicker wires were thought to alleviate this problem as small cold worked wires can warp with annealing, creating additional acoustic discontinuities and signal artifacts.

The state of the art was again summarized by Lynnworth [Lynnworth, 1972]. Thin wire methods were recounted and expanded to include methods for gases and liquids.

Although rhenium was the most attractive sensor material due to its high melting temperature and excellent temperature sensitivity, other refractory metals were also identified as possible high temperature sensor materials [Papadakis, 1974]. Ultrasonic properties of several refractory metals (rhenium, tungsten/rhenium alloys, platinum/rhodium alloys, molybdenum, ruthenium, iridium) were measured using thin wire waveguides. The elastic moduli were calculated from a simplified velocity relation for thin wires (for thin wires only axial deformations are considered, as wave mode conversion and dispersion can be avoided). For ultrasonic thermometry, the key properties are acoustic velocity (a strong function of elastic modulus) and attenuation. Reported measurements indicate that attenuation increases with temperature to some maximum level, and then decreases. Attenuation does not continually increase as temperatures approach the melting point; rather, there is a sharp peak and then decrease (the peak observed for molybdenum occurs around 1750 °C).

In 1975, Lynnworth again summarized progress in this area [Lynnworth, 1975]. This update includes a good introductory explanation of the various phenomena that may be experienced with magnetostrictive transducers and thin wire or ribbon waveguides. An introduction is given to the basics of extensional and torsional transduction, the primary wave modes that may be observed in a waveguide. The signals associated with these waves can be

very confusing due to the propagation of multiple modes travelling at different speeds in both directions along a waveguide. Descriptions are also given for guided wave propagation in thin (though not necessarily round or straight) waveguides. Methods of impedance matching transducers to waveguides and achieving good acoustic coupling are also introduced. Mathematical definitions of reflection, transmission and attenuation coefficients are also stated. Various applications, such as measurement of moduli of wire materials, temperature and temperature profile measurement, were also presented.

In a more recent update, Lynnworth describes multiple methods of generating torsional and flexural waves, both of which have lower velocity than extensional waves which leads to increased resolution and accuracy in temperature measurements [Lynnworth, 1982]. Also discussed is a method of measuring the temperature profile around a circular body using multiple zones created by angled butt welds. A new configuration for a multi-zone thermometer uses a multiple wire bundle, which eliminates reverberations between reflectors. Also described are configurations such as a tube with holes as reflectors and ribbons with notches for reflectors. Titanium and 2% thoriated tungsten are mentioned as the best materials for these new configurations.

Ultrasonic thermometry was also explored over the years at the National Reactor Testing Station (renamed several times before eventually becoming the Idaho National Laboratory). Thoriated tungsten thermometers were developed and used in the Loss Of Fluids Test (LOFT) for measuring fuel temperatures and at the Power Burst Facility (PBF). Each of these tests reached an estimated temperature of 2450 °C. Ultrasonic thermometers were desired for these tests due to the high temperatures (electrical shunting in thermocouples at high temperatures precluded their use), but also because thermal response times of tenths of a

second were necessary for in-core transients to 1800 °C. In addition to the irradiation applications, out-of-core tests to 2600 °C were also performed. Accuracies of approximately 25 °C (1%) were reported. A tungsten-rhenium alloy sensor was used in these tests, as it was known to be stable and ductile in reactor conditions (transmutation effects were not initially considered for these short duration tests). The tantalum sheath used with the W-Re sensor caused sticking at temperatures over 2000 °C. This was corrected by replacing the Ta sheath with a W-Re alloy sheath. Material compatibility tests using depleted fuel were conducted in furnaces to 2600 °C prior to irradiation testing. Minor reactions were observed between a tantalum sheath and fuel. During thermal cycling tests, response times of ultrasonic thermometers were observed to be slightly faster than that of thermocouples of similar dimensions. Transmutation effects were analytically considered after testing. Changes in sensor composition up to fluence of 4.55×10^{20} n/cm^2 (thermal) was considered to have negligible effect on calibration. Ultrasonic thermometers were recommended as replacements for thermocouples for temperatures over 2000 °C, with the caveat that more development was needed first.

Testing was also performed for application of ultrasonic thermometers to liquid metal fast breeder reactor fuel rod centerline measurements up to 2700 °C [Arave, 1972]. Good agreement was observed between ultrasonic temperature measurements and those recorded with refractory thermocouples. Effects of neutron and gamma radiation on calibration were observed to be negligible. Sticking between the sensor and sheath at temperatures above 1800 °C and brittleness of the W-26% Re sheath were described as the primary concerns. Sticking was observed early in the initial test heat-up (beginning at 1800 °C, while heating to 2000 °C). The sticking effect was observed to decrease over time. A temperature of 2000 °C

was held for 7 days. Calibration drift was checked during reactor scrams. No significant changes to the initial calibration were observed. Temperature was increased to 2450 °C, then to 2700 °C. The signal was lost at 2700 °C; this was found to be due to the sheath collapsing onto the sensor. The magnetostrictive transducer driving the thermometer signal (not described) was operated to 10^{19} n/cm^2 (thermal) without significant changes in operation.

Arave compared the performance of four tungsten alloys 100% pure tungsten, tungsten doped with 1%Thoria, tungsten doped with 2%Thoria, and tungsten alloyed with 26% rhenium (a common thermocouple wire) [Arave, 1875]. Tungsten is of significant interest as it has the highest melting point of any metal (approximately 3400 °C). Thermometers constructed from the four alloys were tested for temperature sensitivity, attenuation as a function of temperature, sensitivity as function of driving signal frequency, and attenuation as function of driving signal frequency. W-26% Re was found to have the greatest temperature sensitivity, but also highest attenuation with temperature (this is not surprising, as rhenium has a much higher sensitivity than tungsten). W-26% Re was found to show little temperature related change in attenuation. Frequency was also not a strong factor in attenuation with increasing temperature.

Arave continued working with 2% thoriated tungsten with the primary goals of reducing sticking by use of stand-offs, which were used to provide controlled sticking points [Arave, 1976]. A 2% thoriated tungsten sensor was chosen due to the low attenuation at high temperatures observed in previous tests. A W-26%Re sensor was also tested, but was discounted after decalibration was observed during in-furnace tests. The in-furnace decalibration was attributed to migration of rhenium to the sensor surface and subsequent changes to Young's modulus. Decalibration due to transmutation was also discussed and

considered an important factor for long irradiations, but the associated drift was considered acceptable for fluences up to 10^{18} n/cm^2 (thermal). Compatibility with a 2% thoriated tungsten sheath was demonstrated to 2000 °C and with a W-26%Re sheath to 2400 °C. A ceramic (thoria or hafnia) coating was also used to isolate the sensor from the sheath, and reduce sticking, for temperatures below 2400 °C. Above this temperature, the oxide was observed to vaporize and migrate to cool sections where it would precipitate and bridge the gap between the waveguide and the sheath, causing increased sticking at cool zones. Rings deposited or fabricated onto the inner surface of the sheath were also tested. Sticking was still observed, but with reduced effect. Also, the locations of sticking could be controlled using this method. It was determined that producing sheaths of this nature was impractical. Standoffs consisting of three 0.005 inch beads welded to a 0.015 inch diameter sensor (2-inch sensor length) were also tested, with positive results. Standoffs of this nature can also be used as reflectors.

Tasman [Tasman, 1972] compares ultrasonic thermometry with other methods (pyrometry, noise thermometry, gas thermometry, thermocouples) for use at temperatures over 2000 °C. Thermocouples and ultrasonic thermometers were determined to be the only practical methods available at the time. The primary advantages of ultrasonic thermometers compared to thermocouples are described as increased ruggedness and reduced tendency to decalibrate due to temperature and radiation effects. Tasman considered both multi-sensor time-of-flight and resonance methods, but selected pulse-echo time-of-flight techniques for their multi-point capability. Laboratory tests were performed to temperatures up to 2400 °C for 100 hours with thoriated tungsten sensors. A precision of 30 °C was estimated for a single, 50 mm long sensor. Sticking was encountered at temperatures above 1800 °C. High

temperature signal attenuation was found to be significant for pure tungsten sensors, but not for thoriated tungsten sensors up to at least 2400 °C. Tasman mentions the possibility of connecting the end of the sensor to the end of the sheath to eliminate sticking, as it would fix the end of the sensor and cause the sensor displacement to shear contact bonds between the sensor and sheath. It is unclear if this method was tested.

Tasman was also involved in irradiation testing of ultrasonic thermometers [Tasman, 1977]. Ultrasonic thermometers were evaluated in irradiation tests (TRESON 1 and 2). The estimated thermal conditions at the fuel centerline included a maximum temperature of 2500 °C, a linear heat generation rate of 600 W/cm, and a thermal gradient of several thousand degrees Celsius per centimeter. The designed sensor was 2% thoriated tungsten with a 1 mm outer diameter. Sensors with 2 and 3 segment were used. Segments were formed using diameter reductions. The magnetostrictive transducer consisted of Remendur, a commercialy magnetostrictive alloy of 49% Fe-49%Co-2%V, silver brazed to the cold end of the waveguide. Calibration of the sensors was performed in a vacuum furnace. During the first irradiation test, sticking caused loss of signal after 14 hours at 2400 °C in both sensors. One sensor was partially restored by rapid temperature cycling, differential thermal expansion between sheath and sensor shearing contact bonds. Sticking was thought to be caused by enhanced diffusion of tungsten due to oxygen provided by the fuel. The second irradiation used the same type of sensors as the first. Sticking began again at 14 hours, but this time at 2000 °C. Thermal cycling again restored the signal of one thermometer. This cycling had to be repeated occasionally over the course of irradiation.

Tasman also recognized the advantages (greater temperature sensitivity) and disadvantages (greater sticking or contact sensitivity, more complicated transducer

arrangement) of using torsional waves instead of longitudinal waves [Tasman, 1982]. The main advantage is that torsional waves travel more slowly than longitudinal waves (about half the speed). This implies that a more accurate temperature measurement can be made, as the time of flight will be greater (for the same length of sensor). Conversely, a smaller sensor segment may be used with no loss of temperature accuracy. These advantages are offset by the need for a more complicated transducer configuration. A simple solenoidal coil may be used to generate and receive longitudinal waves, but torsional waves require either a transverse biasing magnetic field or the use of a mode converting transducer (the transducer sits at a right angle to the waveguide). Both of these arrangements make the system larger and more complicated. A second disadvantage is the fact that torsional waves exhibit maximum displacement at the surface of the waveguide. This means that most of the energy of the wave is transported at the surface (or near the surface) of the waveguide, increasing the impact of surface effects like sticking. It is not clear that one configuration is superior. Tasman also considered AKS-tungsten lamp wire (tungsten doped with aluminum, potassium, and silicon) as a possible replacement for thoriated tungsten. AKS-tungsten has increased ductility compared to pure tungsten (due to the dopants causing an irregular, interconnected grain structure), similarly to thoriated tungsten but without the tendency of the thoria to evaporate and cause sticking at high temperatures. Tasman also described several possible sticking solutions. These include limitation of contact by tensioning the waveguide, purposeful contact of many random small areas (threaded waveguide), deliberate contact at specific points (i.e., reflectors similar to those described by Arave), a non-metallic intermediary sub-sheath (also previously described by Arave and Lynnworth, and a movable sensor wire (either axial or rotary motion). A tested rotating sensor design was found to increase sticking through friction

welding.The threaded sensor showed increased sticking due to increased contact pressure at contact points. A tungsten wire wrapped around the sensor was observed to create the same effect. Tasman mentions other researchers had success wrapping the sensor with strips of fine tungsten mesh. Tasman also summarizes the results of 7 different irradiation tests. Sticking was found to be the primary cause of problems in each case.

In 1977, Carlson describes UT evaluations primarily involved with liquid metal fast breeder reactor applications [Carlson, 1977]. Thoriated tungsten sensors were used in fuel (UO_2) melt tests to 2860 °C. These tests used sensors consisting of five 10 mm sensor segments. Temperature resolution of 10 °C was indicated by the calibration data. The magnetostrictive transducers consisted of 2 mm long coils driven by short, high current signals (magnetostrictive material not named). The first tests assumed that the calibration for each sensor segment was identical. This was found to be untrue due to inconsistencies in machining the segments, and subsequent tests calibrated each sensor segment individually.

Carlson also performed an extensive comparison of candidate sensor materials. Materials tested include 302 stainless steel, nickel, Remendur, titanium, platinum, zirconium, vanadium, rhodium, niobium, molybdenum, rhenium, tungsten, and 2% thoriated tungsten. Normalized delay time (effectively inverse acoustic velocity) and attenuation were measured. Impedance matching of wires to yield maximum signal strength was described. Results were averaged over two heating and two cooling cycles. Maximum operating temperature was defined as the temperature where the signal became unmeasurable. The 302 stainless steel sensor was determined to be usable to 1200 °C with good temperature sensitivity. New reflections appeared between 1200-1300 °C, later attributed to annealing of cold work induced during forming of the wire. Nickel sensors were observed to have significant changes

in calibration curve between cycles. A large change in slope between 200-400 °C was thought to indicate a phase change, though none is known. Contamination of the wire material may be a possible explanation. Remendur sensors were included for completeness (Remendur was used in transducers) and were found to work well to 800 °C. Titanium sensors showed very good performance to almost 900 °C, with little attenuation and good temperature sensitivity. A phase change precludes the use of titanium sensors above 880 °C. Platinum sensors had non-reproducible calibration, thought to be due to grain growth, as well as relatively high attenuation. Zirconium sensors performed well for temperatures below 860 °C, at which point a phase change occurs. The tendency for zirconium to become very brittle, coupled with a lower temperature sensitivity, make it a less desirable alternative to titanium. Vanadium sensors evaluations did not yield reproducible calibration curves (possibly due to sticking), an apparent phase change was observed near maximum operating temperature (none indicated in phase diagrams), and the sensor became very brittle. Rhodium sensors showed very good performance to 1300 °C. Attenuation was significantly reduced after an initial heat treat. Niobium sensor behavior was described as bizarre, with small or negative changes in delay time indicating an increase in acoustic velocity. Significant attenuation upon cooling past 500 °C and the appearance of new reflections (a phase change was suspected, though none is known) were also observed. Molybdenum sensors showed low attenuation, but also relatively low temperature sensitivity. Sticking above 1800 °C caused truncation of the test in favor of other materials. This sticking was later determined to be due to a chemical reaction with a zirconia heat shield. Results of rhenium testing led the authors to deem it the "best" material, with good sensitivity and reproducibility to 2600 °C. High attenuation was observed at very high temperatures, but the signal was "clean" enough to offset this. Tungsten testing

demonstrated this material to have the highest temperature operation (2900 °C, the upper temperature limit of the furnace). Tungsten was also described as having low sensitivity and high attenuation at high temperatures. Testing indicated that the 2% thoriated tungsten performed the same as tungsten, but with significantly reduced attenuation due to grain stabilization from thoria. Radiation effects on materials were not considered in this study.

Carlson also used 5 segment ultrasonic thermometers in reactor safety experiments, such as measuring a temperature profile in a molten pool of UO_2/steel, with a maximum temperature of 2860 °C [Carlson, 1979]. Carlson utilized a rotating waveguide design to reduce sticking. This is possible with a magnetostrictive transducer because coupling between the electrical and mechanical systems is done magnetically (i.e., non-contact).

Grossman intended to use UTs for measuring the thermal conductivity of thoria-urania fuel pellets [Grossman, 1982]. Grossman speculated that sticking would be less problematic than in mixed oxide fuels due to a reduced oxygen potential. Like Tasman, Grossman thought of AKS tungsten lamp wire as a superior option to 2% thoriated tungsten wire due to vaporization and relocation of thoria at temperatures over 2500 °C. Grossman also tested welding of the sensor end to the sheath cap to reduce sticking, however without tensioning of the waveguide. Grossman also discussed a clad rod concept. This is similar to the idea of coating the sensor with a ceramic, but generalized to consider any material with a significantly different acoustic impedance from the sensor. This could include ceramics or other metals. The concept is that wave modes can be contained within the core rod if the wavelength is much smaller than the rod diameter. This requires high frequency operation not possible with magnetostrictive transducers at the time; it also brings wave dispersion into consideration.

Shepard compared the performance of several measurement technologies for use in

high temperature nuclear applications [Shepard, 1975]. The tested technologies included a rhenium UT, Johnson Noise Power Thermometers (JNPTs), and tungsten-rhenium thermocouples. The sensors were tested at 900-1500 °C in the High Flux Irradiation Reactor at Oak Ridge National Laboratory for 1000-3000 hours.   Decalibration of the UT and thermocouples due to transmutation was observed. No decalibration was observed for the noise thermometer. Additionally, Remendur based magnetostrictive ultrasonic transducers (used for driving the ultrasonic thermometers) with aluminum and silver wire coils were irradiated to a thermal neutron fluence of 5.8×10^{19} n/cm^2 with no apparent adverse effects. A hafnia insulator inside a tungsten-rhenium protective sheath was credited with preventing collapse of the ultrasonic thermometer sheath. Decalibration of the ultrasonic thermometer, with respect to neutron fluence was observed to be linear. The total accumulated fluences was estimated to be 1.5×10^{22} n/cm^2 (thermal) and 4.6×10^{21} n/cm^2 (fast) at an average temperature of 900-1000 °C. Total decalibration of the ultrasonic thermometer was estimated to be -1070 °C at an actual temperature of 1000 °C (i.e., the UT reads -70 °C). Johnson Noise Thermometry was selected as best choice by authors as it did not decalibrate over the duration of the test.

Gopalsami and Raptis [Gopalsami, 1983] performed tests to 1100 °C with 310 stainless steel, Incoloy 800, sapphire, alumina, and chromium oxide. All candidate materials were observed to have appropriate performance with the exception of chromium oxide, which had a non-singular temperature response. An analytical effort was performed to explore the use of changes to phase shift related to notch width as a possible means to identify reflectors. It was determined that it is possible to identify the reflector producing a specific signal, but it requires high precision in the manufacturing of the notches.

Kulczyk was interested in operation only to 800 °C, and tested thermometers using 304 stainless steel, Inconel 600, and Kanthal as sensor materials [Kulczyk, 1990]. Notches and "posi-notches" (dilations) were used to create sensor segments. Kulczyk's primary contribution is the development of acoustic horn transitions between the transducer and waveguide. Tested geometries were horn-to-horn and reflex-to-reflex couplers. Coupling was achieved via pressure from an acoustic isolation bushing. The developed couplers allowed removal/replacement of the transducer without necessitating removal of the sensor, but did not achieve ideal acoustic coupling unless the materials were identical. Good transmission was achieved over a wide range of frequencies. The removable coupler is not useful in the case that the transducer is located within the reactor.

Laurie, et al. reviewed prior UT research [Laurie, 2008]. Laurie found that US and international applications demonstrated the viability of this technology for light water reactor (LWR), high temperature gas reactor (HTGR), and sodium fast reactor (SFR) test conditions (see Figure 2-2). However, the study noted that prior in-core applications were primarily limited to fuel damage tests that ceased several decades ago. Although such tests clearly demonstrated the ability of UTs to withstand high temperatures (up to nearly 2900 °C), test durations were typically limited to less than 100 hours; and data acquisition was cumbersome due to the limitations of signal processing systems available at the time. The availability of new materials and signal processing techniques suggests that this technology could be ideally suited for irradiations that require robust, high accuracy, compact sensors. Key details of prior US efforts, as reported by Laurie, are summarized in Table 2-2.
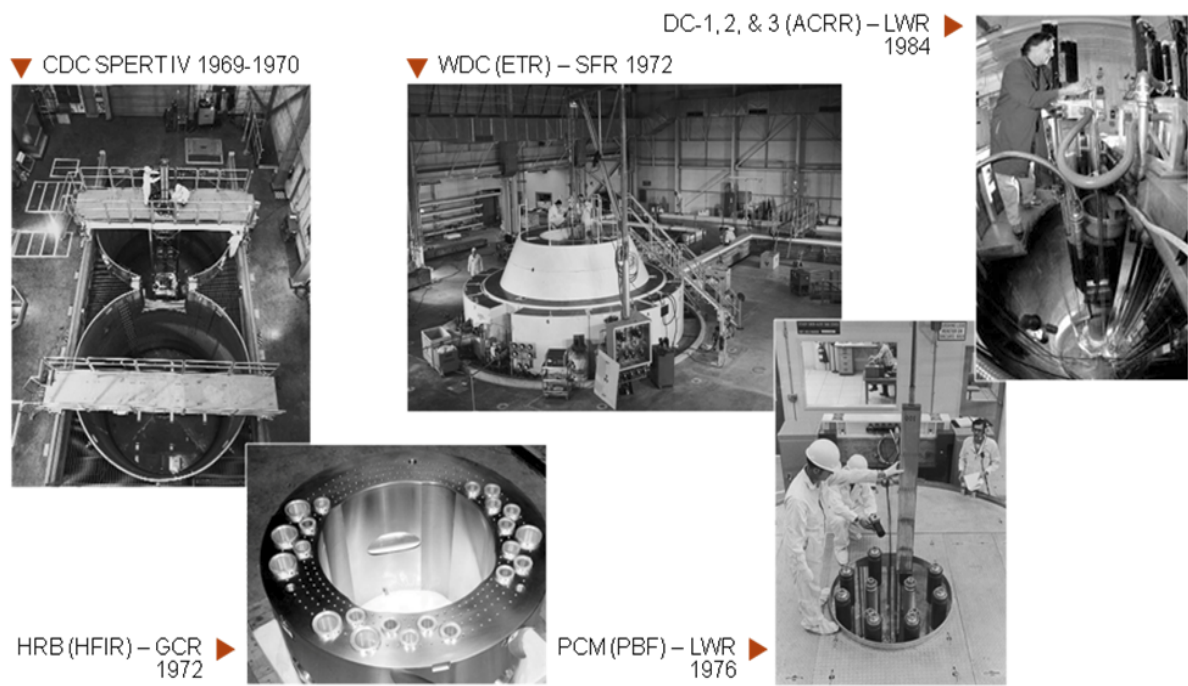
Figure 2-2. Prior UT in-core applications in the US [Laurie, 2008].

Table 2-2. Summary of prior irradiation testing of UTs [Laurie, 2008].

Organization	Test	Maximum Temperature	Sensor Material	Comments
Idaho National Laboratory	WDC-3-5 Engineering Test Reactor	2707 °C	W-25%Re	Minor sticking between sensor and sheath
Idaho National Laboratory	Power Cooling Mismatch	2017 °C	Thoriated Tungsten	Short duration tests, no failures
Idaho National Laboratory	Capsule Driver Core	approximately 1807 °C	W-25%Re	Demonstrated faster response time compared to thermocouples
Oak Ridge National Laboratory	High Flux Isotope Reactor-HRB	907-1107 °C	Rhenium	-1070 °C drift after test due to transmutation of rhenium
Sandia National Laboratory	Molten Fuel Pool	2860 °C	Thoriated Tungsten	5 sensor segments in molten UO_2, thoria sheath, temperature reached in 19 minutes
Nuclear Research and Consultancy Group	RETSON	2000 °C	Thoriated Tungsten	2000 hour test at 2000 °C results in less than 30 °C decalibration
Commissariat à l'énergie atomique/Ispra	FARO	2800 °C	Doped Tungsten	Operation for more than one hour in oxide corium
Commissariat à l'énergie atomique	PHEBUS FPT3	2207 °C	Thoriated Tungsten	Transients in excess of 300 °C/min experienced

The major issues associated with deployment of UTs for irradiation testing included selection of appropriate sensor materials for very high temperature applications, elimination of contact bonding (sticking), and signal processing. Signal processing technology available at the time of prior work was limited, and variations between research efforts are not well

described. The major results of previous research are related to testing of various sensor materials and methods of reducing sticking. These results are summarized in Table 2-3.

Table 2-3. Summary of major results from previous UT research.

Technical Issue	Tested Solution	Comments/Results
Material Selection	Rhenium	High sensitivity. High temperature operation demonstrated to 3180°C. Rapid decalibration due to transmutation.
	Tungsten	High temperature operation demonstrated to 2860°C. Rapid decalibration due to transmutation.
	2% Thoriated Tungsten	High temperature operation demonstrated to 2860°C. Rapid decalibration due to transmutation.
	AKS Tungsten	High temperature operation demonstrated to 2860°C. Rapid decalibration due to transmutation.
	Tungsten-25%Rhenium	High temperature operation demonstrated to 2650 °C. Rapid decalibration due to transmutation.
	Molybdenum	Tested to 1800 °C. Low attenuation observed. Not thoroughly tested due to low melting temperature and similar sensitivity when compared to tungsten.
	Niobium	Flat, non-singular calibration curves.
	Tantalum	Results not reported.
	Platinum	Non reproducible calibration curve. High attenuation.
	Graphite	Results not reported.
	302 Stainless Steel	Good performance to 1200 °C. High temperature sensitivity. Spurious reflections between 1200-1300 °C, attributed to annealing of cold work from wire drawing.
	Nickel	Significant changes in calibration curve between cycles.
	Titanium	Good performance to approximately 900 °C. Low attenuation. High temperature sensitivity. A phase change precludes the use of titanium sensors above 880 °C
	Vanadium	Non reproducible calibration curve. Significant embrittlement.
	Rhodium	Good performance to 1300 °C. Very high thermal neutron absorption cross section.
	Zirconium	Good performance to 860 °C. Not useful above 860 °C due to phase change.

Table 2-3. Summary of major results from previous UT research.

Technical Issue	Tested Solution	Comments/Results
Sticking	Thoria Coating/Sheath	Effective to 2400 °C. Above 2400 °C, vaporization of thoria, migration of vapor to cooler regions, and deposition onto waveguide cause total loss of signal.
	Stand-off Reflectors	Effectiveness not commented on.
	Tensioned Waveguide	Effectiveness not commented on.
	Wire Cloth	Identified as the most effective method.
	Rotating Waveguide	Increases sticking by friction welding.
	Ribbed Sheath	Determined to be impractical to fabricate.
	Threaded Waveguide	Increases sticking due to contact pressure.
	Wire Wrapped Around Waveguide	Increases sticking due to contact pressure.

2.3 Ultrasonic Transducers in Radiation Environments

Ultrasonic measurements have a long and successful history of use for materials characterization, including detection and characterization of degradation and damage [Ensminger, 2012]. Post irradiation examinations (PIEs) have successfully shown that fuel microstructural parameters, such as porosity and grain size, can be correlated to ultrasonic velocity [Phani, 2007]. According to Villard, frequency requirements for such measurements are restricted to greater than 10 MHz [Villard, 2011]. However, lower frequencies can be used for some applications, such as ultrasonic thermometry, where frequency requirements may be 100 – 150 kHz or lower [Lynnworth, 1989]. Prior studies have shown that typically both the piezoelectric and magnetostrictive materials used in transducers degrade when subjected to high temperature and/or radiation [(Holbert, 2005), (Kulikov, 2001), (Shea, 2009), (Wittels, 1957), (Primak, 1975), (Bierney, 1976)]. As discussed below, only limited radiation effects data are available to guide this process.

The use of sensors based on magnetostrictive transducers in Material Testing Reactors (MTRs) has been suggested to measure temperature, liquid level, density, flow, pressure, bubble occurrence and location, and acoustic emissions [(Lynnworth, 1968), (Lynnworth, 1971), (Rogers, 1982)]. Mechanical coupling as well as enhanced guided wave mode generation makes magnetostrictive transduction ideal for low frequency measurements, such as ultrasonic thermometry [Gopalsami, 1984]. As discussed in Chapter 2.2, deployment of these types of sensors has been successful for MTRs for high temperature measurements (up to 2800 °C), but these tests were limited to short-duration severe fuel damage tests. Although ultrasonic thermometers with magnetostrictive transducers have been deployed in MTRs; they have not been used in-core for long duration irradiations.

Many magnetostrictive materials are available for the use and fabrication of ultrasonic transducers. The properties of most relevance to in-core measurements include maximum operating temperature, sensitivity, and resistance to radiation damage. Unlike many of the piezoelectric materials, magnetostrictive materials are primarily metal alloys. Observed effects of radiation on metals differ significantly from observed effects on ceramics. For example, investigations with magnetic Fe-Ni alloys, such as Permalloy, have shown that their magnetic permeability tends to decrease with neutron irradiation [Brown, 1984]. This is attributed to the immobilization of domains due to point- defects generated by displacement cascades. In effect, this would limit the magnetostrictive capabilities of the material. However, magnetostrictive effects have been reported at fluences of up to 5×10^{19} n/cm^2 [Lynnworth, 1971].

2.4 Summary

There is a wide variety of sensors that can be used to monitor temperatures in a wide

variety of environments. However, few temperature sensors are capable of reliably monitoring in-core experiments. This is due to a variety of factors, but degradation of sensors due to irradiation conditions is the most significant factor. The most commonly used sensors are thermocouples, which are robust, accurate, and well developed. For applications below temperatures of 1100 °C, type-K or type-N thermocouples can be used with negligible radiation effects on performance. Above 1100 °C, these thermocouples are unsuitable due to self contamination. Tungsten-rhenium alloy thermocouples are capable of operation at much higher temperatures (up to 2200 °C for short periods of time), but are very sensitive to thermal neutron radiation. These thermocouples can only be used for short periods before they decalibrate due to transmutation of the constitutive elements. A newer thermocouple, the INL developed HTIR-TC, overcomes some of the issues with type-K, type-N, platinum-rhodium, and tungsten-rhenium thermocouples. HTIR-TCs have been tested to temperatures of 1800 °C and are constructed from radiation tolerant materials. However, high temperature degradation of the electrical insulation still limits the temperatures at which the TC may be used (a problem applicable to any temperature sensor based on electrical signals). Thermocouples are also generally limited to a measurement at a single point in space. Multi-point measurements are of interest for the purposes of characterizing the performance of nuclear fuels and structural materials, as well as for validating simulation codes. Multi-point thermocouples can be constructed, but at the cost of increasing the physical size of the sensor (a significant factor when making measurements on small samples, such as nuclear fuel pellets). The only sensor identified in previous studies that provides very high temperature capability, multi-point measurements, and the capability to operate in an intense nuclear radiation environment is the ultrasonic thermometer.

Ultrasonic thermometry development research has been performed since the 1960's using both resonant and pulse-echo techniques. The pulse-echo method has been considered the more promising method due to multi-point capability and lower mass requirements. Despite a great deal of effort, several obstacles remain before ultrasonic thermometry can be considered a viable option for monitoring in-core experiment temperatures. For example, the materials that were identified and tested during previous research were selected based, primarily, on melting point. The materials of most interest, rhenium and tungsten, have relatively high thermal neutron capture cross sections and will transmute during irradiation, leading to decalibration. Other materials with high melting temperatures, such as molybdenum (which also has a low thermal neutron capture cross section), were not tested extensively. Another issue encountered in previous research was sticking, contact bonding between the sensor and its surroundings, which causes spurious signal features and can cause total loss of signal. Many methods of eliminating sticking were identified and tested, but most were found to have limited effect or, worse, to exacerbate the problem. Signal processing was also an area where difficulty was experienced, mostly due to the limited technology available. The signals received from a multi-point ultrasonic thermometer can be very complicated due to many factors, such as acoustic signals reflecting multiple times within the waveguide or the spurious signals created by points of sticking.

Survival of the ultrasonic transducer in a radiation environment is not essential for deployment of this sensor. The transducer can be located remotely from the sensor section with signals transmitted over a distance via waveguide. However, it is advantageous if the magnetostrictive transducer can be located within the reactor vessel. This minimizes the distance that acoustic signals need to travel and reduces the effects of signal attenuation. It

also eliminates the need to have the waveguide, or sheath, pass through a pressure boundary. This eliminates an acoustic barrier in the case of a waveguide and a possible leak path in the case of a sheath (which is essentially a hollow, gas filled tube). Some prior testing has been done in this area, but deployment of an ultrasonic thermometry system in a reactor with high flux, such as the INL's Advanced Test Reactor, will require demonstration of the survival of these transducers in a high radiation environment.

Chapter 3: Theory of Ultrasonic Thermometer Operation

Ultrasonic thermometry is a method of measuring temperature based on changes in the acoustic properties of materials. Ultrasonic (or acoustic) thermometry can be divided into two basic forms; resonance tracking and time domain reflectometry.

The first method, resonant frequency tracking, uses temperature dependant changes in the natural frequency of a resonator. The resonator may be a transducer (a piezoelectric quartz crystal driven into resonance, for example) or a separate component connected to the transducer via a waveguide. In either case, resonant frequency is dependant on both the material and the geometry of the resonator. As the temperature of the resonator changes, the natural frequency also changes, and resonance is lost. The driving frequency is adjusted until resonance is restored. The advantages of this method are its relative simplicity and very high resolution and accuracy (1000 Hz/^{o}C sensitivity or 0.0001 ^{o}C resolution) [Lynnworth, 1989]. Disadvantages of this method include a relatively limited temperature range (-80 to approximately 250 ^{o}C for quartz resonators, though much higher temperatures are possible with refractory metal resonators) and slow response times, due to the mass of the resonator [Lynnworth, 1989], and the ability of the resonant thermometer to measure temperature at only a single point. Examples of resonant thermometer configurations are shown in Figure 3-1.
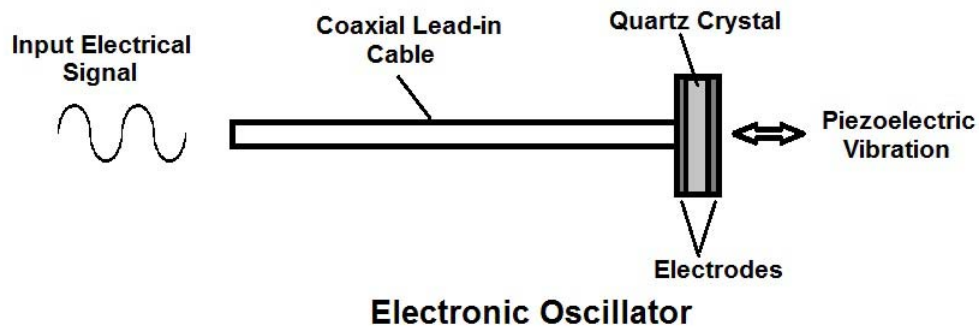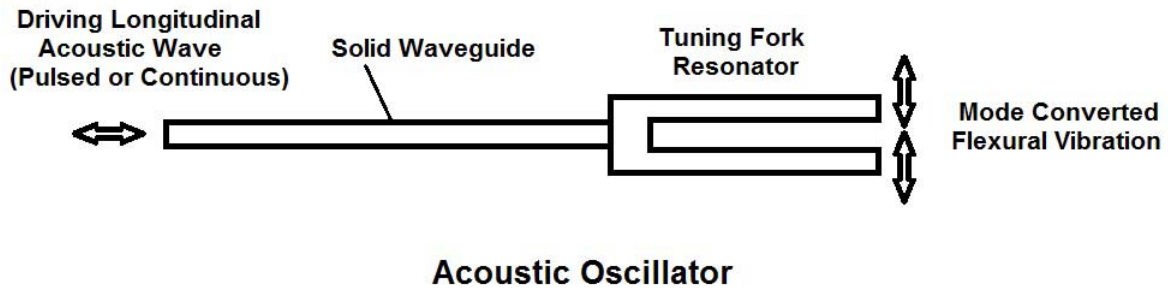
Figure 3-1. Examples of resonant ultrasonic thermometers.

Time domain reflectometry is a method in which the time of flight of an acoustic wave through a material (usually a thin metallic waveguide) is measured, and the average temperature in the material can be related to the wave velocity. This method is the most developed and the most versatile [Lynnworth, 1989]. As any material can conduct sound waves, any material can be used as the sensing element. This is not limited to solid materials, liquids and gases are also useful, though the relationships between temperature and acoustic wave velocity are not the same. The advantages of this method are that the sensor material may be selected to fit the temperature range and operating environment and that acoustic discontinuities may be fabricated into the waveguide at various points along its length,

allowing measurement of temperature at several points with a single sensor. This is the method that has been selected for development in this research effort.

A conceptual design of a basic 'notched-probe' UT, with key components identified, is shown in Figure 3-2. As indicated in this figure, a narrow ultrasonic pulse is generated with an ultrasonic transducer. The ultrasonic pulse propagates to the sensor wire, where a fraction of the pulse energy is reflected at each discontinuity (notches or diameter change). Each reflected pulse is received by the excitation coil, transformed into an electrical signal (amplitude as a function of time), amplified, and evaluated. The time interval between two adjacent echoes is evaluated and compared to a calibration curve to give the average temperature in the corresponding sensor segment. When a number of notches are available on the wire sensor, the various measurements give access to a temperature profile along the probe.
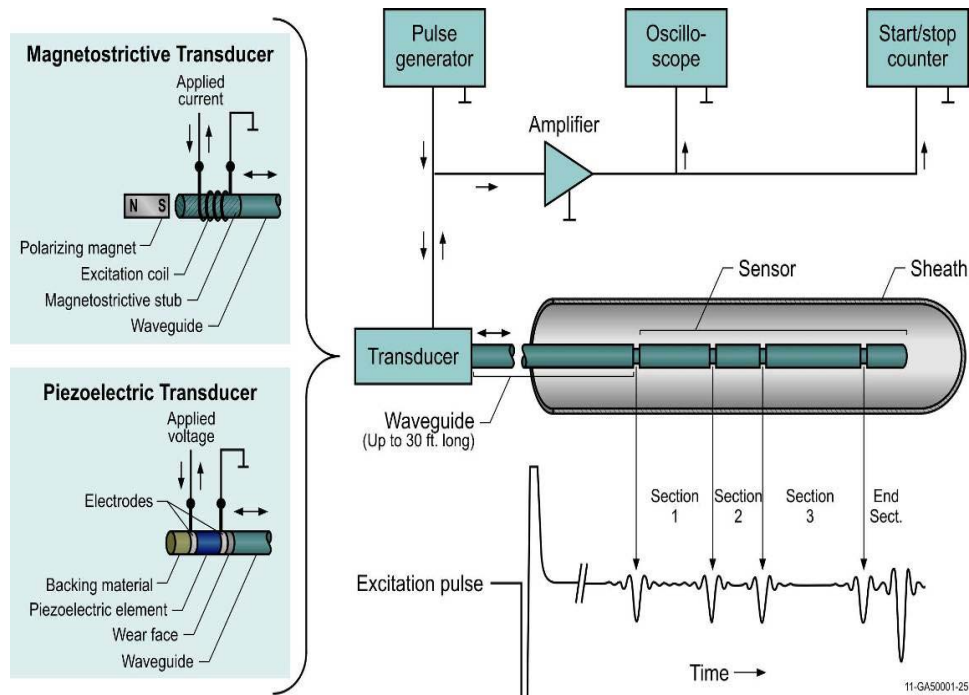

Figure 3-2. Conceptual time domain reflectometry ultrasonic thermometer design [Daw, 2012].

3.1 Ultrasonic Transduction

As shown in Figure 3-2, the transducer is a key component of an ultrasonic thermometer. There are two primary technologies applicable to the current application, piezoelectric and magnetostrictive, discussed in this section. A brief discussion of several other technologies is also presented.

3.1.1 Piezoelectric Transduction

Piezoelectric transducers are the most widely used method of generating and receiving ultrasonic waves. A piezoelectric element consists of a ceramic or single crystal material in which the crystalline structure is composed of polarized molecules or in which there exists a polarization of each unit cell [IEEE, 1987]. Some materials, such as quartz, are permanently polarized, while in others polarization must be induced by a strong external electric field. As such, the element will exhibit no net charge when the crystal is in an undeformed equilibrium state. When a mechanical strain is applied (in the direction of polarization), an electric field will be induced within the crystal as seen in Figure 3-3. This is known as the piezoelectric effect. Conversely, if the element is exposed an external electric field, a mechanical strain is induced through electrostriction. The existence of these inverse phenomena allows the piezoelectric element to be used to transform electrical energy to mechanical energy and vice versa. This means that the element may be used to both generate and sense mechanical waves. A piezoelectric transducer is, therefore, useful as an actuator as well as both a passive and active sensor. For typical applications, piezoelectric transducers are ideal as they can be manufactured to operate at a very wide range of frequencies (DC into the GigaHertz range) and to transduce many different modes of ultrasonic waves.
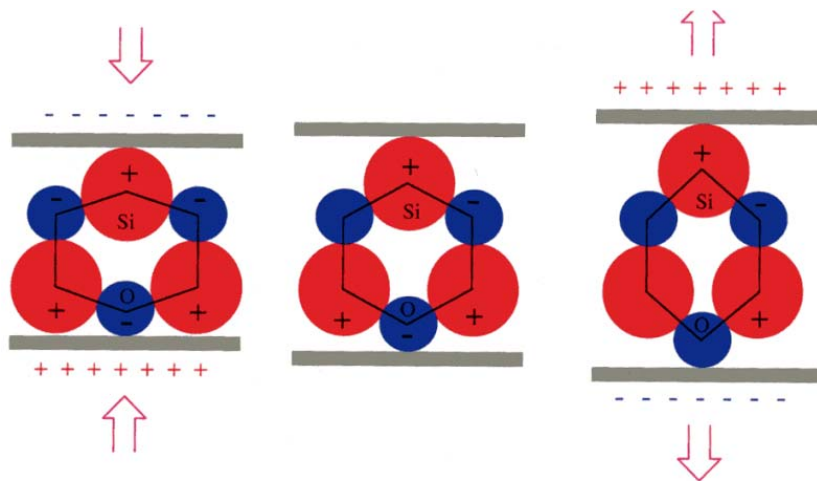
Figure 3-3. Piezoelectric effect in a quartz crystal.

The primary failings of piezoelectric transduction for use in an in-core ultrasonic thermometry application are radiation resistance, difficulty in coupling, fragility, operating frequency, and temperature limitations. The most commonly used piezoelectric materials have been observed to rapidly degrade, in terms of piezoelectric effect, in the presence of neutron and gamma radiation. These same materials typically have Curie temperatures (where piezoelectricity is lost) of approximately 300-350 ^{o}C, with recommendations to use them at no more than half these temperatures. Radiation and temperature resistance issues can, to a degree, be reduced by the use of a waveguide. This is a natural solution as the UT sensor is a waveguide itself and this allows location of the transducer far from the extreme conditions. However, this brings up the problem of coupling. The acoustic impedance of piezoelectric crystals is significantly different than that of likely waveguide materials. This means that most of the acoustic energy produced by the crystal will not be transferred to the waveguide, and most of the energy of returning waves will not be transferred back to the crystal. This is compounded when trying to couple a piezoelectric crystal (with typical diameters of at least 1.5 mm) to metallic waveguides that may have much smaller diameters (as small as 0.25 mm).

Coupling materials (most of which are very low temperature capable organic gels) and impedance matching layers help to alleviate these issues, but none are completely effective. Coupling efficiency is improved with pressure, but the crystals are inherently fragile. Frequency range may seem like an advantage of this technology, but the frequency that a piezoelectric transducer operates at is inversely proportional to the thickness of the crystal. The thicker the crystal, the lower the frequency. Manufacturing piezoelectric crystals in thicknesses that allow operation at frequencies below about 1 MHz is difficult. At frequencies above about 200 kHz, ultrasonic waves in waveguides of 1.5 mm diameter become dispersive, meaning that the waves will change modes from primarily extensional to shear, flexural, etc. As each wave mode travels at a different speed, the signals received will become increasingly difficult to analyze. Higher frequency waves also attenuate more rapidly, as higher frequency waves interact with smaller features (such as grain boundaries). This becomes increasingly problematic at high temperatures, as acoustic attenuation is also a function of temperature.

3.1.2 Magnetostrictive Transduction

Magnetostrictive materials are typically magnetic metals and alloys. Magnetostriction is a phenomenon in which a material undergoes a change in shape under the influence of an externally applied magnetic field. All magnetic materials are magnetostrictive, but most are not useful, because their magnetostrictive effect is very slight. The magnetostrictive transducer is basically identical to a ferritic core solenoidal field coil [Lynnworth, 1989], except that the magnetic permeability of the core changes strongly as a function of the stress state of the material. As such, the coil is used to both generate and receive acoustic signals passing through the core by means of non-contact electromagnetic coupling.
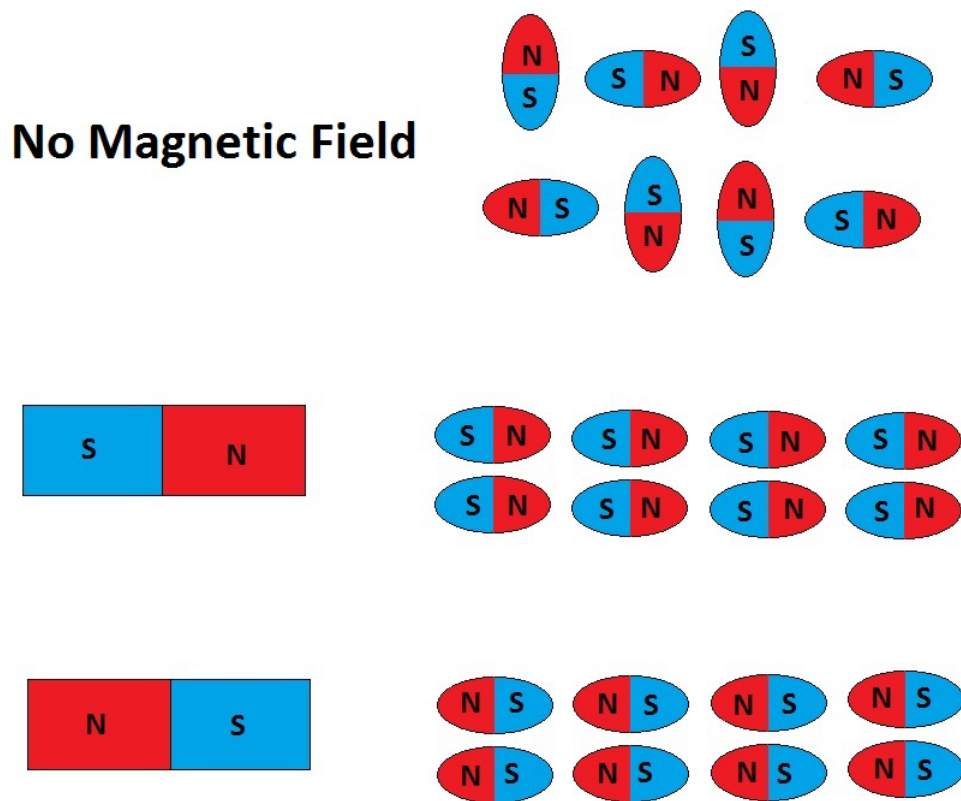
Figure 3-4. Response of magnetostrictive material to externally applied magnetic field.

The primary advantage of magnetostrictive materials over piezoelectric materials is in the ease of coupling to a metallic waveguide. As the magnetostrictive materials are metals or alloys, they can simply be welded, brazed, or soldered to the waveguide. Most metals of interest have acoustic impedances that are quite close to those of common magnetostrictive materials, so efficient acoustic coupling to a cylindrical waveguide can be achieved by using a magnetostrictive rod or wire of proper diameter. As the signals are transferred through electromagnetic (non-contact) means, the coil can be constructed as a separate component from the waveguide, isolating it from the environment and increasing the robustness of the sensor system. A commonly referenced failing of magnetostrictive technologies is that the frequencies of operation are thought to be limited to less than approximately 250 kHz.

However, this is can be an advantage in the current, waveguide based, application as signal attenuation and dispersion are minimized.

3.1.3 Other Methods of Transduction/Generation

There are many other ways of generating and sensing ultrasonic waves, each with advantages and disadvantages.

The electromagnetic acoustic transducer, or EMAT, is very similar to a magnetostrictive transducer. This is a non-contact device that can be used to generate ultrasonic surface waves in any metal, whether magnetic or non-magnetic. The EMAT consists of a coil and a permanent magnet. When placed in close proximity to a metal surface (which must be magnetically pre-biased by the presence of a permanent magnet), an RF signal is pulsed through the coil. Eddy currents induced in the metallic surface generate Lorentz forces along the surface perpendicular to the eddy currents which, in turn, generate acoustic waves in the direction of the biasing magnetic field (mutually perpendicular to the eddy currents and Lorentz forces), as shown in Figure 3-5. In general, EMATs do not transduce efficiently and, therefore, generate weak signals that are not useful for the current application.
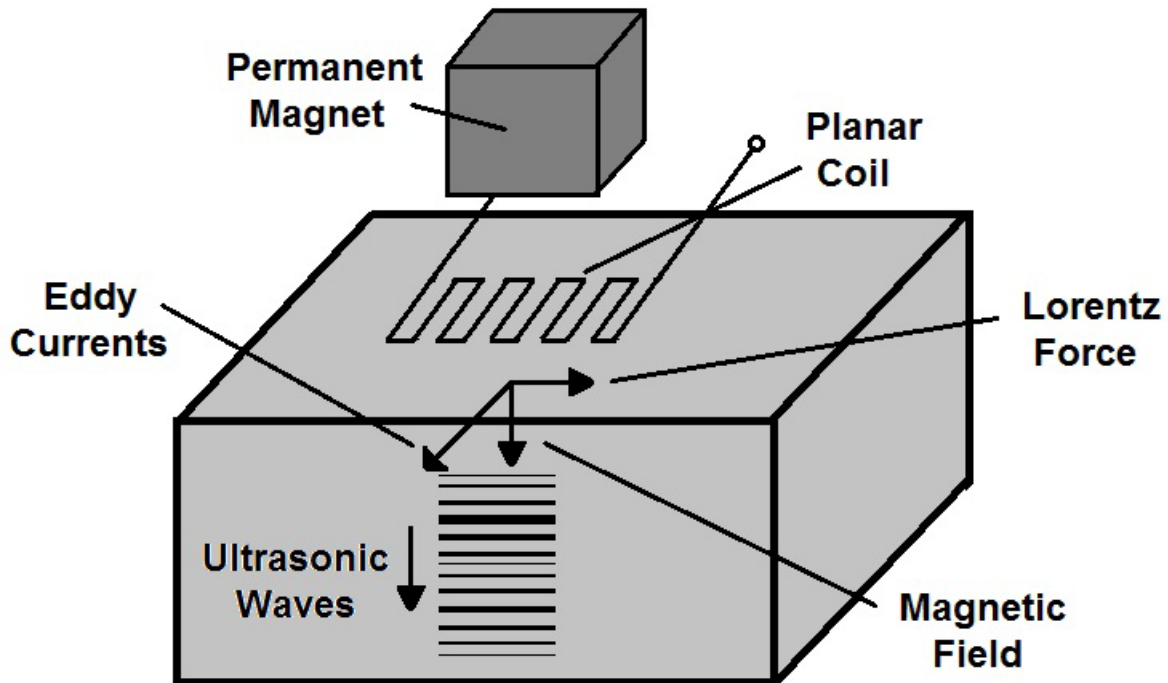
Figure 3-5. EMAT schematic

Laser generation and reception is used outside of the nuclear environment for processes such as laser resonant ultrasound spectroscopy (Figure 3-6). Laser generation of acoustic waves occurs when a laser strikes a material and creates a thermal shockwave. This process is usually ablative and, therefore, not truly non-destructive. Laser based reception is achieved through interferometry and is both very sensitive and very accurate. However, both generation and reception by laser based methods require a line of sight to the object under investigation as well as careful alignment. In the case of in-core testing, this would be achieved through the use of fiber optic cables. These cables, however, have invariably been observed to darken and embrittle in the presence of neutron radiation [Brichard, 2001], resulting in rapid deterioration of signal quality and severely limiting the usefulness of such systems. Fiber optic cables also cannot survive temperatures above approximately 800 °C.
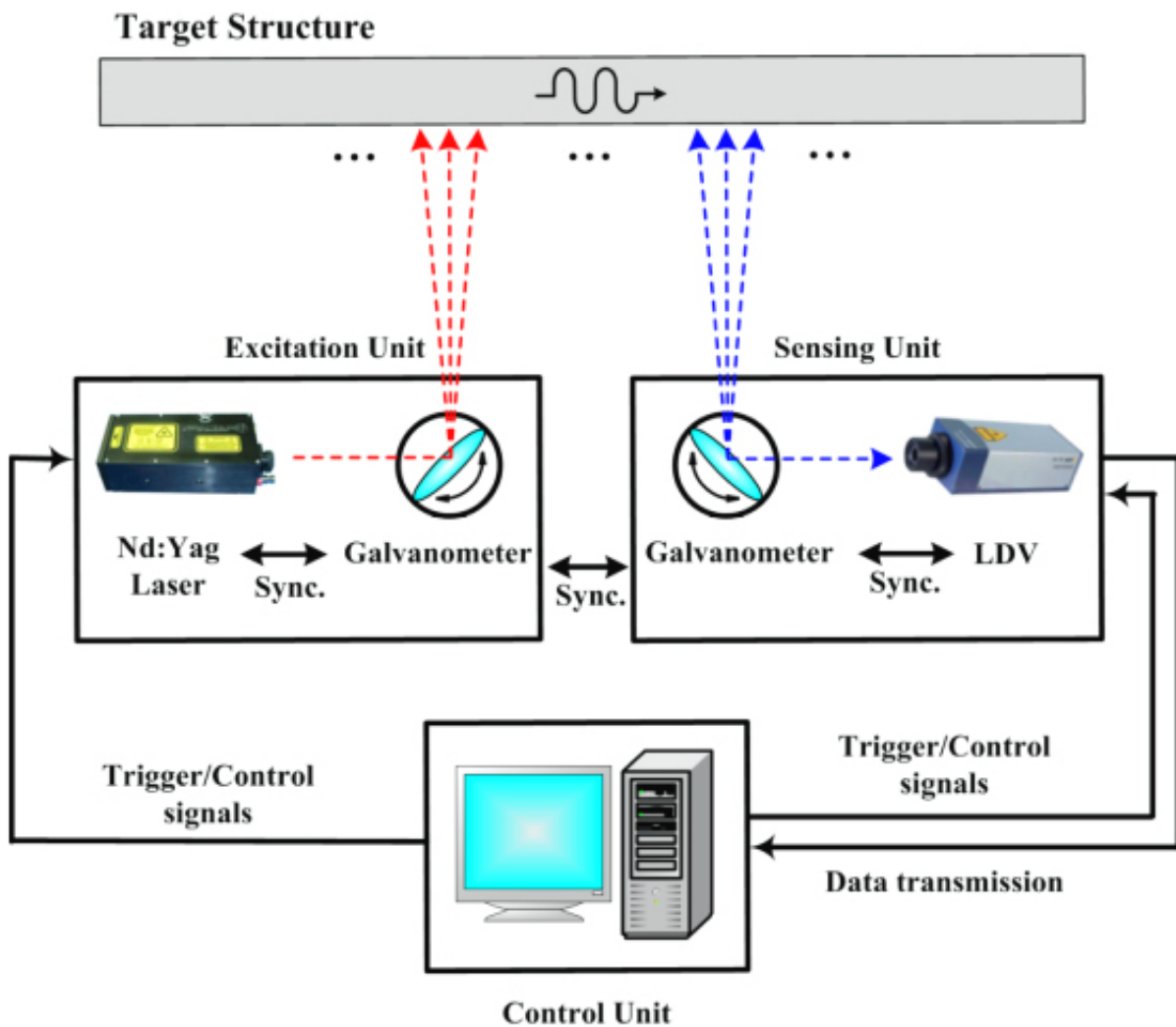
Figure 3-6. Schematic of a typical laser ultrasound system [An, 2012].

Although reception of ultrasonic waves requires a transducer of some sort to convert the acoustic signal to a useful electrical signal, the waves may be generated by any method that causes sound waves to propagate through the sensor. This could be something as crude as hitting the waveguide with a hammer.

3.2 Ultrasonic Wave Propagation

Ultrasonic signals propagate through solids as stress waves. For an infinite isotropic material, the equation of motion can be written as [Graff, 1991]:

$$\rho \frac{\partial^2 \bar{u}}{\partial t^2} = \nabla \sigma \ , \tag{3-1}$$

$$\tag{3-2}$$

where ρ is the material density, σ is the stress tensor, and u is the displacement and ∇ is the gradient operator. For a Hookean material (one that obeys Hooke's law) undergoing small (elastic) displacements, the stress can be related to displacement using Hooke's law as follows [Graff, 1991]:

$$\sigma_{ij} = \lambda \delta_{ij} \varepsilon_{kk} + 2\mu \varepsilon_{ij}, \tag{3-3}$$

where ε represents the strain state of the material, δ is the Kroneker delta, and λ and μ are Lame's first and second constants. In mechanics, Lame's second constant is typically denoted by G, the shear modulus. Lame's constants describe elastic material properties and are related by the bulk modulus, K, as follows [Graff, 1991]:

$$\lambda + \frac{2}{3}\mu = K \quad \text{for a three dimensional body,} \tag{3-4}$$

and

$$\lambda + \mu = K \quad \text{for a two dimensional body.} \tag{3-5}$$

The strain can be related to displacement through the relation [Rose, 1999]:

$$\varepsilon_{ij} = \frac{1}{2}\left(\frac{\partial u_i}{\partial x_j} + \frac{\partial u_j}{\partial x_i}\right). \tag{3-6}$$

Substituting the stress and strain relations into the equation of motion leads to the Navier-Cauchy equation [Kolsky, 1963]:

$$\rho\frac{\partial^2 \bar{u}}{\partial t^2} = (\lambda + \mu)\frac{\partial}{\partial x_i \partial x_i}\frac{\partial u_j}{\partial x_i} + \mu\frac{\partial^2 u_i}{\partial x^2_{\ j}}, \tag{3-7}$$

which can be solved by applying appropriate boundary conditions.

3.2.1 Propagation in Cylindrical Waveguides

In the case of a thin, cylindrical waveguide, the exact solution is given by the Pochhammer-Chree equations (in cylindrical coordinates) [Rose, 1999]:

$$\frac{2\alpha}{r}(\beta^2 + k^2)J_1(\alpha r)J_1(\beta r) - (\beta^2 - k^2)J_0(\alpha r)J_1(\beta r) - 4k^2\alpha\beta J_1(\alpha r)J_0(\beta r) = 0, \tag{3-8}$$

and

$$(\beta r)J_0(\beta r) - 2J_1(\beta r) = 0, \tag{3-9}$$

where r is the radius of the rod, k is the acoustic wavenumber (the inverse wavelength) and, and J_0 and J_1 are Bessel functions of the first kind. α and β are defined by [Shatalov, 2011]:

$$\alpha^2 = \left(\frac{\omega}{c_L}\right)^2 - k^2, \tag{3-10}$$

and

$$\beta^2 = \left(\frac{\omega}{c_T}\right)^2 - k^2, \tag{3-11}$$

where w is the angular frequency, c_L is the velocity of longitudinal waves, and c_T is the velocity of torsional waves. The acoustic wavenumber, k, is related to the angular frequency by [Rose, 1999]:

$$k^2 = \left(\frac{\omega}{c_p}\right)^2 \quad , \tag{3-12}$$

where the quantity c_p is the phase velocity, the propagation rate of the phase of the acoustic wave. The phase velocity is found by solving the Pochhammer-Chree equations numerically, yielding frequency dependant dispersion curves. The phase velocity and wavenumber are then used to calculate the group velocity (the speed at which a wave packet or carrier signal propagates, in the case of a pulsed signal). The group and phase velocities are not necessarily the same. Also, as the acoustic signals typically have non-singular frequency content, components of the wave packet may propagate at slightly different velocities as well. This leads to a gradual spreading of the wave packet known as dispersion. In order for an ultrasonic thermometer to be useful, wave dispersion should be minimized as changes in the mode of propagating waves and to the shape of the acoustic signal can make collected data difficult or impossible to analyze. Figures 3-7 and 3-8 show representative dispersion curves calculated for molybdenum waveguides of two different diameters using the freely available Matlab program pcdisp [Seco, 2009]. The figures plot the velocity of waves of different modes (denoted in the figures as L for longitudinal, T for torsional, and F for flexural) and orders against frequency. Regions where the velocity changes rapidly with respect to frequency are dispersive. These operating frequencies should be avoided in practice.
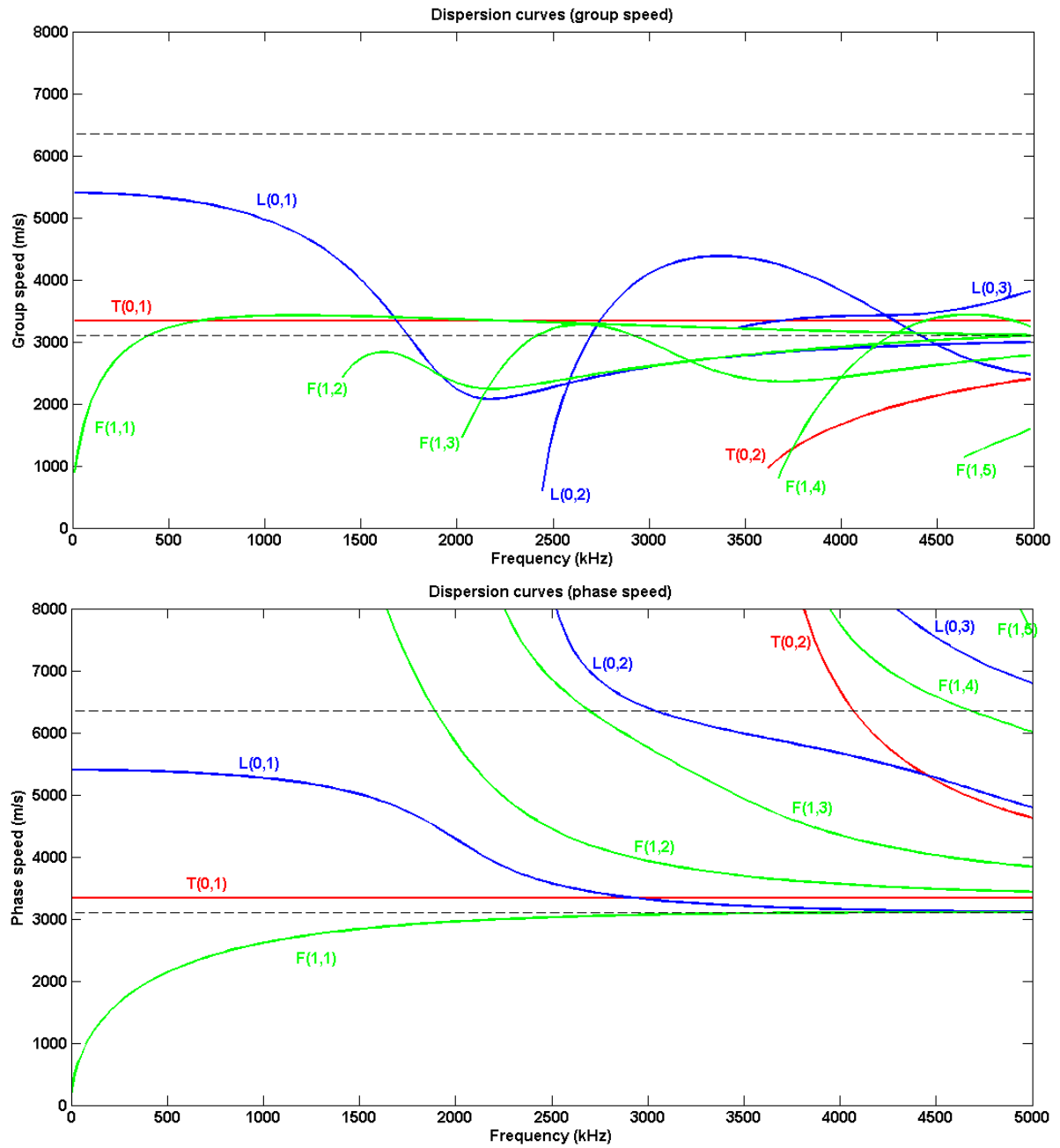
Figure 3-7. Dispersion curves for 1.57 mm diameter molybdenum rod. Calculated using pcdisp [Seco, 2009].
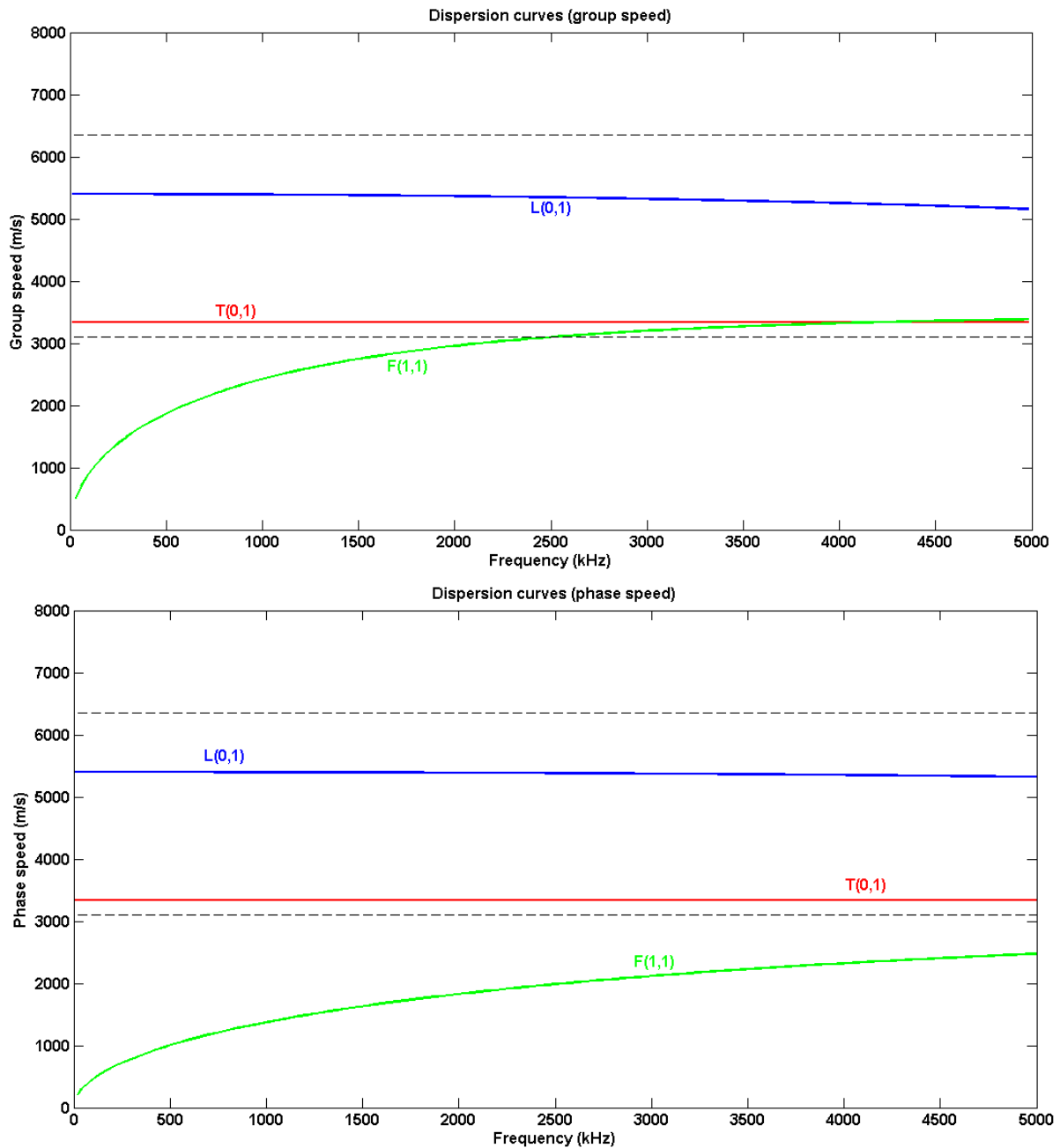
Figure 3-8. Dispersion curves for 0.25 mm diameter molybdenum wire. Calculated using pcdisp [Seco, 2009].

Figures 3-7 and 3-8 also indicate that more higher order wave modes may be supported for a larger diameter rod, assuming equal operating frequency. For the most part,

this is not a concern as only one wave mode is excited by a carefully designed driving transducer (i.e. 2nd, 3rd, etc. order modes of the three base wave types). Typically, the lowest order longitudinal (L(0,1)) or torsional (T(0,1)) mode would be used for a UT system. Other modes interfering with the received signal could be created through excitation of these higher order modes, or through mode conversion; for example, a sharp bend in the rod could convert longitudinal waves to flexural waves.

3.2.2 Temperature Dependant Velocity

For a solid material, the acoustic velocity is dependent on both the mechanical stiffness of the material and its density. In a thin (diameter of waveguide less than one tenth acoustic wavelength, as a rule of thumb) waveguide, the temperature dependant velocity, c_L, of a longitudinal wave can be simplified to [Lynnworth, 1989]:

$$c_L = \sqrt{\frac{E}{\rho}} \qquad \textbf{(3-13)}$$

where E is the Young's modulus of elasticity. Both of these parameters are functions of temperature, and both tend to decrease with increasing temperature. However, changes to the Young's modulus tend to dominate changes to the density. This means that the acoustic velocity of a material tends to decrease with increasing temperature. There is a separate effect on the time of flight of an acoustic wave through the material that comes from thermal expansion. This effect is typically negligible in comparison to the change in acoustic velocity. In a practical system, the time of flight is related to the temperature through calibration of the system against a standard, typically a thermocouple for temperatures below approximately 1500 $^\circ$C and a pyrometer for temperatures above 1500 $^\circ$C.

Chapter 4: Ultrasonic Thermometry

4.1 Basic Thermometer Design

As described in Figure 3-2, a basic pulse-echo ultrasonic thermometer consists of an ultrasonic transducer acoustically coupled to a waveguide. UTs operate on the principle that the speed at which sound travels through a material (acoustic velocity) is dependant on the temperature of the material. By introducing an acoustic signal to the sensor (typically a metallic rod) and measuring the time delay between the initial pulse and received echoes, temperature may be derived. UTs have several advantages over other temperature sensors. First, UTs can be made with very small diameters while maintaining a high level of durability, as the sensor consists simply of a small diameter rod (typical diameters of 1 mm, though a sheath may be required for some environments). As discussed in Chapter 3.2.2, a smaller diameter rod is desirable; as wave dispersion is avoided when the rod diameter is sufficiently smaller than the acoustic wavelength [Lynnworth, 1989]. Also, if enough acoustic power can be introduced into the sensor, temperature measurements may be made near the melting point of the transducer material. As no electrical insulation is required, shunting effects found in thermocouples and resistance temperature devices are eliminated. A clear line of sight is not required, as is the case for most optical pyrometry applications. With proper selection of materials, UTs may be used in very harsh environments, such as high temperature steam or liquid metals. Most attractive, however, is the ability to introduce multiple acoustic discontinuities to the sensor, as this enables temperature measurements at several points along the sensor length (allowing temperature profiling with a single sensor). The following sections detail the process of selecting appropriate components for application to in-core tests.

4.1.1 Coil

Ultrasonic thermometers using magnetostrictive transduction use a solenoidal coil to both generate and detect the magnetic field changes necessary for generation of longitudinal ultrasonic waves via the magnetostrictive effect. The frequency of a magnetostrictive transducer is primarily a function of the transducer (i.e., coil or rod) length, with the transducer length equating to one half of its acoustic wavelength [Krautkramer, 1969]. Dimensions and material properties of the magnetostrictive core also have some effect on the frequency. The resolution of an ultrasonic system is partially dependent on the operating frequency of its transducer. As mentioned in Chapter 3.1.1, higher frequencies allow detection of smaller physical features (such as reflectors) as well as greater time resolution of signal features (such as zero crossings). Increasing frequency necessarily requires decreasing length. However, decreasing transducer length also decreases signal strength. To overcome this, a new coil type, capable of higher frequency operation, was developed. As part of this research, additional development was completed to produce a high frequency transducer capable of operating at high temperatures (200-900 °C). At this time, a patent for the high frequency transducer design is currently being pursued by the United States Department of Energy (DOE); and the design specifics cannot be discussed [Daw, 2012].

4.1.2 Waveguide

For application to in-core temperature measurement of fuel centerline temperatures, the environment (temperature, radiation, etc.) limits selection of certain components and strongly influences others. The high temperatures limit waveguide materials to high melting temperature metals; specifically refractory metals in the extreme case of sodium fast reactors with ceramic fuels where temperatures may exceed 2600 $^\circ$C. The high neutron radiation

levels also restrict material selection to those with small neutron absorption cross sections (in order to reduce transmutation induced calibration drift).

4.1.3 Damping

Ultrasonic transducers generate acoustic waves in both directions (both toward and away from the sensor section of the waveguide in the case of a magnetostrictive transducer). The waves propagating away from the sensor strike the free end of the waveguide and are reflected back toward the transducer, where they may interfere with the signals being used for measurement. To eliminate this problem, the free end of an ultrasonic transducer is damped. This is typically accomplished (in the case of piezoelectric transducers) by compressing a highly attenuating material against the free side of the transducer crystal. This is not an option with a small wire waveguide, as the wire end area is too small.

For magnetostrictive transducers, the typical method used to obscure the undesired free-end echo was to place the end of the magnetostrictive rod at the center of the driving coil. While this does effectively eliminate the free-end echo, it significantly reduces the strength of the ultrasonic pulse. This method also does nothing to reduce the interfering effects of reflections created by the weld between the magnetostrictive rod and the waveguide. As part of this research a new method was developed which utilizes a material with an acoustic impedance similar to that of the waveguide. The free end of the magnetostrictive rod was placed in a tube filled with loose attenuating material. The tube was then compacted onto the rod. The effect is that acoustic energy from the rod is transferred from the rod to the damper over the length of the damper and is then scattered within the damping material. If the damper has sufficient length, this results in an efficient cancellation of the undesirable reflections.

4.1.4 Signal Processing

A signal processing method described by Roberts, et al. [Roberts, 2006], was used during initial acoustic velocity characterization testing. This method consists of cross-correlating the time series data to a known signal (typically either the input signal or the expected reflection), then squaring and low pass filtering the correlated data. Steps for the selected method using data obtained from a 0.254 mm diameter 302 stainless steel wire at 20 ^{o}C are shown graphically in Figure 4-1.
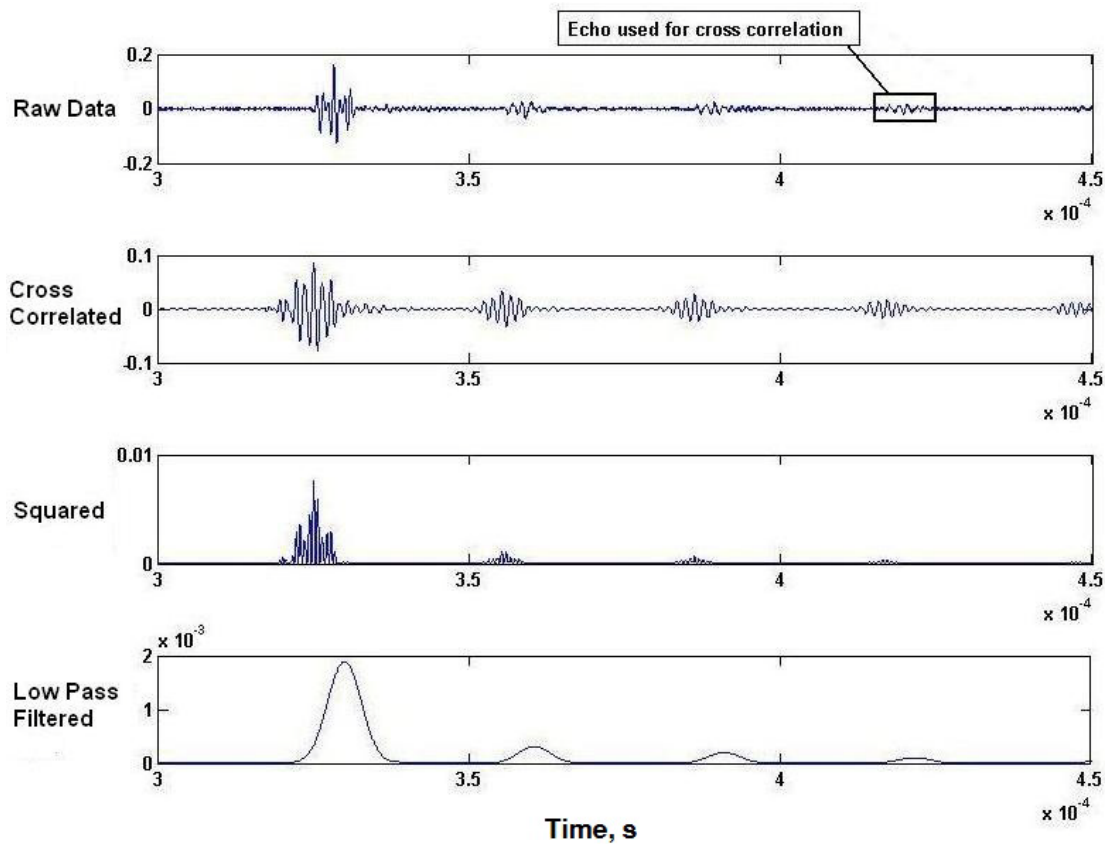
Figure 4-1.   Graphical representation of data analysis process.

This method greatly increased the signal-to-noise ratio and simplified identification of reflections, even in the presence of significant noise. The input signal used for these tests was

a simple square pulse, and could not be used in the cross-correlation. Two issues were observed with this initial method. First, the short (80×10^{-9} s) square pulse is best suited for powering high frequency, voltage based transducers (such as piezoelectric crystals). The inductive coils used to drive the magnetostrictive transducers require more time to fully charge and develop a strong magnetic field. The use of the short square pulse results in a clean, but weak, signal that could be overwhelmed by noise in an extreme environment or by excessive attenuation at high temperatures. The second issue observed is that although the input pulse is very short, the measured signals are quite long and require a large amount of space between reflectors for sufficient echo separation. Use of the above signal processing method results in broad, flat peaks instead of sharp, easily resolved signals.

The first issue has been resolved by switching the driving signal from a short square pulse to a longer tone-burst. The tone-burst is a sinusoidal signal several periods in length. This input results in a signal many times more powerful than the simple square pulse, without making the received signals significantly more complex (the echo shape is unchanged if the burst length is not overly long). As both the length and the frequency of the tone-burst can be varied, the signal may be optimized for different sensors and testing conditions.

The second issue is also partially solved by use of the tone-burst input signal. Although the input signal has longer duration than the square pulse, the frequency content of the input is narrow. This results in less ringing of the transducer. This means that the received signals are of similar duration to those observed with the square pulse, but with greater amplitude.

4.2 Experimental Results

The following sections discuss experiments and results used to characterize components of a UT system.

4.2.1 Acoustic Velocity Experimental Setup

As an initial step in the UT system development effort, acoustic velocity characterization tests were completed in order to reduce the number of candidate sensor materials by comparing temperature response, ease of fabrication, transmitted signal quality, etc. The tests were also used to evaluate and make appropriate adjustments to a signal processing technique for UT applications. The steps required to perform these tests (candidate material selection, test sample fabrication, test setup, and signal processing adaptation) are summarized in this section.

The materials selected for initial evaluations are listed in Table 4-1 with relevant material properties and envisioned irradiation environments. Candidate sensor materials were selected based on melting temperature, thermal neutron capture cross section, and compatibility with anticipated in-core test conditions. For higher temperature applications, such as inert gas-filled tests of oxide fuels, refractory metals are an obvious choice due to their high melting temperatures. Tungsten and rhenium were not considered (despite high melting points and previous use in UTs for very short term measurements) due to their high thermal neutron capture cross sections, as both are known to be prone to decalibration due to transmutation. Molybdenum and niobium have high melting points and low thermal neutron capture cross sections. Variations of these materials, KW-molybdenum (e.g., molybdenum doped with small amounts of potassium, silicon, and tungsten) and niobium-1% zirconium were selected for initial testing. Prior experience with these materials indicates that they retain

ductility better than pure metals after heating. For lower temperature tests (less than 1000 °C) in liquid metal or liquid sodium bonded metallic fuels, stainless steel and Inconel 606 were selected for cost, corrosion resistance, and ease of fabrication.

Table 4-1. Candidate sensor materials.

Material	Melting Temperature, °C [Touloukian, 1973]	Thermal Neutron Capture Cross Section, Barns [Mughabghab, 1981]	Identified Irradiation Test Application
302 Stainless Steel	1510	3.02	Liquid Metal Bonded Metallic Fuel (T<1000 °C)
304 Stainless Steel	1510	3.03	
Inconel 606	1400	4.35	
Molybdenum	2620	2.51	Inert Gas Filled Ceramic Fuel (T>1000 °C)
KW-Molybdenum	2620	2.51	
Niobium-1%Zirconium	2470	1.14	

Test specimens were isolated from each other in alumina tubes, which were installed in a tube furnace equipped with an argon purge gas system (note that Figure 4-2 shows a single installed sample, but a total of six were included in the test). Signals were generated using a commercial pulser/receiver system, and coils were hand fabricated in-house. Data were monitored and recorded using a high speed digital oscilloscope. Temperatures were measured using a National Institute of Standards and Technology (NIST) traceable Type-S thermocouple. Data were collected in 100 °C increments from room temperature to 1300 °C. Equipment used to generate and record the ultrasonic signals is shown in Figure 4-3.
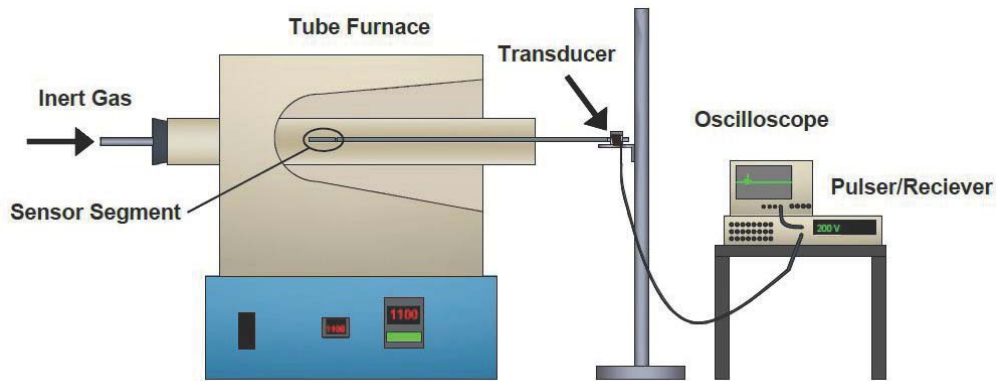
Figure 4-2.   Acoustic velocity characterization test setup.
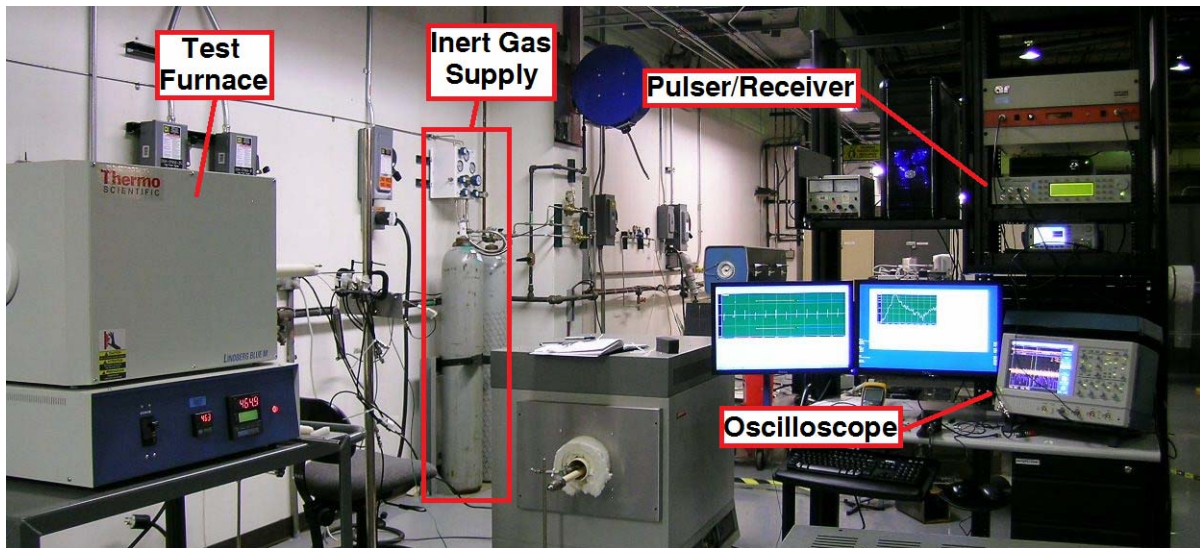
Figure 4-3.   Test equipment used to evaluate test devices.

4.2.2 Acoustic Velocity Results

Acoustic velocity was calculated from the delay time between the maxima in the filtered data and the known length of the sensor segment (after correcting for thermal expansion) using the following equation:

$$c_L = \frac{2(l + \Delta l)}{\Delta t}$$

(4-1)

where c_L is the acoustic velocity of the longitudinal sound wave, l is the initial sensor length at room temperature, Δl is the change in length due to thermal expansion, and Δt is the delay time between maxima.

As will be discussed in the next section, results from the acoustic velocity characterization tests indicate that stainless steel and doped molybdenum are ideal candidate sensor materials for the two temperature ranges considered in the current evaluations.

Stainless Steel

Figure 4-4 compares measured acoustic velocities of 302 and 304 series stainless steel samples to values calculated from reference mechanical property data [(Touloukian, 1973), (Chavez, 1994)]. As shown in this figure, calculated velocities based on test data are somewhat higher than reference values found in the literature (about 5% for temperatures below 800 °C). This difference can be attributed to differences in the manufacturing process used in production of the wires. However, the trend is appropriate for UT applications. High temperature attenuation increased signal noise and eventual loss of signal for temperatures above 1100 °C for the 0.254 mm diameter sample and above 1200 °C for the 1.58 mm diameter sample. It was also observed that the increased signal noise remained after cooling the sample. This is due to straightening the wire prior to heating. In order to achieve a "clean" signal, the wire should be free from small diameter bends and kinks. With stainless steel, it is possible to stretch the wire a small amount, inducing some cold work. As the wire is heated and begins to anneal, the cold work is relieved; and the small bends are partially restored.
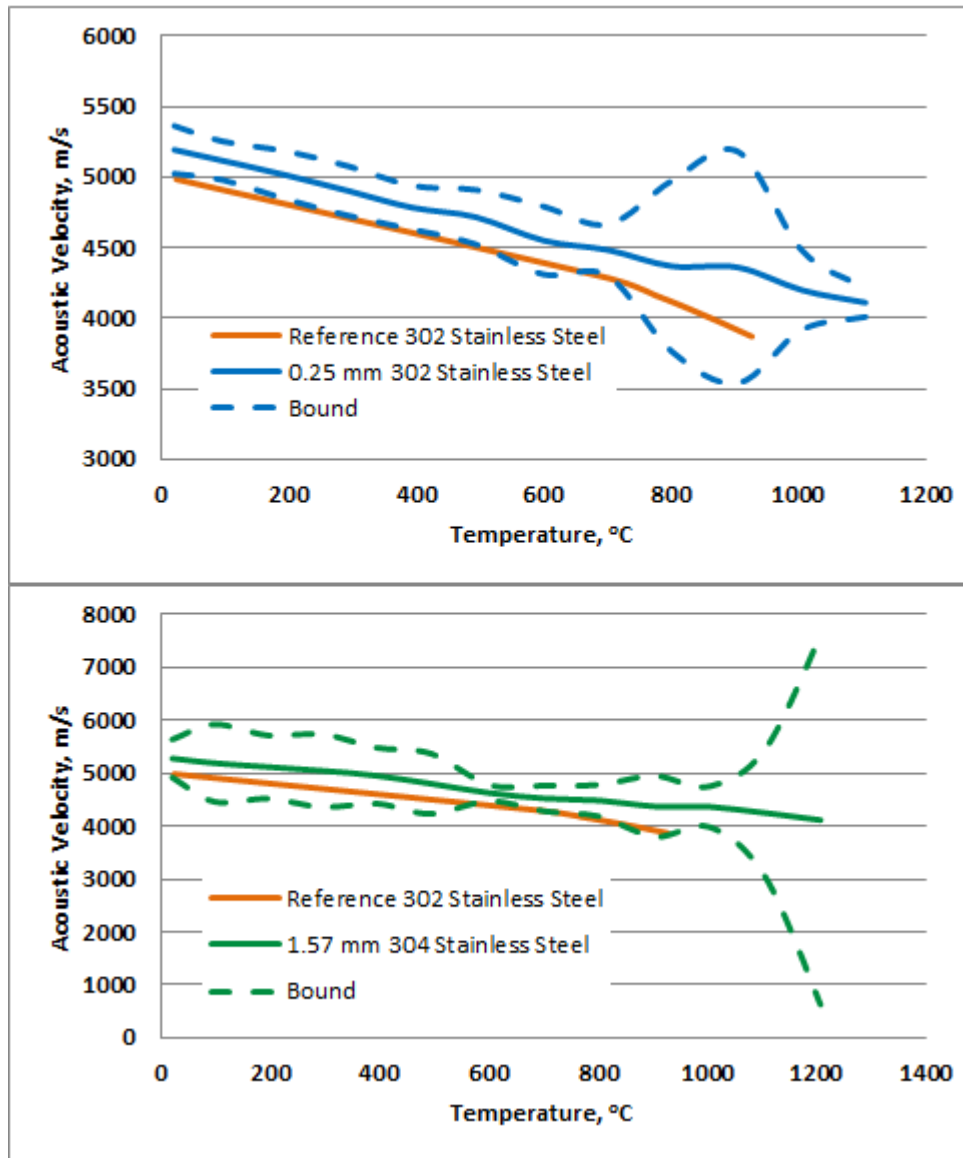
Figure 4-4. Comparison of measured acoustic velocity of stainless steel to calculated reference values.

Molybdenum

Figure 4-5 compares measured acoustic velocities for pure molybdenum and KW-molybdenum samples to values calculated from reference mechanical property data [(Touloukian, 1973), (Syre, 1961)]. The temperature response of the molybdenum samples is close to values inferred from the literature, except at the highest and lowest test temperatures.

Signals for molybdenum samples did not attenuate significantly over the evaluated temperature range.
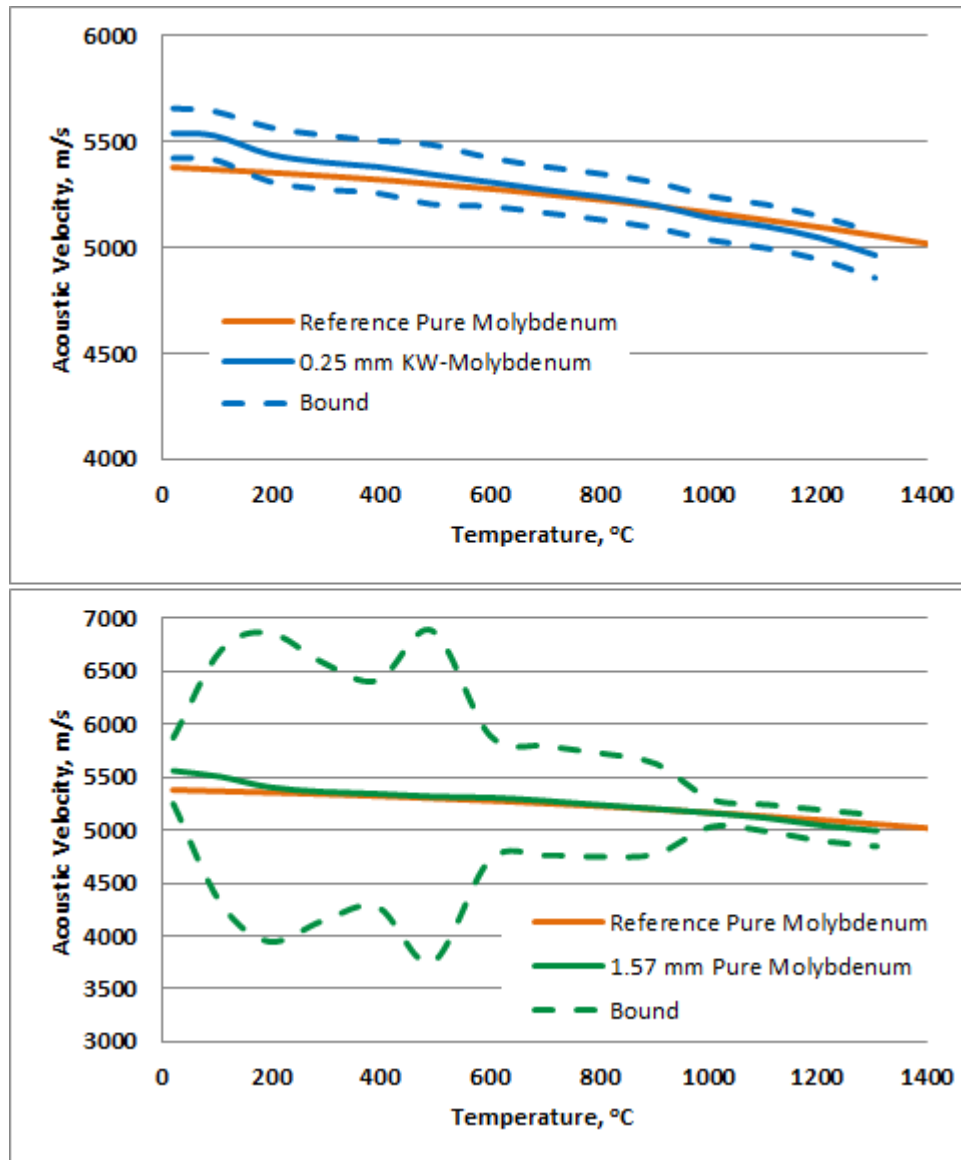
Figure 4-5. Comparison of measured acoustic velocity of molybdenum to calculated reference values.

Inconel 606

Figure 4-6 compares the acoustic velocity of Inconel 606 to values calculated from reference mechanical property data [(Touloukian, 1973), (Chavez, 1994)]. As with other materials evaluated, the velocity values of the tested samples are somewhat higher (better than 5% for temperatures up to 1100 °C) than velocities calculated with reference data.
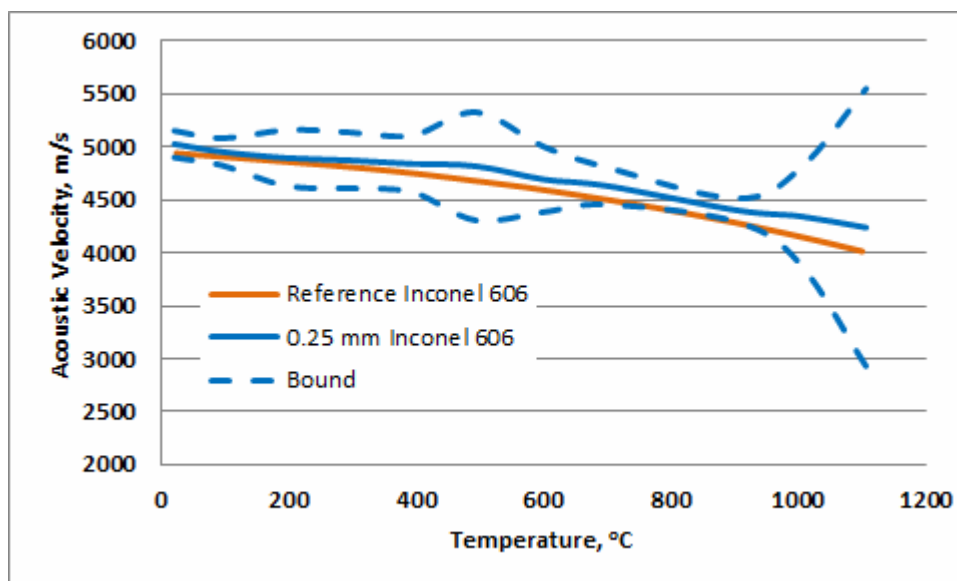
Figure 4-6.   Comparison of measured acoustic velocity of Inconel 606 to calculated reference values.

Sticking, a form of contact bonding between the sensor and its surroundings that can interfere with and obscure acoustic signals, occurred for Inconel 606 at temperatures above 1000 °C. As discussed in Chapter 2.2 sticking was only observed at temperatures above 1800 °C in previous research [(Carlson, 1971), (Tasman, 1982), (Grossman, 1982)]. This sticking could have been due to contact bonding between the sample and the alumina tube. However, due to the relatively low test temperature, it is more likely due to binding between the sample and the tube caused by differential thermal expansion. The sample was verified as

"stuck" upon attempted removal from the alumina guide tube. An example of the effect of sticking is shown in Figure 4-7 for an Inconel 606 sample tested at temperatures between 1000 °C and 1300 °C. Sticking appears to begin at 1100 °C and has completely obscured the reflector signal at 1200 °C. Though the observed sticking obscured the signal at high test temperatures, Inconel 606 does appear to be a good candidate for lower temperature irradiation test use. However, due to the sticking problem, the performance of candidate stainless steel materials appears superior.
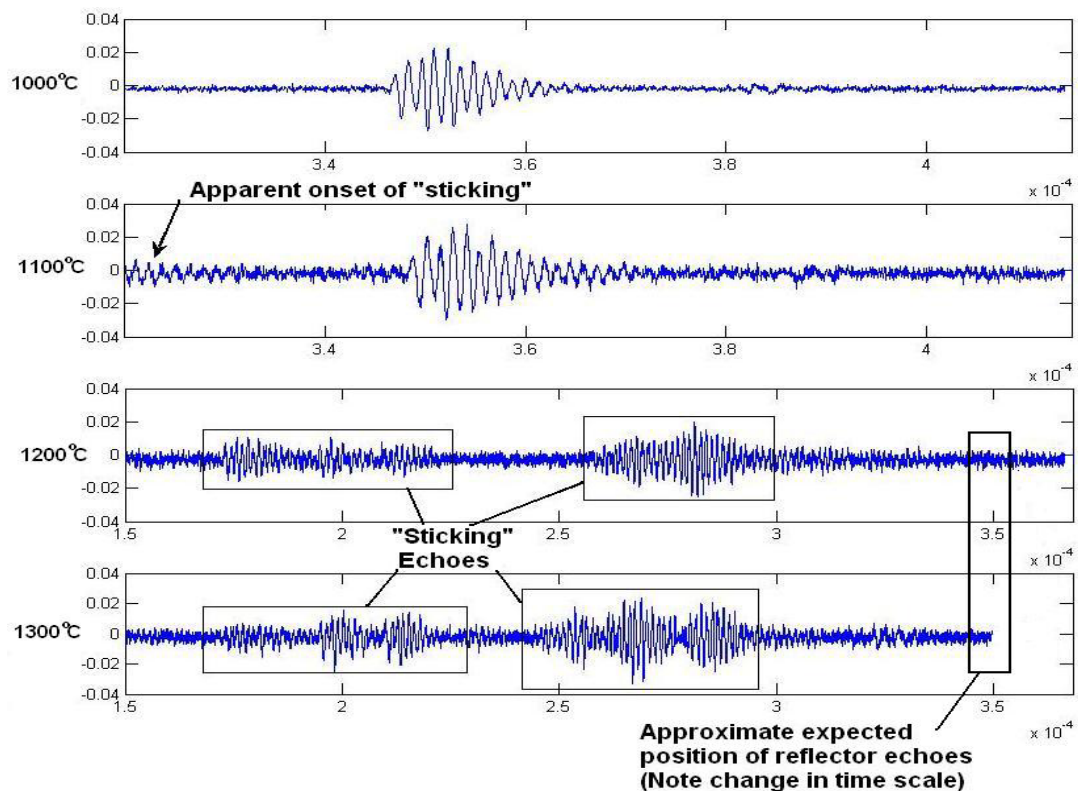
Figure 4-7.   Progression of "sticking" observed for Inconel 606 sample.

Niobium-1% Zirconium

The temperature response of the niobium-1% zirconium sample differed from values calculated from reference mechanical property data, although the velocity values are close at

room temperature. Reference data for density [Senor, 1990] and elastic modulus [Wojcik, 1994] predict a decrease in acoustic velocity with increasing temperature, as for the other tested samples. However, recorded data show a clear increase in velocity with temperature (see Figure 4-8).

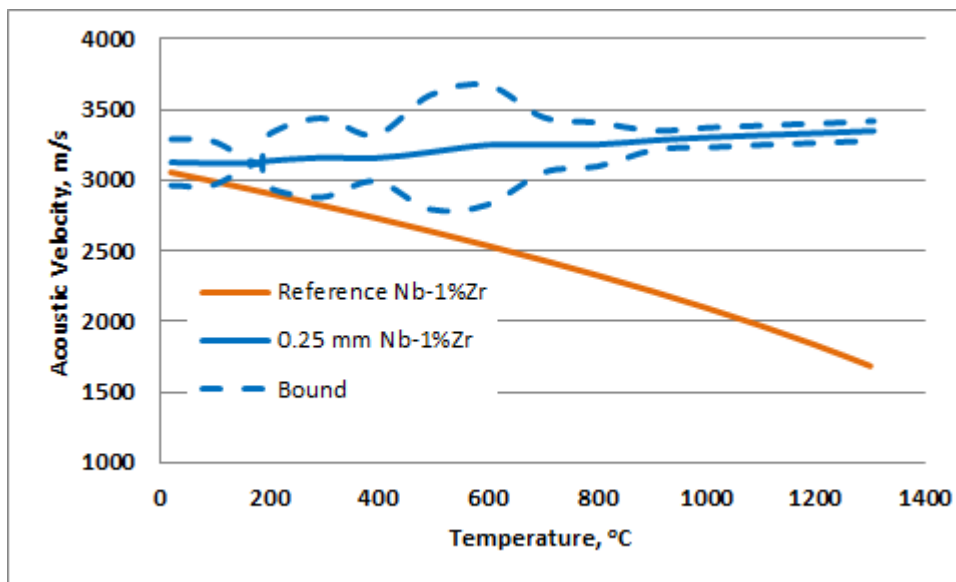**Figure 4-8.**   Comparison of measured acoustic velocity of Nb-1%Zr to calculated reference values.

Difficulties in fabricating the niobium alloy sample may partially explain this discrepancy. For example, welding the niobium to the magnetostrictive stub with a laser welder was observed to significantly embrittle the wire. To overcome this, a small amount of nickel wire was melted onto the weld in order to strengthen the joint, causing a slight bulge. The embrittlement also made the "dilation" type reflector problematic and led to the use of a double bend in the wire as a reflector. Ringing in the magnetostrictive stub, due to the diameter increase, was observed to cause the acoustic pulse to spread. The double bend reflector, as it was not a sharp acoustic discontinuity, could have also increased measurement uncertainties. This "spread out" nature of the signals can be seen in Figure 4-9, which shows

two reflection signals used to calculate acoustic velocity. Although the non-ideal signals could lead to increased error in the calculation of acoustic velocity, a comparison of signals recorded at different temperatures appears to verify the increase in velocity. Lines of equal slope were used to connect an easily identifiable feature common to both reflections starting at 20 °C. The line perfectly connects this feature in the leading reflection (at around 5×10^{-4} s). However a slight adjustment to the slope was required to fit the trailing reflection. This indicates a reduction in delay time with increasing temperature and, therefore, an increase in acoustic velocity. As discussed next, the increase in acoustic velocity is judged to be most likely due to the alloying of the base niobium with zirconium. This could cause a change in the relative effect of elastic modulus, compared to density, on the acoustic velocity by causing the sample to retain stiffness at elevated temperatures.
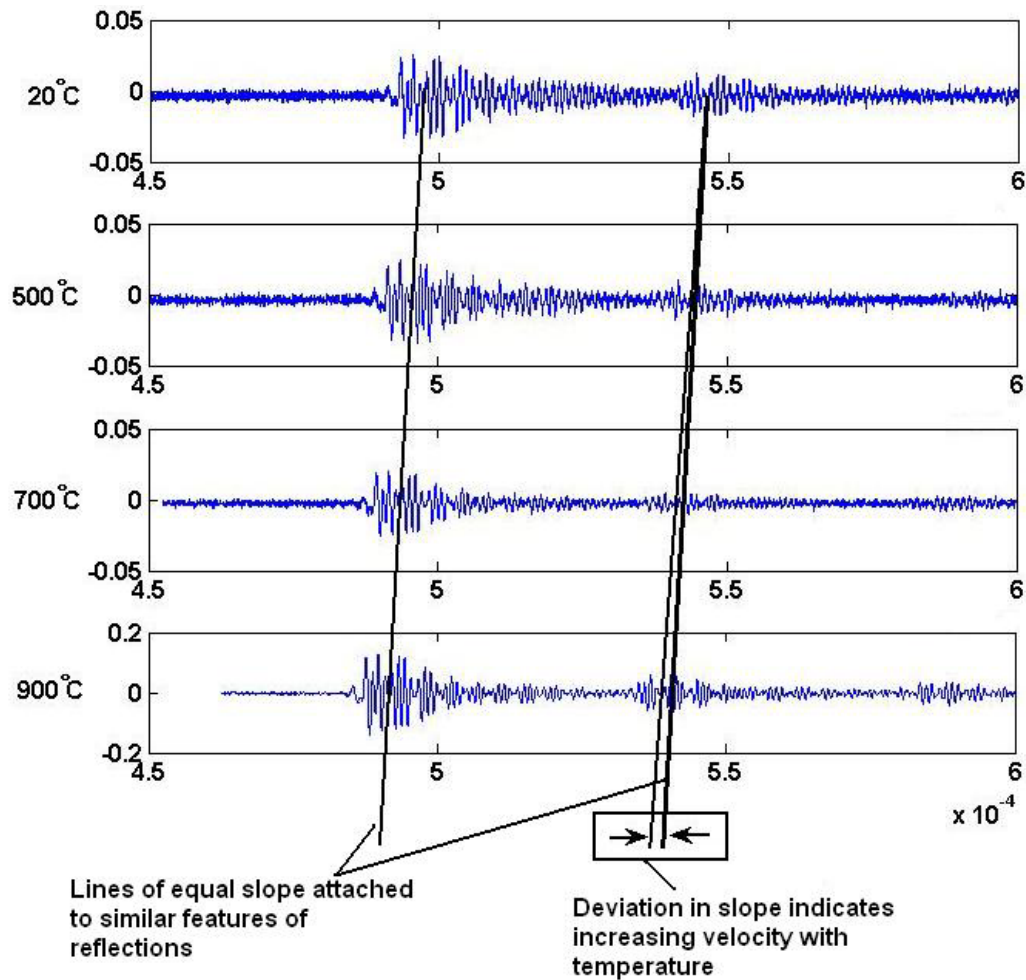
Figure 4-9. Time series data for Nb-1%Zr sample showing increase in acoustic velocity with temperature.

Figures 4-10 and 4-11 show temperature dependant elastic modulus data for niobium and some of its common alloys. From the plots it is apparent that the stiffness of niobium alloys is not strongly dependant on temperature, changing very slightly and in some cases increasing slightly. This is thought to be a behavior very specific to niobium and depends on microstructural processes such as annealing, recrystallization, and grain growth as a function of temperature, including time at temperature.
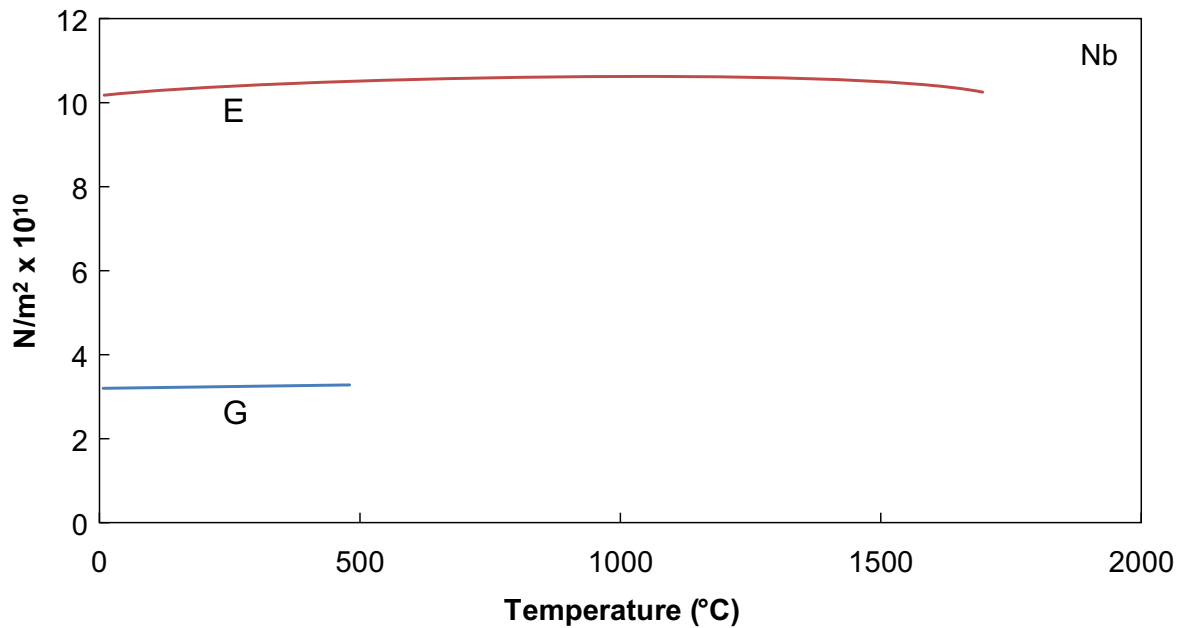
Figure 4-10. Temperature dependant elastic and bulk modulus for pure niobium found by ultrasonic methods. Reproduced from [Farraro, 1979]
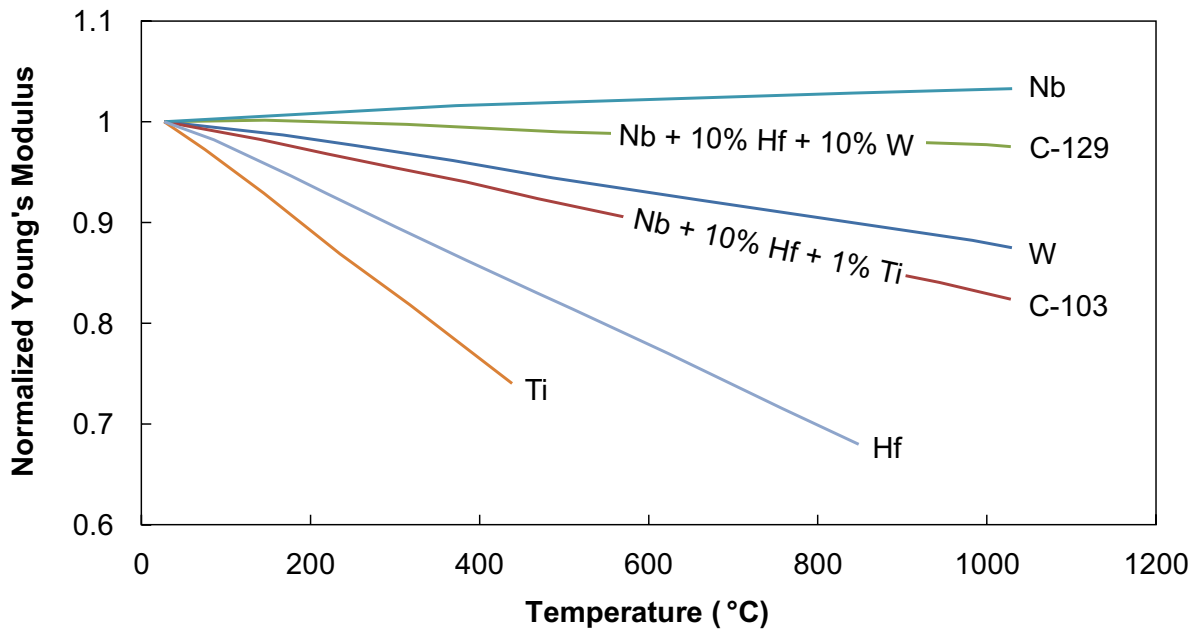
Figure 4-11. Temperature dependant elastic modulus for pure niobium and selected alloys found by ultrasonic methods. Reproduced from [Carneval, 1965]

An uncertainty analysis of acoustic velocity testing results was performed and is detailed in Appendix A. With the exception of the signal to noise ratio contribution, the measurement uncertainty had a nearly constant value of approximately 2%. The signal to noise ratio contribution was seen to vary significantly. This is due to the fact that the signal to noise ratio is affected by many phenomena, both physical (signal attenuation, mode conversion, background noise) and within the signal acquisition process (signal amplification, digitization, etc.), many of which are temperature dependant. Primarily, a poor signal to noise ratio was observed and has been determined to have been caused by non-ideal selection of driving electronics. Namely, the pulser/receiver system selected for this test was designed for use with capacitive loads, such as those experienced with piezoelectric transducers. The available pulse width of 80×10^{-9} s was insufficient to provide peak signal amplitude with the inductive loads characteristic of magnetostrictive transducers. This effect and the overall measurement uncertainty are discussed in more depth in Appendix A.

4.2.3 Reflector Spacing Tests and High Frequency Coil

The primary effect of increasing the operating frequency of the transducer is in reducing the required distance between reflectors on the waveguide. This increases the spatial resolution of the system and allows for smaller temperature sensor segments (producing a temperature measurement that is less "blurred" due to averaging over the length of the segment). A goal of this research was to achieve the ability to distinguish reflectors spaced one centimeter apart or smaller. This spacing was requested by researchers from DOE programs as the required resolution for fuel irradiation data resolution needed to validate new fuel analysis models [Rempe, 2011]. The bench test configuration shown in Figure 4-12 was used to compare the performance of transducers operating at different frequencies, and to

evaluate the spatial resolution available with each, with a 0.25 mm waveguide. Copper clips were used to create reflections with easily varied spacing.
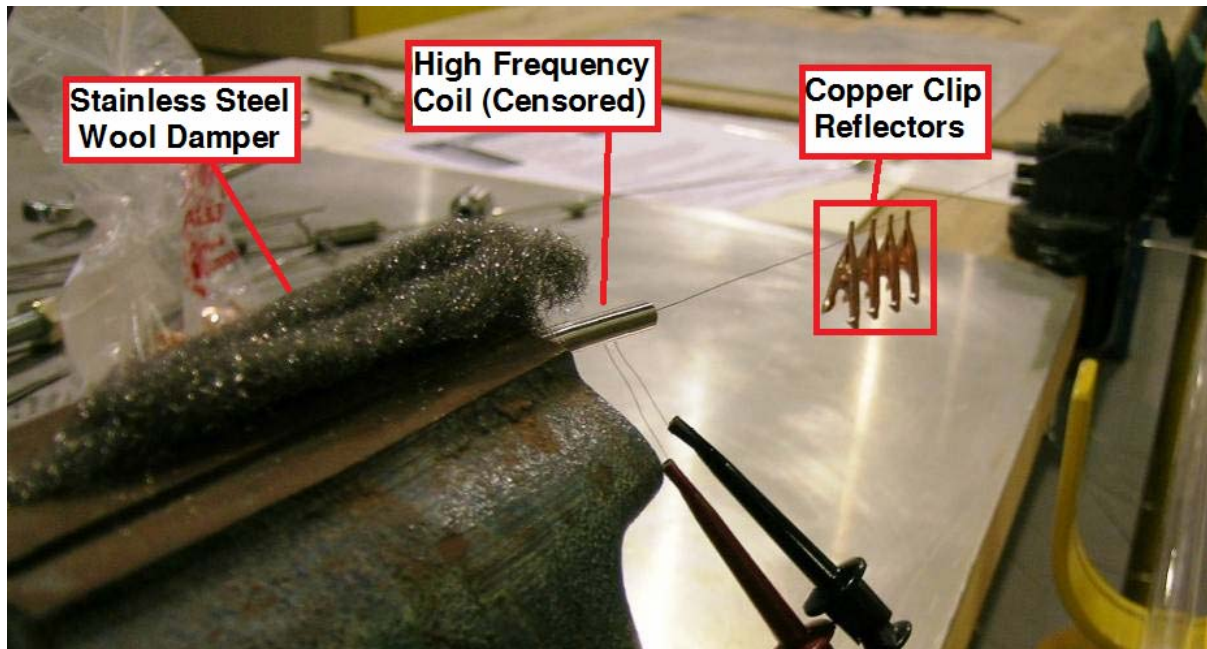
Figure 4-12.   Test configuration used to test effect of transducer frequency on spatial resolution.

At the beginning of this research effort, the magnetostrictive transducers that were available were limited to frequencies up to approximately 200 kHz. Figure 4-13a shows a recorded waveform captured using a 200 kHz transducer and a waveguide with reflectors separated by 2.5 cm. The reflector configuration did not allow the use of more than two reflectors at this frequency, as the amplitude became too small to detect. Figure 4-13b shows a recorded waveform captured using a 500 kHz transducer and a waveguide with reflectors separated by 1.7 cm. The reflector configuration did not allow the use of more than three reflectors at this frequency, as the amplitude became too small to detect. Figure 4-13c shows the signal recorded for a transducer operating at 1.9 MHz with reflectors spaced 0.7 cm apart. The multiple period reflections are due to the need to pulse the tone-burst for several cycles in

order to generate a sufficiently strong signal. Even so, the four reflections are clearly separated. It is expected that if sufficient energy could be introduced into the transducer over a single tone-burst cycle, the spacing between reflectors could be reduced even further. The effect of reverberations is less pronounced for the higher frequency transducer, allowing four reflectors to be clearly distinguished. This is attributed to the fact that the fraction of acoustic energy reflected at each clip is a function of frequency. The reflected waveforms are more consistent in amplitude than those observed with lower frequency transducers, and the reverberations appear to attenuate more rapidly.

4.2.3.1 Damping

A damping method was developed that allows complete damping of the back end echo when used with a small waveguide (i.e., 0.254 mm diameter). For a thin wire waveguide, a short section of metallic tubing is filled with an attenuating material and swaged onto the free end of the waveguide, compressing the damping material (see Figure 4-14). However, this method becomes significantly less effective as waveguide diameter increases.

For in-core testing with a stainless steel or Remendur waveguide, most common damping materials (i.e., polymers and greases/gels) are not usable, as they rapidly degrade in the radiation environment. Therefore, crushable oxides and stainless steel wool were selected as potential damping materials. It was determined that the signal improvement yielded by a swaged damper is primarily dependent on two properties; the acoustic impedance mismatch between the damping material and the waveguide, and the compression of the damper. For a 26% reduction in damper diameter (0.55 mm/ 76 mm damper length), complete back-end echo attenuation was observed for dampers constructed with stainless steel wool or magnesium oxide powder.
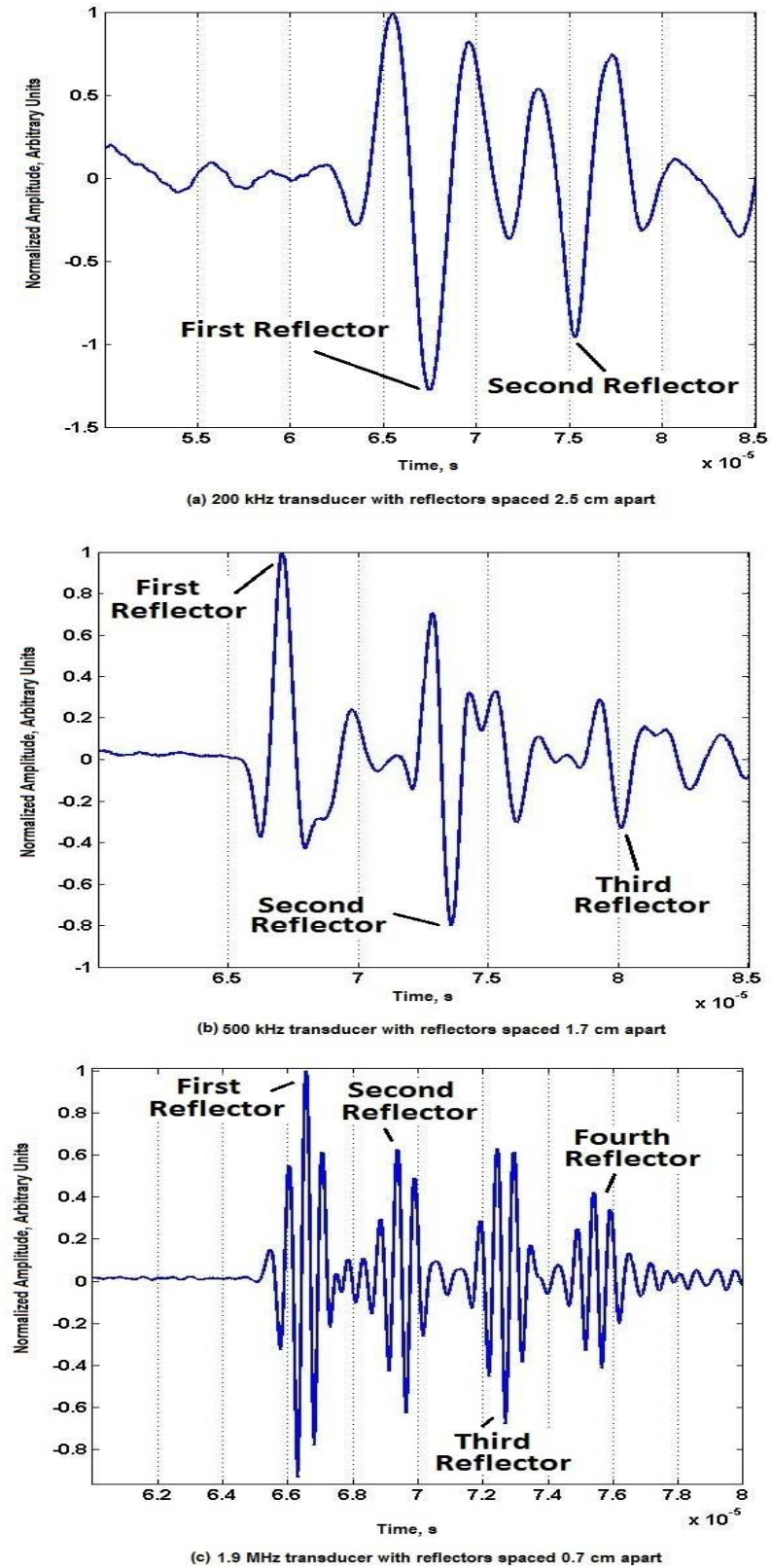
Figure 4-13. Comparison of detectable reflections with different frequency transducers.
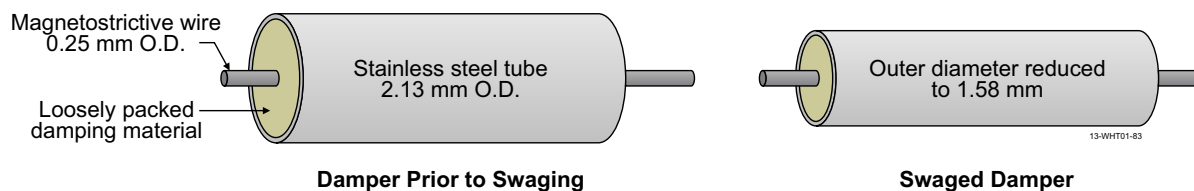
Figure 4-14. Description of swaged damper.

As damping eliminates back-end echoes and higher-order reflections, it is not always advantageous. Higher-order reflections consist of acoustic pulses that have travelled through the sensor segment multiple times. As such, utilizing the higher-order reflections in a temperature measurement effectively increases the length of the sensor, each additional reflection effectively doubling the length. This means that the both the temperature sensitivity and measurement accuracy of the thermometer are increased. Damping can, however, be important for thermometers with very short lead-in waveguide lengths, as the initial back-end echo can interfere with the sensor reflections.

4.3 Ultrasonic Thermometer Conceptual Design

Figure 4-15 shows the conceptual design for an improved ultrasonic thermometer for use in fuel and material irradiation tests. The UT is fully encapsulated, utilizing a 0.25 mm wire as the sensing element and lead-in waveguide. Reflectors are formed by laser welding small amounts of material to the sensor waveguide. The reflector material is the same as the sensor, but a finer wire is used to control the reflection coefficient. The coil design is currently dependant on the operating temperature of the transducer and the spacing requirements on the sensor segments. Closely spaced sensor segments require the newly developed high frequency coil, which cannot currently be made from high temperature capable materials. The transducer housing length can be designed to accommodate a damper, if necessary. The housing is filled with inert gas and joints are laser welded for leak tightness. The lead-in cable is a metal

sheathed coaxial cable using a powdered silicon dioxide dielectric and copper center conductor and shield.
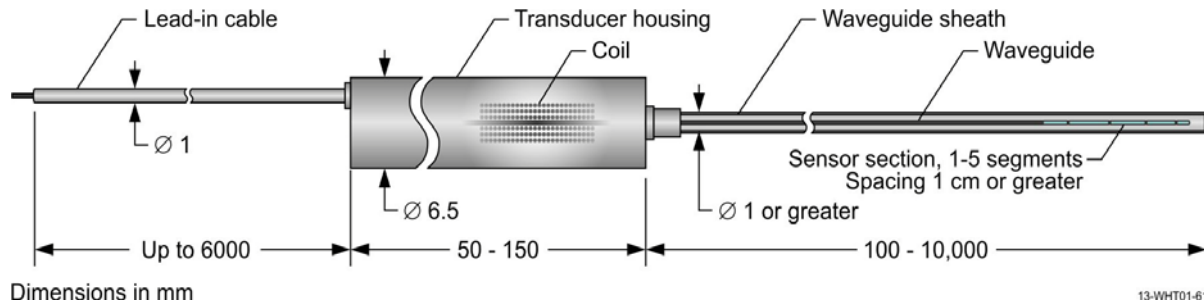
Figure 4-15. Ultrasonic thermometer improved design.

4.4 Conclusions and Future Work

Considerable progress was made toward the deployment of an ultrasonic thermometer for in-core experiments. The primary progress was made in the areas of material selection and improved spatial resolution. KW-molybdenum and 304 stainless steel were identified as preferred sensor materials, based on material properties, ease of fabrication, and the results of acoustic velocity characterization tests. Stainless steel is recommended for applications in which temperatures will not exceed 1000 °C, while molybdenum doped with tungsten and potassium silicate was identified for applications between approximately 1000 °C and 2500 °C. A new, high frequency coil was developed and used to improve spatial resolution of reflectors by allowing minimization of reflector spacing. This effect is enhanced by the use of a new method of damping developed to remove "back end" reflections, eliminating interference caused by them and simplifying signal processing. A signal processing method was also identified and tested, which changed the difficult identification of Gaussian sinusoids into simple peak detection.

Expected future work includes fabrication and testing of the conceptual UT with the identified doped molybdenum sensor in a high temperature environment (anticipated maximum test temperature of 2600 ^{o}C) and quantification of the temperature resolution possible with various reflector spacings. After furnace evaluations are complete, irradiation testing of the sensor is anticipated. Irradiation test design will be based on the ultrasonic transducer irradiation test detailed in Chapter 5.

Chapter 5: Transducer Irradiation Test

The ULtrasonic TRAnsducer irradiation test (ULTRA), which is funded by the Department of Energy (DOE) Advanced Test Reactor (ATR) National Scientific User Facility (NSUF) and the Nuclear Energy Enabling Technology (NEET) programs, is a collaborative effort involving Idaho National Laboratory (INL), Pacific Northwest National Laboratory (PNNL), Argonne National Laboratory (ANL), the Pennsylvania State University (PSU), the Massachusetts Institute of Technology (MIT), and the French Alternative Energies and Atomic Energy Commission (CEA). As discussed in Chapters 3 and 4, transducer performance during irradiation is a significant issue that must be addressed prior to in-core deployment of ultrasound-based sensors. This test addresses this uncertainty by evaluating candidate materials capable of generating and receiving ultrasonic waves after exposure to high neutron fluences. As part of this dissertation research, a test capsule design was developed that includes both piezoelectric and magnetostrictive materials, transducers, and sensors. Test conditions exceeding fluences evaluated in prior ultrasound transducer irradiations were selected. As part of this thesis research, a new design of magnetostrictive transducers was developed, fabricated, evaluated in a laboratory setting, and provided to MIT for this irradiation. As discussed within this chapter, several of the transducer materials included in this irradiation appear promising for in-core ultrasound sensors for measuring temperature and other parameters of interest such as gas composition and pressure, crack initiation and growth, etc.

5.1 Transducer Irradiation Test Design

The ULTRA test consists of a heavily instrumented test capsule irradiated in the Massachusetts Institute of Technology Research Reactor (MITR). The test results identify the

most promising magnetostrictive and piezoelectric transduction materials for use in future sensor development. This test is an instrumented lead test, meaning that data are collected in real time from sensors used to monitor test conditions and test transducers.

5.1.1 MITR Design

Relevant MITR design information is summarized here to provide perspective about the design of the ultrasonics transducer capsule and test conditions developed by this project.

The MITR is a tank-type research reactor [MITR User's Guide, 2012]. It is currently licensed for 6 MW operation. The irradiation position and flux condition of the location where the ULTRA test capsule is located in the MITR is shown in Figure 5-1. The ULTRA capsule is inserted into the reactor core at a location where the thermal flux is approximately 3.6×10^{13} n/cm^2-s and fast flux (Energy > 0.1 MeV) is 1.2×10^{14} n/cm^2-s.

Geometric constraints within the in-core experiment tube limit the test capsule dimensions to 46 mm in diameter and 610 mm in length. It was proposed that the test exceed fast neutron fluences of prior piezoelectric transducer irradiations (e.g., $> 1\times10^{21}$ n/cm^2 at Energy>1.0 MeV). In order to observe rapid changes at relatively low fluences, the test was started with the reactor coming to power slowly. This enables data collection at low fluence levels, where failures were observed in prior piezoelectric transducer irradiations. The expected steady state fast flux (Energy>1 MeV) is 3.5×10^{13} n/cm^2-s with the reactor running at 5.8 MW power. At this level of fast flux, it is estimated that approximately 390 full power days, or 23 calender months, will be required to reach the desired fluences.

Figure 5-1 shows the position of the test capsule within the MITR core. Based on thermal analysis performed at MIT, the operating temperature for the test at steady state was predicted to be between 350 and 450 °C. After startup, the target temperature is controlled by

variation of the composition of a gas gap between the test capsule and the in-core experiment tube. The gas is a mixture of helium and neon. Once the reactor reaches a power level sufficient to maintain the target temperature, the experiment is placed on automatic temperature control (e.g., the helium/neon mixture is varied based on temperatures from thermocouples included in the test).
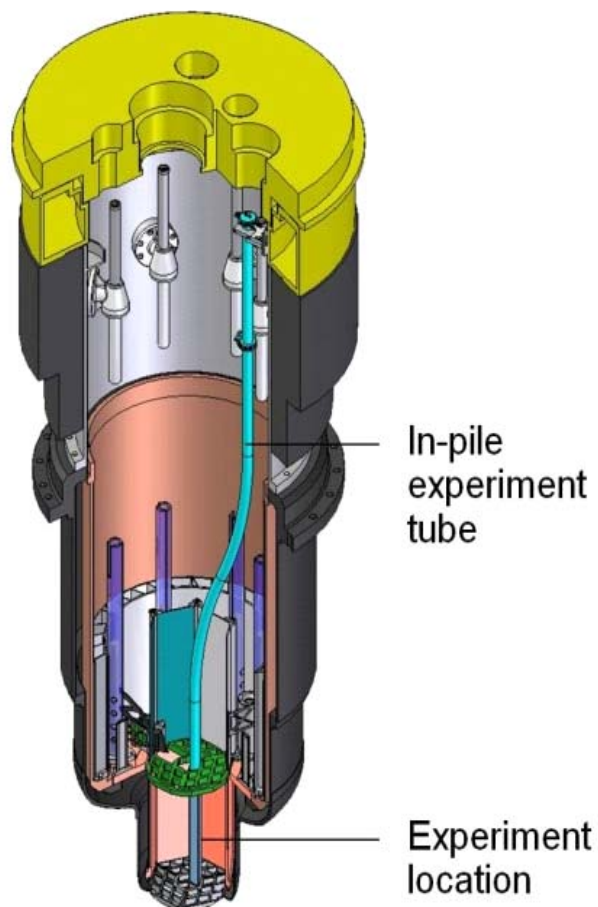
Figure 5-1. Position of irradiation capsule within MITR core.

5.1.2 Candidate Magnetostrictive Transducer Materials

Many magnetostrictive materials are available for the use and fabrication of ultrasonic transducers. The properties of most relevance to in-core measurements include maximum operating temperature, sensitivity, resistance to radiation damage, and resistance to becoming

highly activated during irradiation. Unlike many of the piezoelectric materials, magnetostrictive materials are primarily metal alloys. Observed effects of radiation on metals differ significantly from observed effects on ceramics. For example, investigations with magnetic Fe-Ni alloys, such as Permalloy, have shown that their magnetic permeability tends to decrease with neutron irradiation [Brown, 1984]. This is attributed to the immobilization of magnetic domains due to point-defects generated by displacement cascades. Although this would limit the magnetostrictive capabilities of the material, magnetostrictive effects have been reported at fluences of up to 5×10^{19} n/cm^2 [Lynnworth, 1971].

Magnetostrictive materials considered for the ULTRA irradiation may be generally categorized into three types: pure metals, alloys, and "giant" magnetostrictive materials. Typical saturation magnetostriction for pure or alloyed magnetostrictives are on the order of tens of microstrains, whereas the giant magnetostrictives may produce up to one thousand microstrains of elongation. The pure metals include the ferromagnetic elements nickel, iron, and cobalt. Alloys typically consist of combinations of the pure magnetostrictive materials with other alloying materials, such as chromium. The "giant" magnetostrictive alloys are newer materials that have significantly improved magnetostrictive response.

As previously detailed, most magnetostrictive applications require the use of a biasing magnet. Most materials appropriate for use as biasing magnets contain constituent elements that are not well suited for use in a reactor environment. Typically, this means the presence of cobalt or materials with high thermal neutron capture cross sections, such as boron, samarium, or neodymium. The primary magnetic materials considered were Alnico (an aluminum-nickel-cobalt alloy), Nd-B-Fe (a neodymium-boron-iron ceramic), and Sm-Co (a samarium-cobalt ceramic). Alnico provides the weakest magnetic field strength of these options, but it

also has the highest Curie temperature (the temperature at which a magnet loses magnetization) of the candidates. Activation of the cobalt is the primary concern with this material. Prior testing has shown that Alnico magnets can retain their field for at least half the accumulated fluence proposed for this test. Samarium cobalt magnets have high field strength and moderately high Curie temperatures. The concerns with this material are activation of the cobalt and transmutation of the samarium. Prior testing indicates that the nuclear environment does not strongly affect the performance of these magnets. The strongest magnets available are Nd-B-Fe. These magnets are not considered suitable as the Curie temperature is below the proposed test temperature. Another option for generating the biasing magnetic field is the use of a DC biasing coil. This option is not preferred as the coil may increase the volume of the transducer and would necessarily add an additional electrical lead to each magnetostrictive transducer.

This table also lists properties of interest related to suitability for ultrasound applications with respect to performance, availability, and fabricability. This section describes the process used to determine which materials were ultimately included in the ULTRA test.

5.1.2.1   Magnetostrictive Material Down-Selection

Nickel [Olabi, 2008]

Although nickel is widely used in nuclear applications (i.e., nickel alloys such as Inconel 600), the low Curie temperature and weak magnetostrictive response make it a poor magnetostrictive transducer candidate.

Iron [Olabi, 2008]

Iron has a suitable Curie temperature; however, its saturation magnetostriction is very low. This makes iron a poor candidate, as the signals produced by this material are likely to be too weak to be of use.

Cobalt

Cobalt has the highest magnetostriction of any pure metal and a very high Curie temperature. However, the likely activation of cobalt under irradiation, as well as the availability of cobalt based alloys with greater magnetostriction, make pure cobalt a poor candidate.

Remendur

Remendur has the most history of use in nuclear applications of all the magnetostrictive alloys, having been used previously for short duration ultrasonic thermometry applications [Laurie, 2010]. Remendur has a high Curie temperature and high magnetostriction. Given this, and its previous use, Remendur was highly recommended for testing, despite the presence of cobalt. Although Remendur is no longer commercially available, several identical alloys are available under different names such as Vacoflux 50.

Vacoflux® [Vacuumschmelze]

Vacoflux 50 is an alloy chemically identical to Remendur, which has been used in European ultrasonic thermometry applications. It was recommended as a possible alternative to Remendur.

Vacoflux 17 is essentially a reduced cobalt variant of Vacoflux 50. As such, it does still contain cobalt and has significantly reduced magnetostriction. Vacoflux 17 was not recommended for inclusion, as Vacoflux 50/Remendur is the preferred alternative.

Arnokrome^{TM} [Arnokrome 3, Arnokrome 4, Arnokrome 5 Datasheets]

Arnold Magnetics produces several magnetostrictive alloys, Arnokrome 3, Arnokrome 4, and Arnokrome 5. Because Arnokrome 3 contains cobalt and has much lower magnetostriction than Remendur, it deemed to not be of interest. Arnokrome 4 and 5 have similar magnetostriction to Arnokrome 3, but without the presence of cobalt. Although not as promising as some candidates, Arnokrome 4 or 5 were considered as desirable for inclusion in the irradiation test.

Galfenol [Etrema, Galfenol]

Galfenol is a relatively new alloy of iron and gallium. Galfenol is a member of the "giant" magnetostrictive alloys and has a very large saturation magnetostriction. It also has an appropriately high Curie temperature. Neither constituent element reacts strongly with neutron radiation. All of these factors made Galfenol the most appealing magnetostrictive material candidate included in the ULTRA irradiation test.

Terfenol-D [Etrema, Terfenol-D]

Terfenol-D has the highest saturation magnetostriction of any known material and is widely used in the design of actuators. However, Terfenol-D contains both terbium and dysprosium, both of which have high thermal neutron absorption cross sections (particularly dysprosium). Additionally, Terfenol-D has a low Curie temperature of 380 ^{o}C, which is below the anticipated irradiation temperature of 400-450 ^{o}C. Due to these factors, Terfenol-D was not included in the ULTRA test.

Selected Materials

Because the ULTRA test could only accommodate two types of magnetostrictive materials, the recommended candidate materials, Remendur and Galfenol were included in test transducers in the ULTRA test, with Arnokrome 4 and Arnokrome 5 included as loose samples. As Galfenol is a relatively new alloy, it has very limited availability; and a variation containing trace amounts of niobium-carbide was selected as a substitute.

Magnetostrictive materials considered for this irradiation are summarized in Table 5-1.

Table 5-1. Summary of candidate magnetostrictive materials. Materials included in transducers are highlighted in blue. Materials included as stand-alone samples are highlighted in green.

Material	Composition	Key Properties	Comments
Nickel	100% Ni	25-50 μ-strain max. magnetostriction, Curie temperature 358 ^{o}C	Pure metal, easy to acquire/manufacture, low magnetostriction, low Curie temperature
Iron	100% Fe	10-20 μ-strain max. magnetostriction, Curie temperature 770 ^{o}C	Pure metal, easy to acquire/manufacture, low magnetostriction
Cobalt	100% Co	50-60 μ-strain max. magnetostriction, Curie temperature 1130 ^{o}C	Pure metal, low magnetostriction, activcation of cobalt
Remendur	49%Fe-49%Co-2%V	70-100 μ-strain max. magnetostriction, Curie temperature 950 ^{o}C	No longer manufactured, identical/similar alloys available, activation of cobalt
Vacoflux 50	49%Fe-49%Co-2%V	70 μ-strain max. magnetostriction, Curie temperature 950 ^{o}C	Activation of cobalt
Vacoflux 17	81%Fe-17%Co-2%Cr	25 μ-strain max. magnetostriction, Curie temperature 920 ^{o}C	Activation of cobalt
Arnakrome 3	60%Fe-30%Cr-10%Co	10-40 μ-strain max. magnetostriction, Curie temperature 625 ^{o}C	Activation of cobalt
Arnakrome 4	95%Fe-5%Cr	10-40 μ-strain max. magnetostriction, Curie temperature 770 ^{o}C	Low magnetostriction
Arnakrome 5	92%Fe-8%Mn	10-40 μ-strain max. magnetostriction, Curie temperature 770 ^{o}C	Low magnetostriction
Galfenol	81%Fe-19%Ga	100-400 μ-strain max. magnetostriction, Curie temperature 700 ^{o}C	Relatively new, small amounts of data, may be difficult to acquire
Terfenol-D	Tb0.3-Dy0.7-Fe1.95	1000-2000 μ-strain max. magnetostriction, Curie temperature 360 ^{o}C	Very brittle, strong biasing field/prestress required

5.1.2.2 Magnet Material Selection

Alnico

Alnico magnets are considered primarily because they have a very high Curie temperature. The magnetic field strength is not high, compared to ceramic rare-earth magnets, but is sufficiently high for use as a biasing field source. Alnico magnets do have some history of testing in-core, being irradiated to approximately half the target fluence of the current study with little loss of performance [Sery, 1961]. The low coercive force is a concern as this indicates that the magnets lose strength over time.

Nd-B-Fe

Neodymium-boron-iron magnets are the strongest commercially available permanent magnets. They are also very resistant to demagnetization. However, their low Curie temperature (310 ^{o}C) means that they would be rendered non-magnetic at the expected test temperatures. Previous irradiation testing indicates that Nd-B-Fe magnets are not tolerant to neutron irradiation. Additionally, these magnets contain boron, which has a high neutron absorption cross section and a less desirable irradiation sensor material [Liu, 2007].

Sm-Co

Samarium-cobalt magnets have magnetic properties nearly as desirable as Nd-B-Fe magnets and Curie temperatures nearly as high as Alnico magnets. Although samarium has a high thermal neutron absorption cross section, previous irradiation testing indicates that neutron irradiation has a negligible effect on its magnetic properties [Liu, 2007].

Magnetic materials considered for this irradiation are summarized in Table 5-2.

Table 5-2. Summary of candidate magnet materials.

Material	Composition	Key Properties	Comments
Alnico 5	51%Fe-24%Co-14%Ni-8%Al-3%Cu	Curie temperature 860 $^{\circ}$C, Max. Energy Product 43.8 kJ/m^3, Residual Induction 12800 Gauss, Coercive force 640 Oersteds.	High Curie temperature, low magnetic strength, demagnetize over time, cobalt present.
Alnico 9	34%Fe-35%Co-15%Ni-7%Al-4%Cu-5%Ti	Curie temperature 860 $^{\circ}$C, Max. Energy Product 71.6 kJ/m^3, Residual Induction 10600 Gauss, Coercive force 1500 Oersteds	High Curie temperature, low magnetic strength, demagnetize over time, cobalt present.
Nd-B-Fe	$Nd_2X_{14}B$, X=Fe or Co	Curie temperature 310 $^{\circ}$C, Max. Energy Product 190-400 kJ/m^3, Residual Induction 10000-14100 Gauss, Coercive force 9600-13000 Oersteds	Low Curie temperature, very high magnetic strength, brittle, presence of neodymium and boron.
Sm-Co	SmCo5	Curie temperature 750 $^{\circ}$C, Max. Energy Product 130-180 kJ/m^3, Residual Induction 8300-11600 Gauss, Coercive force 7500-10600 Oersteds	High Curie temperature, high magnetic strength, brittle, presence of samarium and cobalt, higher cost.
Sm-Co/	Sm_2Co_{17}	Curie temperature 825 $^{\circ}$C, Max. Energy Product 190-240 kJ/m^3, Residual Induction 10000-11600 Gauss, Coercive force 6000-10600 Oersteds	High Curie temperature, high magnetic strength, brittle, presence of samarium and cobalt, higher cost.

5.1.3 Transducer Design for Irradiation Test

The magnetostrictive transducer design for inclusion in the irradiation test was originally based on the ultrasonic thermometer design developed in Chapter 4. The transducer consists of a magnetostrictive wire welded to a stainless steel waveguide, a high temperature capable coil, a swaged damper and a tensioning spring. The transducer components are

housed within a thin walled stainless steel housing (an attempt was made to minimize the mass of components to reduce gamma and neutron heating within the test capsule). A schematic drawing and x-ray of the prototype transducer is shown in Figure 5-2.
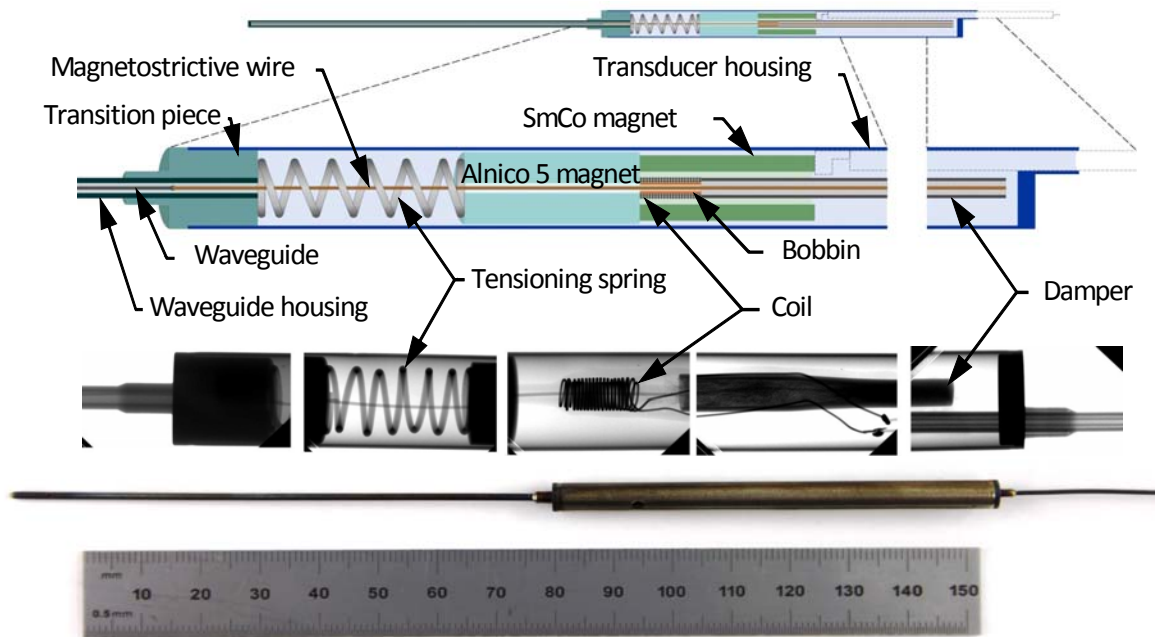
Figure 5-2. Initial transducer design for irradiation test based on UT design (dimensions in mm).

Construction of high temperature magnetostrictive transducer coils is a multi-step process that involves several heat treatment steps. First, the coil is formed by wrapping several layers of silver-palladium wire around an alumina bobbin (Figure 5-3a). The wire is coated in a standoff insulation (a particulate alumina-silica mixture with a burnable binder). The insulation requires a heat treatment step prior to high temperature use, and becomes brittle after heating (Figure 5-3b). After heat treatment, the coil is coated with alumina cement and heat treated a second time to cure the cement (Figure 5-3c). The coil is then securely placed in a fixture, and the wire leads are laser welded to a high temperature coaxial cable (one lead to the center conductor and one to the sheath as shown in Figure 5-3d). As the welds

are fragile, the end of the cable and the coil are coated in another layer of alumina cement and cured. The magnetostrictive wire (previously welded to the waveguide) is next threaded through the coil. The assembly is then placed into a pre-fabricated transducer housing and seal welded (possibly after vacuum purging and backfilling with an inert gas, depending on anticipated service environment; see Figure 5-3e). The transducer housing is composed of stainless steel. For higher temperature thermometry (applications in which the waveguide would be exposed to temperatures over 1000 °C), a molybdenum waveguide housing would be used. The assembled transducer is shown in Figure 5-3e.
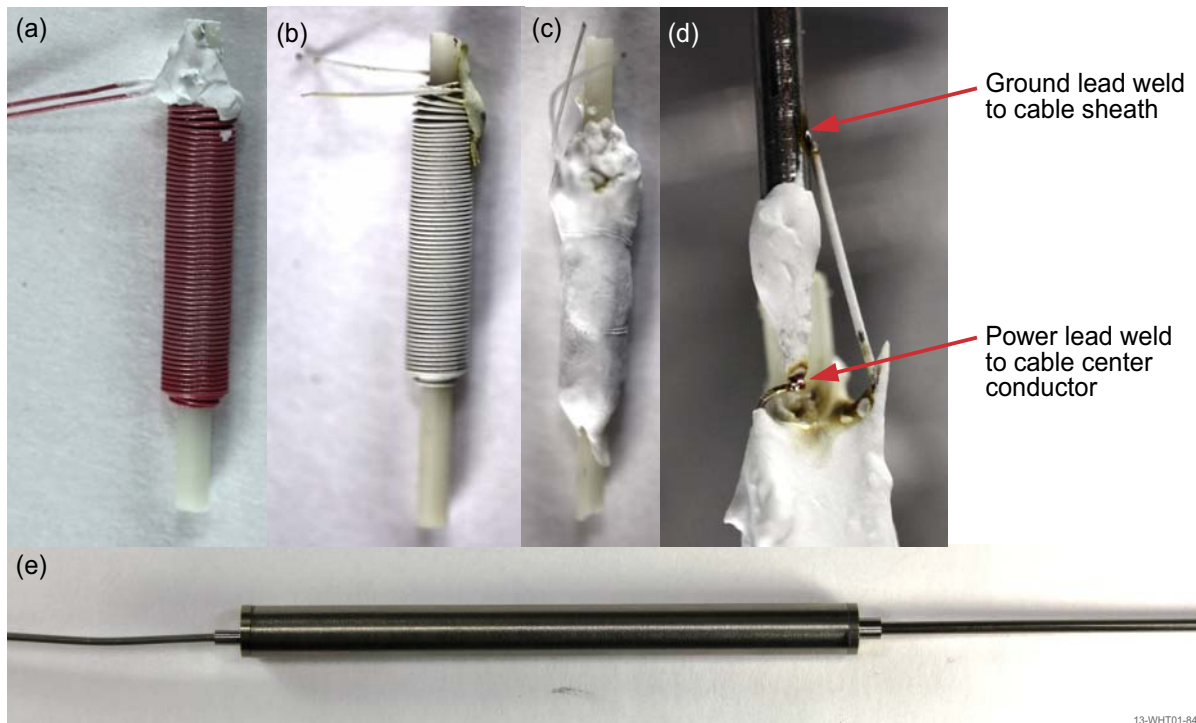
Figure 5-3. Steps involved in making high temperature capable magnetostrictive transducer.

Initial testing of this prototype, in furnaces held at temperatures up to 670 $^{\text{o}}$C, revealed several issues with the design. Many of the components included in the design were not necessary and were removed from the final design. The spring was intended to keep tension in the waveguide in order to reduce the chances of sticking. Initial testing revealed that this

spring was unnecessary in the temperature range expected for the MITR irradiation test. The stainless steel waveguide was also eliminated, and the magnetostrictive wire length was increased to maintain the total waveguide length. This eliminated the weld between the two wires and simplified the design. The damper was also determined to be unnecessary, as the signals recorded from a simple wire (no additional reflectors) do not interfere with each other. The initial testing also revealed problems with transducer performance at test temperatures. A plot of the signal magnitude as a function of temperature is shown in Figure 5-4. The "Heating" data points were recorded as the transducer was heated, in steps, to 670 ^{o}C; and the "Cooling" data points were recorded during cooling. The transducer performed with steady amplitude from room temperature to 300 ^{o}C. Then, the signal amplitude attenuated with increasing temperature. Upon cooling, the signal amplitude did not recover. The data also show apparent intermittent shorting within the coil, as indicated by the low amplitude data points observed during the heating process (but not observed during cooling). This seems to indicate that the heat treatment of the coil was insufficient, and some moisture may have been retained in the ceramic cement used to isolate and strengthen the coil.
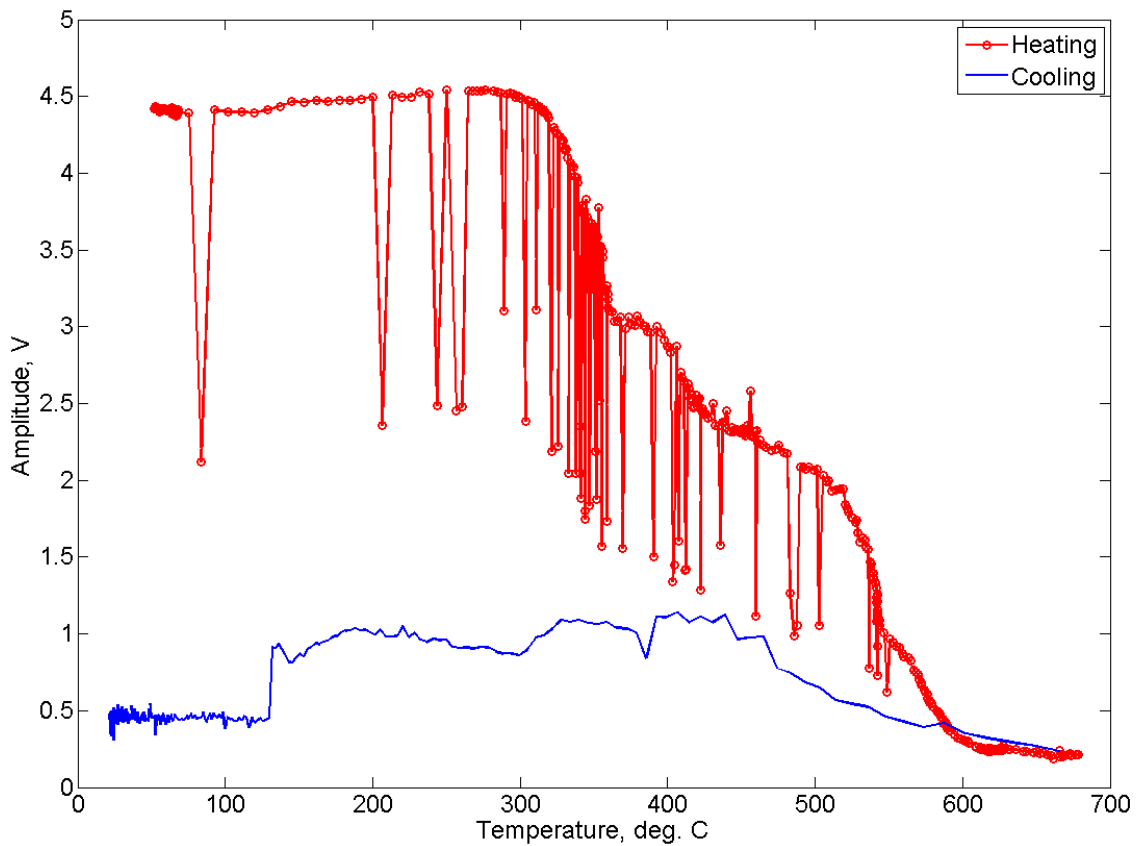
Figure 5-4. Temperature performance of prototype magnetostrictive transducer.

Further testing of prototype coils has shown that the magnets used to pre-bias the magnetostrictive wire cause signal attenuation at elevated temperatures. As the coil is operated at temperature, the magnetostrictive wire becomes weakly magnetized and, in effect, self biased. The self biasing remains after cooling and appears to be permanent, or at least long lasting. This effect has been observed in samples several months after heating.

The stainless steel waveguide, tensioning spring, and damper were removed for the final design of the magnetostrictive transducers as they were deemed unnecessary and complicated the construction process. The biasing magnets were also eliminated due to the detrimental effect on the signal after exposure to elevated temperatures.

5.1.4 Piezoelectric Transducers

In addition to the magnetostrictive transducers, piezoelectric transducers were also included in the ULTRA test. The piezoelectric transducers are of interest as many ultrasonic sensor systems require operating frequencies greater than are currently achievable with magnetostrictive materials. The piezoelectric materials were selected by PSU, and the transducers were provided by PSU. Four piezoelectric transducers are included in the ULTRA test. The transduction materials are bismuth titanate, aluminum nitride, and zinc oxide. A second aluminum nitride transducer was included for redundancy.

5.1.5 Test Capsule Design

A preliminary test capsule, designed as part of this research, is shown in Figure 5-5. The design incorporated room for six piezoelectric and three magnetostrictive samples as well as instrumentation for monitoring temperature, thermal neutron flux, and gamma flux.
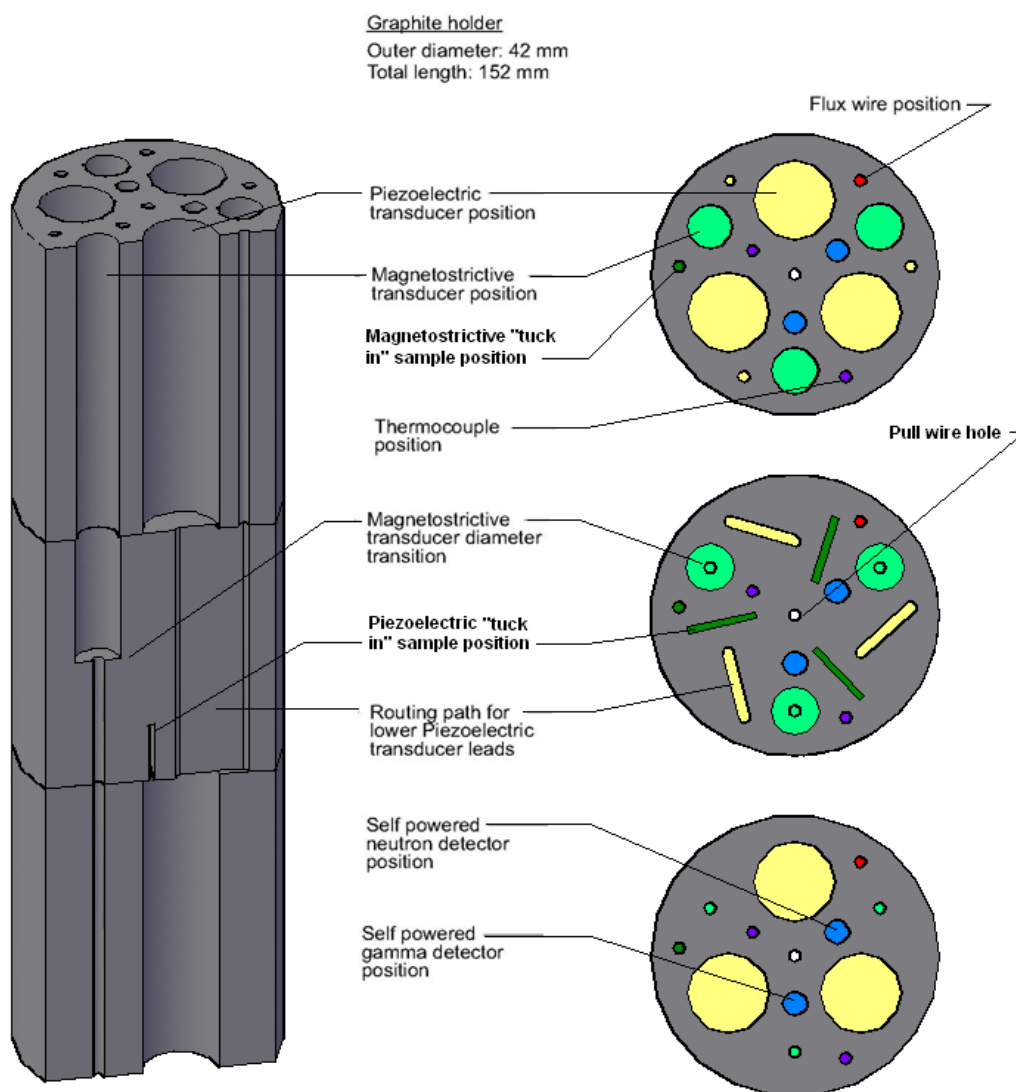
Figure 5-5. Initial test capsule graphite sample holder design with sample and instrumentation positions detailed.

Gamma heating evaluations were completed by MIT indicating that the mass of the materials in this initial capsule design would lead to piezoelectric transducer materials being exposed to temperatures that could cause thermal degradation. Thermal analyses performed by MIT indicated that temperatures could reach over 540 $^{\circ}$C with the preliminary design. Figures 5-6 and 5-7 show temperatures calculated by MIT using the ANSYS code [ANSYS, Inc., 2012] for the initial design of the graphite sample holder and the transducer outer

surfaces [Carpenter, 2013].
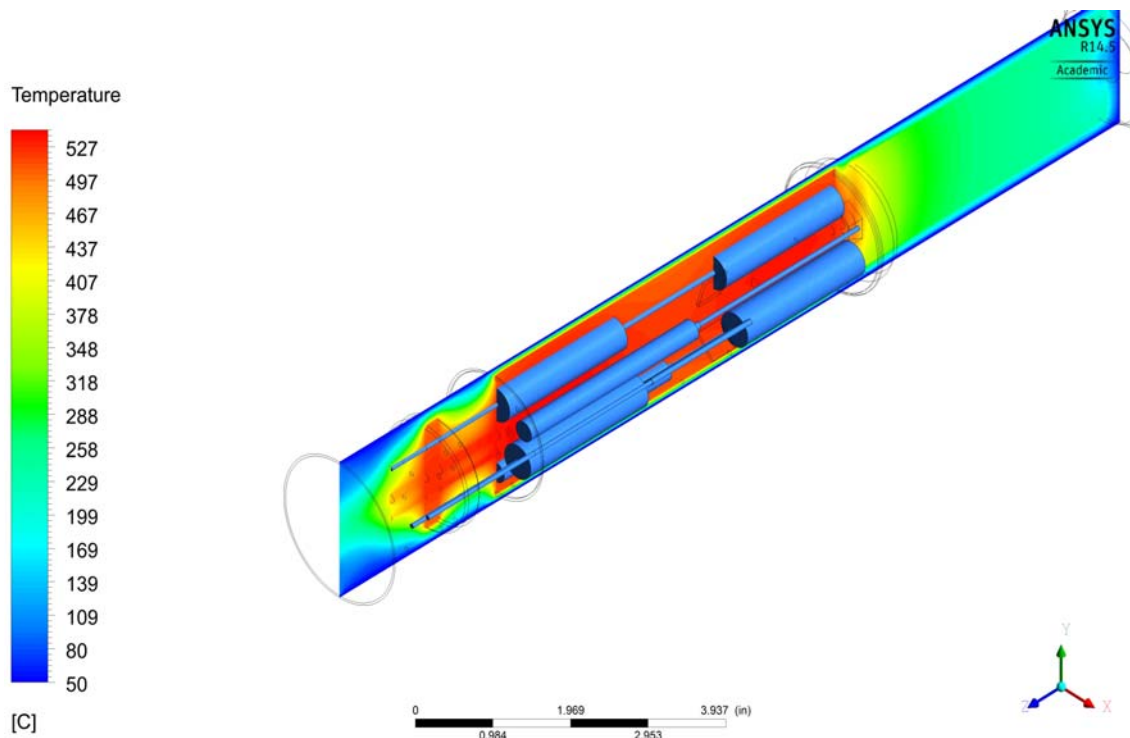
Figure 5-6. Calculated temperature distribution within graphite sample holder.[Carpenter, 5/14/2013]

To reduce temperatures, it was necessary to reduce the mass of materials included within the capsule. Specifically, the number of transducers were reduced (eliminating materials that laboratory evaluations conducted by PSU and INL deemed less promising as well as unnecessary redundancies), and the graphite holder was redesigned. The final design accommodates four piezoelectric transducers and two magnetostrictive transducers. All of the originally selected transducer materials were included, but only the aluminum nitride piezoelectric transducer has a redundant transducer. A key feature of the redesigned capsule is the staggering of the vertical position of each piezoelectric transducer. This feature spreads the mass of the transducers across a greater volume, and reduces the concentrated gamma heating. The final design is shown in Figure 5-8. As shown in this figure, this design includes stand-
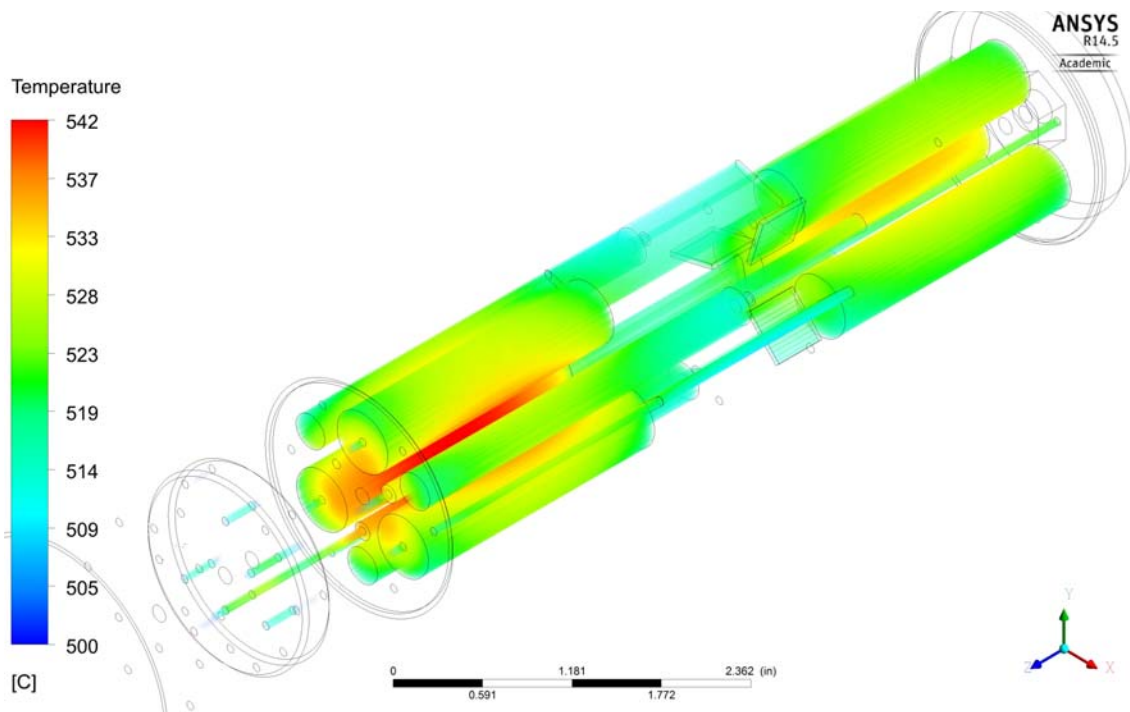
Figure 5-7. Calculated surface temperature distribution for test transducers.[Carpenter, 5/14/2013]

alone samples of candidate transducer materials (so that post-irradiation evaluations can be

completed to evaluate degradation) and all of the planned instrumentation to monitor test

conditions (e.g., temperature, neutron flux, and gamma fields). Temperatures for the

redesigned capsule are predicted to reach a maximum of approximately 430 $^{\circ}$C, as shown in

Figure 5-9 (thermal analysis of the redesigned capsule).
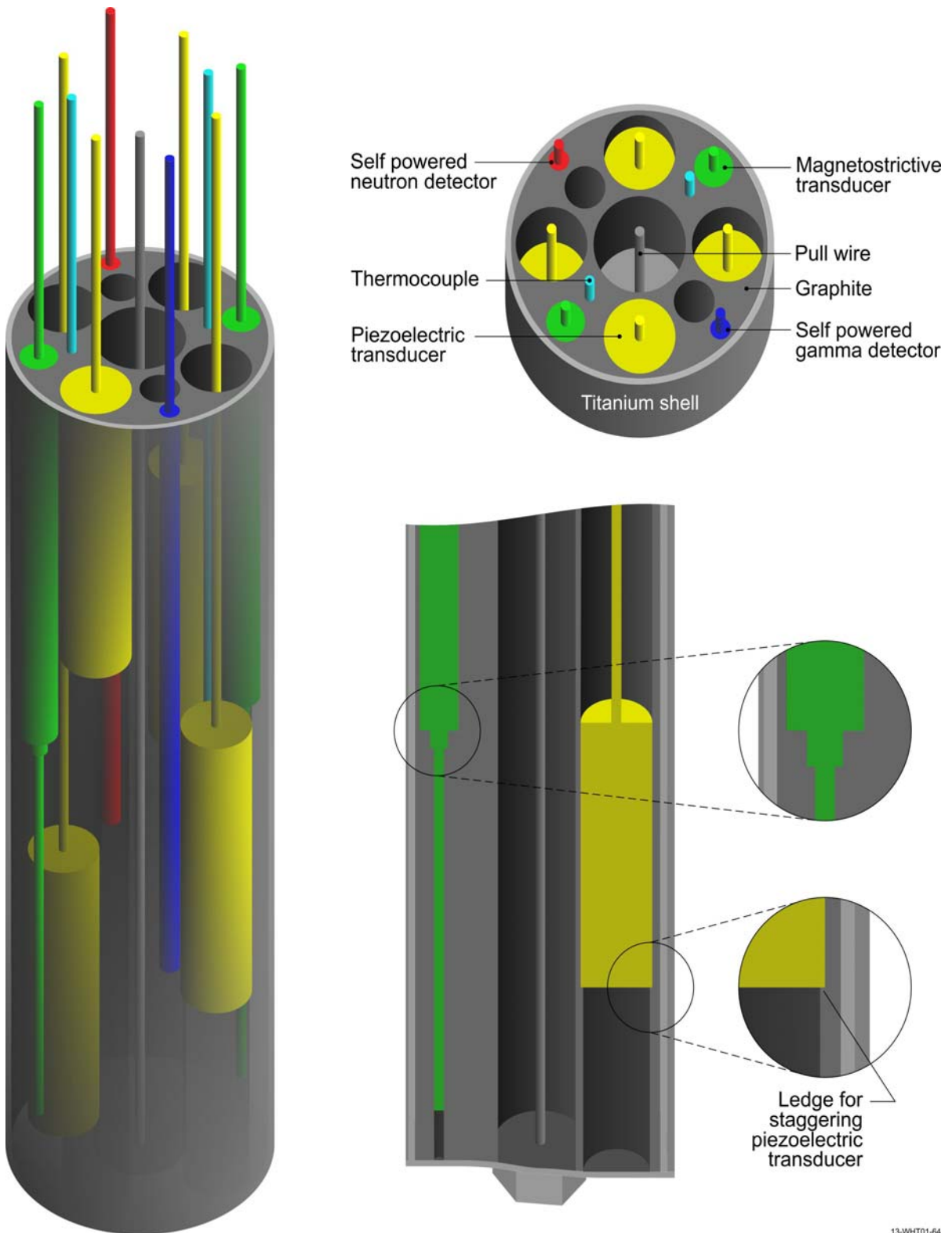
Figure 5-8. Final test capsule graphite sample holder design with sample and instrumentation positions detailed.
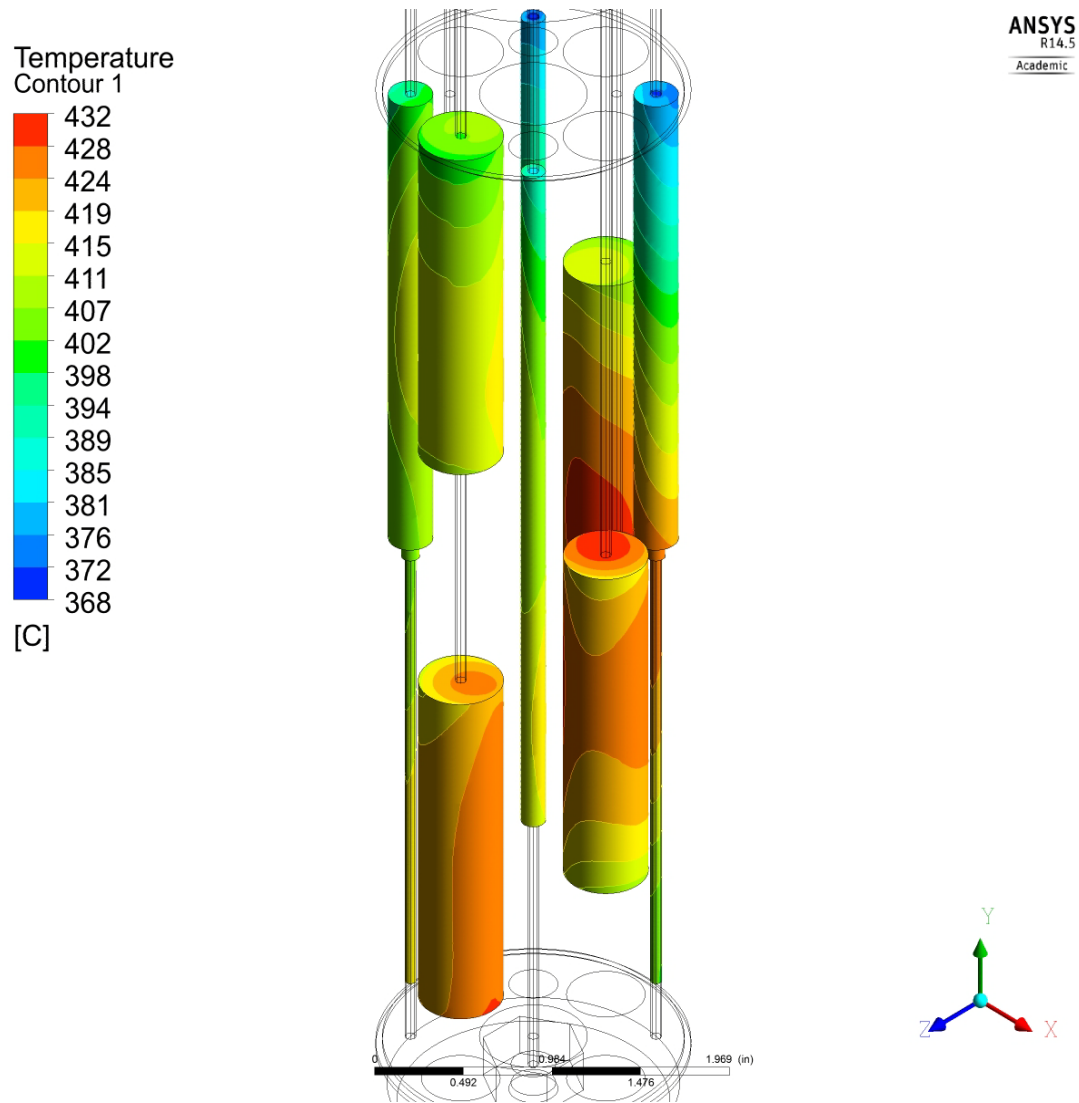
Figure 5-9. Results of thermal analysis of redesigned test capsule predicting lower transducer surface temperatures.[Carpenter, 6/24/2013]

5.1.5.1 Sensors

Clearly, in order to characterize ultrasonic transducer degradation during irradiation, real-time data are needed to characterize the irradiation test conditions. As discussed within this section, the ULTRA test includes diverse and redundant instrumentation for obtaining such data.

Irradiation test temperatures are monitored online by two Type-K thermocouples. Thermal neutron flux are monitored online by a vanadium emitter Self Powered Neutron

Detector (SPND). Gamma flux are monitored online by a platinum emitter Self Powered

Gamma Detector (SPGD). A schematic diagram of the SPND and SPGD is shown in Figure

5-10 (Sensors have identical configuration and dimensions, selected sheath materials (Inconel

600), and insulation material (Al_2O_3). Differences are limited to the selected emitter (e.g.,

vanadium for the SPND and platinum for the SPGD).
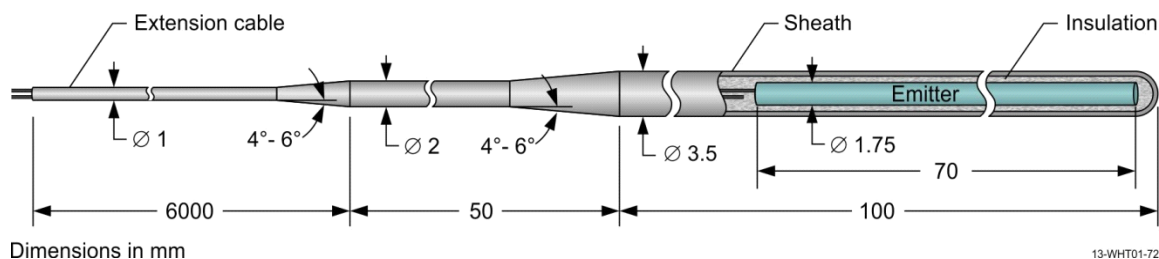
Figure 5-10. Schematic diagram of SPND and SPGD (dimensions are the same for each).

In addition to the thermocouples, the maximum temperature reached at selected

locations during the irradiation will be verified using melt wires encapsulated in a quartz tube.

Five wire compositions are included, with melting temperature ranging between

approximately 327 and 514 ^oC. Melting temperatures of the wires have been verified using a

Differential Scanning Calorimeter (DSC) system at the Idaho National Laboratory High

Temperature Test Laboratory (HTTL). Melt wire compositions and melting temperatures are

listed in Table 5-3, and a photo of a quartz-encapsulated melt wire capsule is shown in Figure

5-11. Integrated thermal and fast neutron fluences at selected locations will be evaluated

through post irradiation analysis of Fe-Ni-Cr flux wires.

5.2 Irradiation Results to Date

The irradiation test started in late February 2014 and will run until either the target fast

fluence (at least 1.0×10^{21} n/cm^2, Energy>1 MeV) is reached or all test transducers have failed.

To date, a total fluence of 4.6×10^{20} n/cm^2 has been accumulated. To this point, both

Table 5-3. Compositions and melting temperatures of melt wires.

Material Composition, %	Melting Temperature, °C
100 Pb	327.5
94 Zn-6 Al	381.0
85 Te-15 Sn	401.0
100 Zn	419.6
80 Sb-20 Zn	507.8-514.3

Figure 5-11. Example melt wire capsule with four wire types.

magnetostrictive transducers are still functioning. Signal changes, which reflect both radiation

and temperature effects, are difficult to separate analytically. As such, only changes occurring

while the reactor is operated at steady state (i.e., constant temperature) can be used to estimate

the effects of radiation alone. Figure 5-12 shows the power and temperature history of the test

to date.
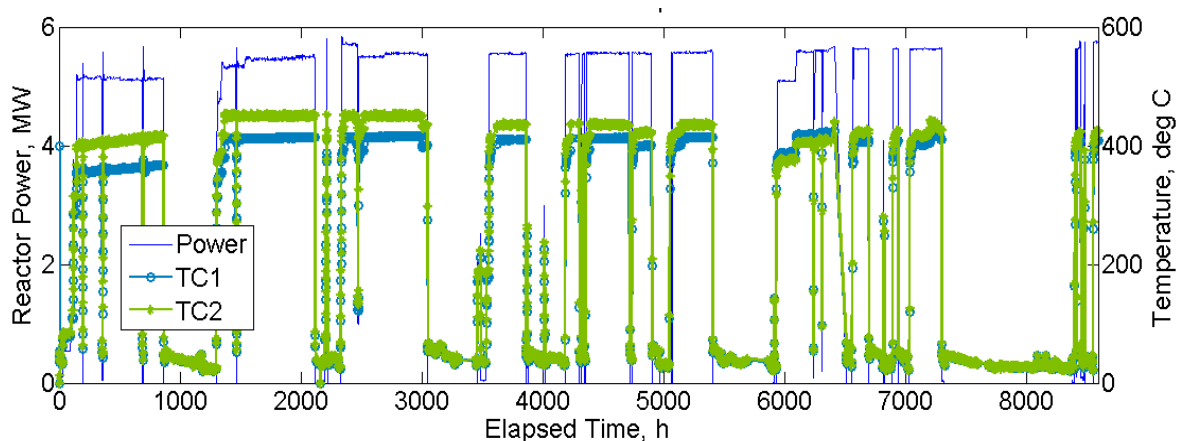
Figure 5-12. Reactor power and temperature history for ULTRA test.

Performance of the transducers is characterized by an amplitude measurement. Figure

5-13 shows the recorded waveform for the Remendur transducer at the beginning of the test

(room temperature and zero fluence). The first acoustic reflection is highlighted. The absolute maximum value of the fast Fourier transform of this reflected signal is used to track the percent change in signal strength (normalized to the signal when the reactor reached full power).
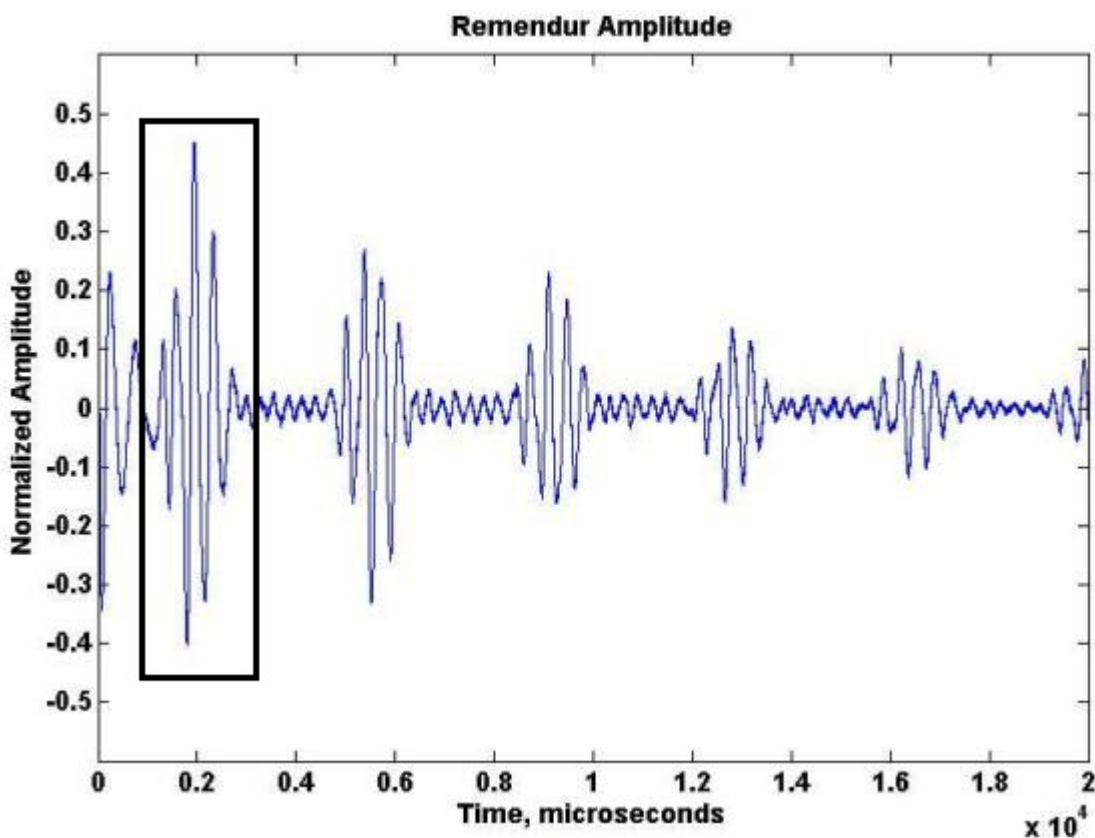
Figure 5-13. Recorded Remendur transducer waveform at start of irradiation test.

Figure 5-14 shows the peak to peak amplitude history for the Remendur transducer. The upper plot shows the Remendur performance and reactor power as a function of accumulated fast fluence. The lower plot shows Remendur performance and test temperature history as a function of elapsed test time. From these plots, it is apparent that the test temperatures have a more significant impact on the signal amplitude than the radiation. This is partially due to changes in the waveform shape as the Remendur was heated. This is most

likely caused by mechanical binding, or strong contact, between the Remendur wire and the alumina coil bobbin. This cannot be verified until post irradiation examination of the transducer. It should be noted that the apparent noise and signal decrease observed for the highest fluences is an artifact of the logarithmic scale (e.g., more data are compressed into the same area) and a scheduled reactor shut down for refueling. Increased noise after the reactor was restarted after refueling may indicate an intermittent short in the drive coil. Additionally, there were three reactor scrams prior to this shut down; a strong recovery in signal strength was observed during each scram.
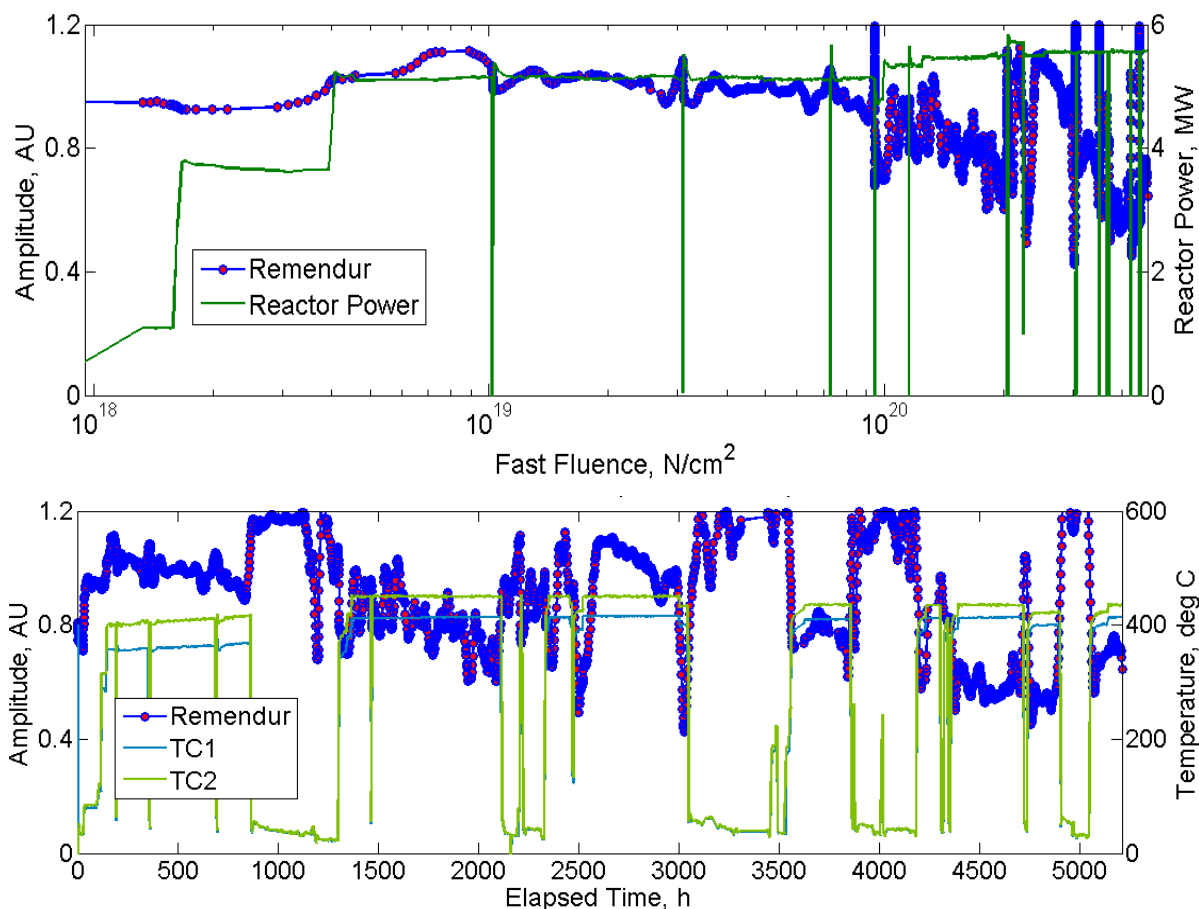
Figure 5-14. Amplitude of Remendur signal as functions of fast fluence and temperature.

Figure 5-15 shows the Remendur transducer recorded waveform after the reactor reached full power. The difference in signal shape is clear, as the reflected signals have spread and become "blurred."
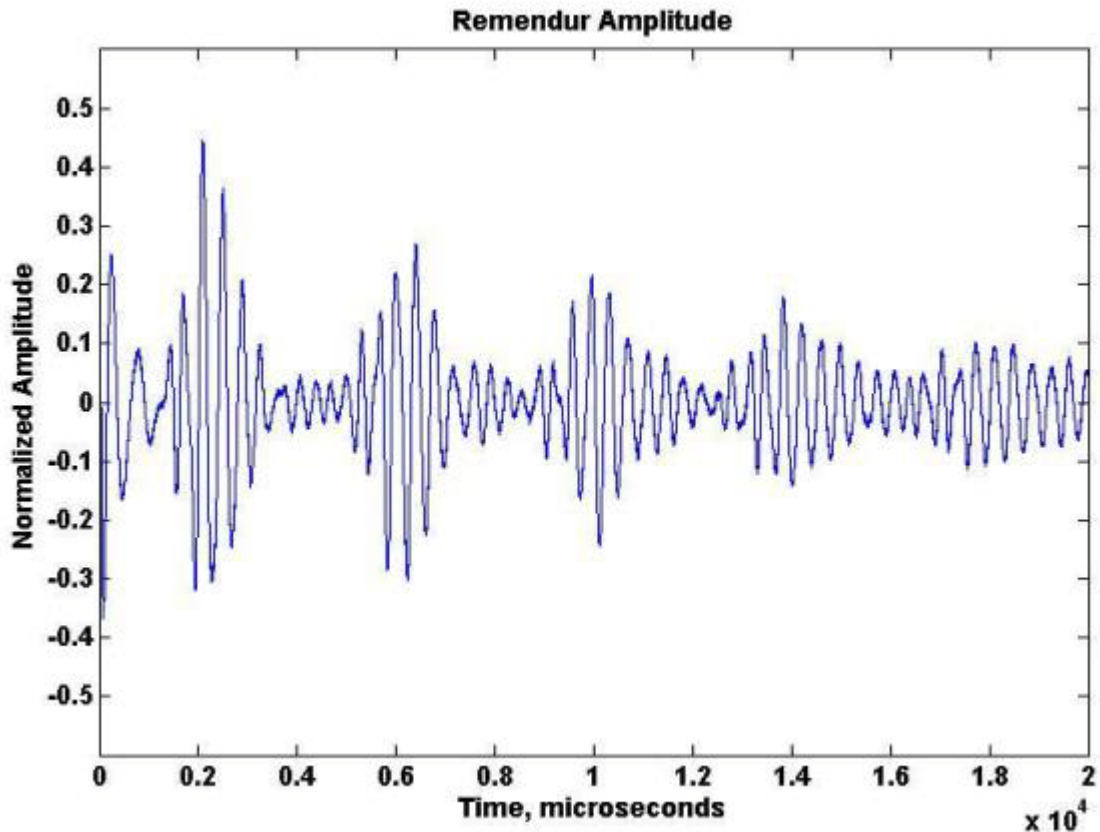
Figure 5-15. Recorded Remendur transducer waveform after full reactor power was reached (fast fluence of 4×10^{18} n/cm^2).

Total reduction in the Remendur signal amplitude from the onset of full reactor power to the most recent data is approximately 12% during the steady temperature region of the irradiation test (first reactor cycle), after which changes to the reactor power and temperature make comparisons more complex. The minimum normalized Remendur signal is approximately 50% of the original signal strength, but the signal is observed to recover to pre-irradiation levels during periods of low temperature operation (shut down cycles).

The Galfenol transducer has shown very stable operation over the course of the irradiation, though the amplitude is typically on the order of one third what is observed for Remendur. Figure 5-16 shows the peak to peak amplitude for the Galfenol transducer as a function of accumulated fluence. The upper plot shows the Galfenol performance and reactor power as a function of accumulated fast fluence. The lower plot shows Galfenol performance and test temperature history as a function of elapsed test time. Temperature effects are not as pronounced for the Galfenol transducer as for the Remendur (though they are still present), and the change in waveform shape has not been observed.
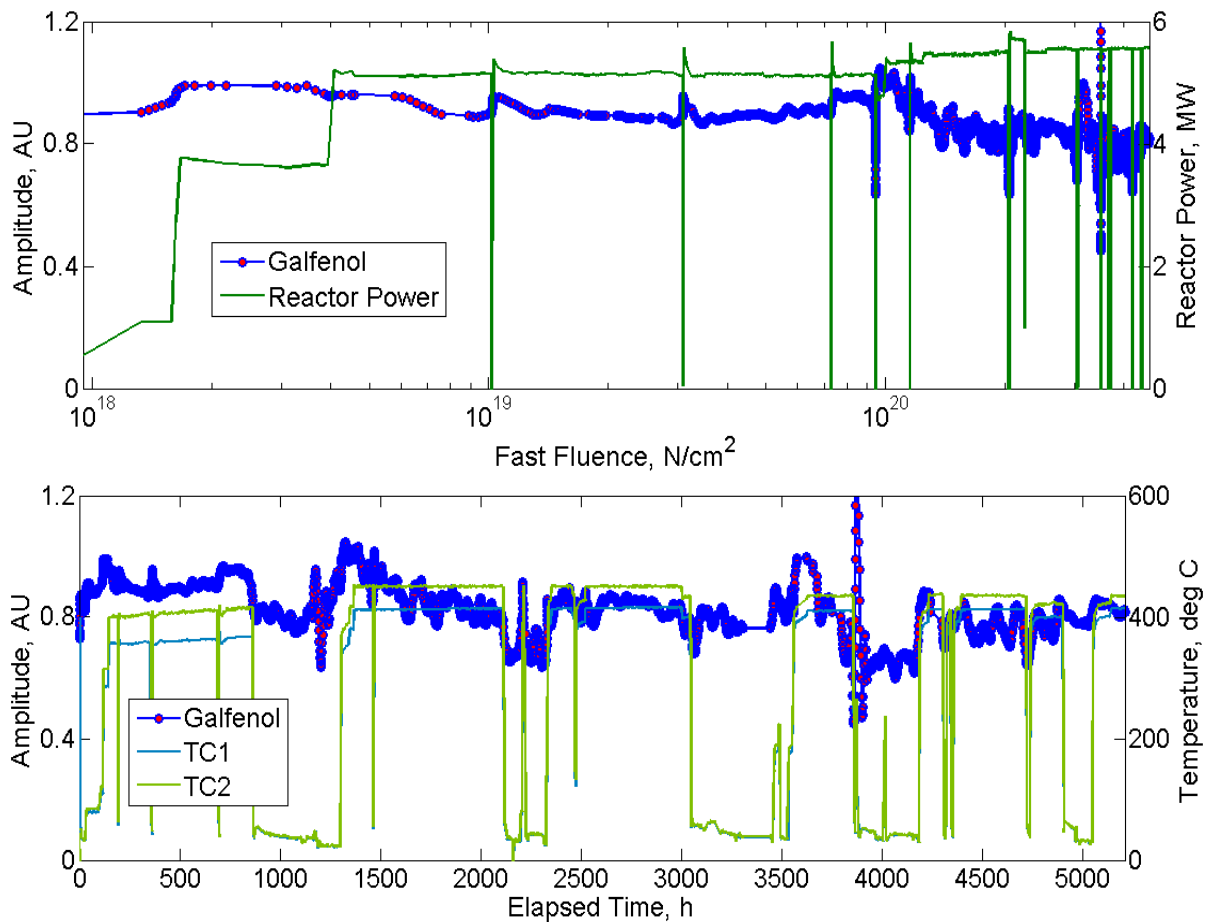
Figure 5-16. Amplitude of Galfenol signal as functions of fast fluence and temperature.

Total degradation of the Galfenol transducer signal is approximately 10% during the steady temperature region of the irradiation test (first reactor cycle), after which changes to the reactor power and temperature make comparisons more complex. To date, the normalized Galfenol signal is approximately 80% of the original signal strength at startup. Temperature effects, while present, are less pronounced for the Galfenol transducer than are observed for the Remendur transducer. The temperature response of the Galfenol transducer is opposite that of the Remendur, signal strength is greater during operating cycles when the temperature is elevated.

5.3 Conclusions and Future Work

Results of irradiation testing performed in the MITR shows ultrasonic transducers based on magnetostrictive materials to be highly resistant to degradation caused by neutron and gamma radiation. This result has several significant benefits to the design and application of an ultrasonic thermometer. First, if the transducer is located within the reactor vessel, the distance from the transducer to the sensor can be reduced. This could become critically important during very high temperature operation, as attenuation along the waveguide can be minimized. Second, reducing the length of the lead-in waveguide reduces the chances that the waveguide must be bent for installation. Although curvature of the waveguide does not affect performance, hard bends in the waveguide or strong points of contact with the sheath near bends could cause the acoustic signal to become corrupted. Finally, the small diameter waveguide design is likely to require a protective sheath, which is essentially a hollow tube. If the transducer must be located outside the reactor vessel, the sheath would have to cross a pressure/containment boundary and would represent a possible leak path. By locating the transducer inside the vessel, only a mineral insulated cable must cross the boundary. A

complete estimate of the irradiation effects on the magnetostrictive transducers cannot be made until post irradiation examination has been performed (anticipated for mid 2015). It is anticipated that PIE efforts will include operation of the test transducers after removal from the reactor, visual analysis of transducers and stand alone samples, and testing of stand alone samples with specially fabricated coils. Scanning electron microscopy may also be performed on stand alone samples.

Future work in the transducer development will include adaptation of the high frequency transducer design for higher temperature operation. Further irradiation testing should be conducted at low temperatures, if possible, to assess the effect of elevated temperatures on the irradiation effects observed in the ULTRA test. Although data obtained from this MITR irradiation already demonstrates the feasibility of proposed magnetostrictive transducers for the UT considered in this research effort, the test is not expected to be completed until mid-2015.

Chapter 6: Conclusions and Recommendations

The objective of this research was to enable deployment of Ultrasonic Thermometers (UTs) in irradiations of ceramic and metallic fuels. UTs has many potential advantages over commonly used thermocouples. These include higher temperature capability and the ability to measure a temperature profile with a single probe. Ultrasonic thermometry is a subject that has received significant attention in past research efforts. However, several technical issues have made UTs difficult to deploy routinely for in-core testing. These issues include selection of appropriate materials for the temperatures and radiation conditions the sensors are likely to be exposed to, contact bonding of the sensor to its surroundings, and cumbersome signal processing. Research was broken into two main areas; out-of-core development and testing of the UT and its components in a laboratory environment and in-core assessment of the radiation tolerance of the magnetostrictive transducers used to generate and sense the acoustic signals.

6.1 Conclusions

Significant progress was made toward the deployment of an ultrasonic thermometer for in-core experiments. The primary progress was made in the areas of material selection and improved spatial resolution. KW-molybdenum and 304 stainless steel were identified as preferred sensor materials, based on material properties, ease of fabrication, and the results of acoustic velocity characterization tests. Stainless steel is recommended for applications in which temperatures will not exceed 1000 °C, while molybdenum doped with tungsten and potassium silicate was identified for applications between approximately 1000 °C and 2500 °C. A new, high frequency coil was developed and used to improve spatial resolution of reflectors by allowing minimization of reflector spacing. This effect is enhanced by the use of

a new method of damping developed to remove "back end" reflections, eliminating interference caused by them, and simplifying signal processing. A signal processing method was also identified and tested, which changed the difficult identification of Gaussian sinusoids into simple peak detection.

The ULTRA irradiation test was the first to include both piezoelectric and magnetostrictive materials and is scheduled to surpass other ultrasonic transducer irradiations in terms of total fluence. The included transducers were operated during irradiation; and the test capsule was heavily instrumented with real time sensors, resulting in a high degree of confidence in the results. The results shows ultrasonic transducers based on magnetostrictive materials to be highly resistant to degradation caused by neutron and gamma radiation. This result has several significant benefits to the design and application of an ultrasonic thermometer. First, if the transducer is located within the reactor vessel, the distance from the transducer to the sensor can be reduced. This could become critically important during very high temperature operation, as attenuation along the waveguide can be minimized. Second, reducing the length of the lead-in waveguide reduces the chances that the waveguide must be bent for installation. Although curvature of the waveguide does not affect performance, hard bends in the waveguide or strong points of contact with the sheath near bends could cause the acoustic signal to become corrupted. Finally, the small diameter waveguide design is likely to require a protective sheath, which is essentially a hollow tube. If the transducer must be located outside the reactor vessel, the sheath would have to cross a pressure/containment boundary and would represent a possible leak path. By locating the transducer inside the vessel, only a mineral insulated cable must cross the boundary.

6.2 Recommendations for Future Work

Future ultrasonic thermometry work will include fabrication and testing of the developed conceptual UT design in a high temperature environment and quantification of the temperature resolution possible with various reflector spacings. After furnace evaluations are complete, irradiation testing of the sensor is needed before the sensor can be deployed to monitor in-core experiments.

Future transducer development work should include adaptation of the high frequency transducer design for higher temperature operation. Further irradiation testing should be conducted at low temperatures, if possible, to assess the effect of elevated temperatures on the irradiation effects observed in the ULTRA test.

References

An, Y-K., Park, B., Sohn, H., "Complete noncontact laser ultrasonic imaging for automated crack visualization in a plate," *Smart Materials and Structures*, Vol. 22, Num. 2, Dec, 2012.

ANSYS Inc., ANSYS Ver. 14.5, http://www.ansys.com, 2012.

Arave, A.E., Meservey, R.H., "A High Temperature Ultrasonic Thermometer for Measuring Reactor Fuel Temperature," IN-1413, Idaho Nuclear Corporation, 1970.

Arave, A.E., Panisko, F.E., Christiansen, J.A., "High-Temperature Ultrasonic Thermometer In-Reactor Fuel Rod Centerline Temperature Test Results," ANCR-1091, Aerojet Nuclear Company, 1972.

Arave, A.E., "Comparison of Four Tungsten Alloys for Use as Ultrasonic Thermometer Sensors," ANCR-1225, Aerojet Nuclear Company, 1975.

Arave, A.E., Buchenauer, J., "Use of Tungsten-2% Thoria Ultrasonic Transmission Line and Sensor to Improve the Performance of High-Temperature Ultrasonic Thermometry," TREE-NUREG-1021, Idaho National Engineering Laboratory, 1976.Bell, J.F., "A Solid Acoustic Thermometer," Ultrasonics, pp. 11-14, January, 1968.

Arnokrome 3 Datasheet Rev. 01-11-11, www.arnoldmagnetics.com/WorkArea/ DownloadAsset.aspx?id=5262, Accessed 08/09/2012.

Arnokrome 4 Specification Rev. 1/11/11, www.arnoldmagnetics.com/WorkArea/ DownloadAsset.aspx?id=5263, Accessed 08/09/2012.

Arnokrome 5 Specification Rev. 2/24/11, www.arnoldmagnetics.com/WorkArea/ DownloadAsset.aspx?id=5328, Accessed 08/09/2012.

ATR Users Guide July 2009, ATR National Scientific User Facility, INL/EXT-08-14709, 2009.

Bliss, P., Fanciullo, S., "High Temperature Thermometry at Pratt & Whitney Aircraft-CANEL" *Internal Pratt & Whitney Report-462,* 1965.

Brichard, B., Borgermans, A., Fernandez Fernandez, K., Lammens, K., Dectreton, M., "Radiation Effect in Silica Optical Fiber Exposed to Intense Mixed Neutron-Gamma Radiation Field," I*EEE Transactions on Nuclear Science*, Vol. 48, No. 6, pp. 2069, 2001.

Brown, R.D., Cost, J.R., Stanley, J.T., "Effects of neutron irradiation on magnetic permeability of amorphous and crystalline magnetic alloys," J. Appl. Phys., 55, pp. 1754-1756, 1984.

Carlson, G.A., Sullivan, W.H., Plein, H.G., "Application of Ultrasonic Thermometry in LMFBR Safety Research," SAND-77 1157, Sandia Laboratories, 1977. (Also: 1977 Ultrasonics Symposium Proceedings)

Carlson, G.A., Plein, H.G., "Refractory Metals for Ultrasonic Thermometry Application," NUREG/CR-0368 SAND78-1382 R-7, Sandia Laboratories, 1978.

Carlson, G.A., Sullivan, W.H., Plein, H.G., Kerley, M., "An Ultrasonic Thermometry System for Measuring Very High Temperatures in Reactor Safety Experiments," SAND79-0621, Sandia Laboratories, 1979.

Carnevale, E.H., Lynnworth, L.C., Ultrasonic Measurements from 1000 to 10,000 K, Proc. 5th International Congress on Acoustics (5e Congres International d'Acoustique), Liege 7-14 September 1965.

Carpenter, D., *Personal communication (Massachusetts Institute of Technology)*, 5/14/2013.

Carpenter, D., *Personal communication (Massachusetts Institute of Technology)*, 6/24/2013.

Chavez, S.A., Korth, G.E., Harper, D.M., Walker, T.J., "High-temperature tensile and creep data for Inconel 600, 304 stainless steel and SA106B carbon steel," Nuclear Engineering and Design, 148, pp. 351-363, 1994.

Currell, G., "Analytical Instrumentation: Performance Characteristics and Quality," Wiley, 2000.

Daw, J. E., Rempe, J. L., Knudson, D. L., Wilkins, S. C., Crepeau, J. C., "Extension Wire for High Temperature Irradiation Resistant Thermocouples," *Measurement Science and Technology*, 19, February 2008.

Daw, J. E., Crepeau, J. C., Rempe, J. L., Wilkins, S. C., Knudson, D. L., Condie, K. G., "Initial Results from Investigations to Enhance the Performance of High Temperature Irradiation-Resistant Thermocouples," J*ournal of the Japanese Society of Mechanical Engineers (JSME) Journal of Power and Energy Systems, invited paper, 15th International Conference on Nuclear Engineering (ICONE15) Special Edition*, 2, No. 2, pp 854-863, 2008.

J.E. Daw, J.L. Rempe, J.C. Crepeau, "Update On Ultrasonic Thermometry Development At Idaho National Laboratory," *8th International Topical Meeting on Nuclear Plant*

Instrumentation, Control, and Human Machine Interface Technologies (NPIC&HMIT 2012), San Diego, CA, July 22-26, 2012.

Joshua Daw, Steven Cheney Taylor, Joy Lynn Rempe, "High Frequency Magnetostrictive Transducer for Waveguide Applications," IDR #BA-767, submitted August 8, 2012, Elected by DOE to pursue as a patent, July 2014.

Etrema Products, Inc.,"What is Galfenol?", http://www.etrema-usa.com/core/galfenol/, Accessed 08/09/2012.

Etrema Products, Inc.,"Data Sheet Terfenol-D", http://www.etrema-usa.com/documents/Terfenol.pdf, Accessed 08/09/2012.

Farraro, R.J., McLellan, R.B.,"High Temperature Elastic Properties of Polycrystalline Niobium, Tantalum, and Vanadium," Metallurgical Transactions A, Volume 10A, p.1699, Nov. 1979.

Fenton, A.W., "How Do Thermocouples Work?," *Nuclear Energy*, p.61, Feb. 1980.

Figliola, R. S., Beasley, D. E., "Theory and Design for Mechanical Measurements," 3rd Edition, Wiley, 2000.

Gopalsami, N., Raptis, A.C.. "Simultaneous Measurement of Ultrasonic Velocity and Attenuation in Thin Rods with Application to Temperature Profiling," Ultrasonics Symposium, pp. 856-860, 1983.

Grossman, R.J., "Ultrasonic-Thermometry Development for In-Situ Measurement of Nuclear-Fuel Temperatures (AWBA Development Program)," KAPL-4160, General Electric Company Knolls Atomic Power Laboratory, 1982.

IEEE Standard on Piezoelectricity, ANSI/IEEE Std 176-1987, 1987.

Joint Committee for Guides in Metrology 100: 2008, "Evaluation of Measurement Data-Guide to the Expression of Uncertainty in Measurement (GUM)," 2008.

Kolsky, H., "Stress waves in solids," Dover Publications, 1963.

Krautkramer, J., Krautkramer, H., Grabendorfer, W., Niklas, L.,"Ultrasonic Testing of Materials," Springer-Verlag New York Inc., 1969.

Kulczyk, W.K., Smith, G.W., Jackson, G.A., "Ultrasonic Distributed Temperature Sensor," Sensors and Actuators, A21-A23, pp. 663-669, 1990.

Laurie, M., Magallon, D., Rempe, J., Wilkins, S., Pierre, J., Marquié, C., Eymery, S., Morice, R., "Ultrasonic High Temperature Sensors: Past Experiments and Prospective for Future Use," Joint International Symposium on Temperature, Humidity, and Moisture and Thermal Measurements in Industry and Science, Portorož, Slovenia, May 31 - June 4, 2010.

Lineberry M., Allen T., "The Sodium-Cooled Fast Reactor (SFR)," Argonne National Laboratory, US Department of Energy. ANL/NT/CP-108933, 2002.

Linnemann, K., Klinkel, S., Wagner, W., "A Constitutive Model for Magnetostrictive and Piezoelectric Materials," *International Journal of Solids and Structures*, Vol. 46, Issue 5, pp. 1149-1166, March, 2009

Liu, et al., "Thermal Stability and Radiation Resistance of Sm-Co Based Permanent Magnets," Paper 2036, Proceedings of Space Nuclear Conference, 2007.

Lynnworth, L.C., Carnevale, E.H., "Final Report-Ultrasonic Temperature Measuring Device," NASA CR-72339, August, 1967.

Lynnworth, L.C., Carnevale, E.H., Carey, C.A., "Ultrasonic Thermometry in Solids and Gases at Elevated Temperatures," Proceedings of the Fifth Temperature Measurement Society Conference and Exhibit, Hawthorne CA, March, 1967.

Lynnworth, L.C., Carnevale, E.H., McDonough, M.S., Fam, S.S., "Ultrasonic Thermometry for Nuclear Reactors," IEEE Transactions on Nuclear Science, Vol. NS-16, P. 184-187 1968.

Lynnworth, L.C., "Use of Ultrasonics for High-Temperature Measurements," Presented at American Society for Nondestructive Testing Meeting, Boston, MA, Mar. 20, 1968.

Lynnworth, L.C., "Sound Ways to Measure Temperature," Instrumentation Technology, 17, Number 4, pp. 47-52, April, 1969.

Lynnworth, L.C., Patch, D.R., "New Sensors for Ultrasound: Measuring Temperature Profiles," Materials Research and Standards, 10, Number 8, pp. 6-11, August, 1970.

Lynnworth, L.C., "Nuclear Reactor Thermometry," US Patent Application 3,597,316: 3 Aug 1971.

Lynnworth, L.C., Carnevale, E.H., "Ultrasonic Thermometry Using Pulse Techniques," Temperature: Its Measurement and Control in Science and Industry, Vol. 4, Part 1, pp. 715-732, 1972.Lynnworth, L.C.,"Magnetostrictive Ultrasonic Probes," Panametrics Technical Memorandum (UR-141), May 30, 1975.

Lynnworth, L.C.,"Temperature Profiles Using Multizone Ultrasonic Waveguides," Temperature: Its Measurement and Control in Science and Industry, Vol. 5, Part 2, pp. 1181-1190, 1982.

Lynnworth, L.C., *Ultrasonic Measurements for Process Control: Theory, Techniques, Applications*, Academic Press, 1989.

MITR Users Guide Rev. 3 July 2012, Massachusetts Institute of Technology, 2012.

Mughabghab, s., Sivadeenam, M., Holden, N.,"Neutron Cross Sections from Neutron Resonance Parameters and Thermal Cross Sections," Academic Press,1981.

NIST Technical Note 1297, 1994 Edition, "Guidelines for Evaluating and Expressing the Uncertainty of NIST Measurement Results," 1994.

NIST Type-S Thermocouple Data Tables, http://srdata.nist.gov/its90/download/type_s.tab

Olabi, A.G., Grunwald, A., "Design and application of magnetostrictive materials," *Materials and Design*, 29, pp 469-483, 2008.

Papdakis, E.P., Lynnworth, L.C., Patch, D.R., Carnevale, E.H., "Ultrasonic Thermometry in LMFBR Systems," Final Report NYO-3906-13, Panametrics Inc. 1972.

Papdakis, E.P., Fowler, Lynnworth, L.C., Robertson, A., Zysk, E.D., "Ultrasonic Measurements of Young's Modulus and Extensional Wave Attenuation in Refractory Metal Wires at Elevated Temperatures with Application to Ultrasonic Thermometry," Journal of Applied Physics, 45, Number 6, pp. 2409-2420, June, 1974.

Priest, J."*Temperature and Its Measurement*," *Encyclopedia of Energy, Volume 6*, p.45, 2004.

Rempe, J., Wilkins, S.C., "High Temperature Thermocouples for In-Pile Applications," *Paper 143, Proceedings of the 11th International Topical Meeting on Nuclear Reactor Thermal-Hydraulics (NURETH-11)*, Popes Palace Conference Center, Avignon, France, October 2-6, 2005.

Rempe, J. L., Knudson, D. L., Condie, K. G., Wilkins, S. C., "Evaluation of Specialized Thermocouples for High-Temperature In-Pile Testing," *Proceedings of the 2006 International Congress on Advances in Nuclear Power Plants (ICAPP'06)*, Reno, NV, June 4-8, 2006.

Rempe, J. L., Knudson, D. L., Condie, K. G., Wilkins, S. C., Crepeau, J. C., Daw, J. E., "Options Extending the Applicability of High Temperature Irradiation Resistant Thermocouples," invited paper for *NURETH12 Special Edition, Nuclear Technology*, 167, pp 169-177, July 2009.

Rempe, J., MacLean, H., Schley, R., Hurley, D., Daw, J., Taylor, S., Smith, J., Svoboda, J., Kotter, D., Knudson, D., Wilkins, S.C., Guers, M., Bond, L., Ott, L., McDuffee, J., Parma, E., Rochau, G., "New In-Pile Instrumentation to Support Fuel Cycle Research and Development," FCRD-FUEL-2011-000033, (also issued as INL/EXT-10-19149), January 2011.

Roberts, M.J., Holcomb, D.E.,Kisner, R.A., "Signal Processing Algorithm Implementation for In Vessel Level Measurement," https://inlportal.inl.gov/portal/server.pt/gateway/PTARGS-0-2-3310-277-2604-43/http%3B/inlpublisher%3B7087/publishedcontent/publish/communities/inl-gov/ about-inl/gen-iv-technical-documents/signal-processing-algorighm.pdf,September 2006.

Rose, J., "Ultrasonic Waves in Solid Media," Cambridge University Press, 1999.

Seco, F., *PCdisp*, http://www.iai.csic.es/users/fseco/pcdisp/pcdisp.htm, 2009.

Senor, D.J., Thomas, J.K., Peddicord, K.L., "Thermophysical property correlations for the niobium-1% zirconium alloy," Journal of Nuclear Materials, 173, pp. 261-273, 1990.

Sery, R.S., et al., "Radiation Damage Thresholds for Permanent Magnets," NOLTR 61-45, 1961.

Shatalov, M., Marais, J., Fedotov, I., Tenkam, M.,"Longitudinal Vibration of Isotropic Solid Rods: From Classical to Modern Theories," Advances in Computer Science and Engineering, InTech, 2011.

Shepard, R.L., Borkowski, C.J., East, J.K., Fox, R.J., Horton, J.L., "Ultrasonic and Johnson Noise Fuel Centerline Thermometry," International Colloquium on High-Temperature In-Pile Thermometry, EUR-5395, 1975.

Swenson, C.A., Quinn, T.J., "*Thermometry,*" *Encyclopedia of Physical Science and Technology*, p. 705, 2004.

Syre, R., "Niobium, Molybdenum, Tantalum and Tungsten: a Summary of Their Properties with Recommendations for Research and Development," AGARDograph, 50, 1961.

Taylor, B. N., Kuyatt, C. E., "Guidelines for Evaluating and Expressing the Uncertainty of NIST Measurement Results," NIST Technical Note 1297, 1994.

Tasman, H.A., Schmidt, H.E., "The Ultrasonic Thermometer-Construction, Application, and Operating Experience," High Temperatures- High Pressures, Vol. 4 pp. 477-481, 1972.

Tasman, H.A., Schmidt, H.E., Richter, J., Campana, M, Fayl, G., "The TRESON Experiments: Measurement of Profiles in Nuclear Fuels by Means of Ultrasonic Thermometers," High Temperatures- High Pressures, Vol. 9 pp. 387-406, 1977.

Tasman, H.A., Campana, M., Pel, D., Richter, J., "Ultrasonic Thin-Wire Thermometry for Nuclear Applications," Temperature: Its Measurement and Control in Science and Industry, Vol. 5, Part 2, pp. 1191-1196, 1982.

Touloukian, Y. S., et al., Thermophysical Properties of Matter, IFI/Plenum Publishing, New York, New York, 1973.

Ugural, A., Fenster, S., "Advanced Strength and Applied Elasticity, Fourth Edition," Prentice Hall, 2010.

Vacuumschmelze, "SOFT MAGNETIC COBALT-IRON-ALLOYS," http://www.vacuumschmelze.com/fileadmin/Medienbiliothek_2010/Downloads/HT/PTH%20004%20Vacoflux-Vacodur% 20engl.pdf, Accessed 08/09/2012.

Wilkins, S.C., Evans, R. P., "Assessment of High Temperature Measurements for Use in the Gas Test Loop," INL/EXT-05-00298, May, 2005.

Wohlfarth, E. P., "Ferromagnetic Materials. a Handbook on the Properties of Magnetically Ordered Substances Volume 2," North-Holland, 1980.

Wojcik, C.G., "Processing, properties, and applications of high temperature niobium alloys," MRS Symposium, Materials Research Society, Pittsburgh, PA, 322: pp. 519–30, 1994.

Appendix A: Uncertainty Analysis

Uncertainties in the acoustic velocity measurements were calculated on a percent error basis and were combined using the "Root Sum Square" (RSS) method [(Figliola, 2000), (Taylor, 1994)]. Error components that were considered were uncertainty of the reference (NIST traceable Type S) thermocouple and associated thermocouple reader, resolution of the precision ruler used to measure sensor lengths, aliasing of the analog to digital conversion performed by the pulse/receive system, time and voltage resolution and time jitter of the oscilloscope, and random noise in the recorded time-series data. The contribution of random noise to the measurement uncertainty was estimated using the signal to noise ratio. Signal to noise ratio (SNR) is not a straight-forward calculation when real data sets are involved. Typically, a true signal to noise ratio value must be calculated using a "clean" signal, a signal without noise, for comparison with the noisy signal. This is accomplished using mathematical models to estimate the true signal to noise ratio in a practical system. For real signals, the signal to noise ratio can be estimated as the ratio of the signal variance to the noise variance as long as the signal is zero-mean. For systems with relatively large signal to noise ratios (signal amplitude greater than approximately10 times the noise floor), the fractional uncertainty due to noise can then be expressed as the inverse of the signal to noise ratio [Currell, 2000]. Estimations of uncertainty in thermal expansion data were not included in reference materials and have not been accounted for. All uncertainty components, with the exception of the signal to noise ratio, are Type-B uncertainties as defined by both NIST and european standards [(NIST, 1994), (JCGM, 2008)]. Signal to noise ratio is considered as a Type-A uncertainty,

Pertinent specifications for equipment used in testing are provided in Table A-1.

Table A-1. Specifications for equipment used in acoustic velocity testing.

Equipment	Use	Relevant Specifications/Comments
Ruler	Measure length of sensor segments	0.5 mm resolution.
Tektronix TDS 5104B Oscilloscpe	Record and measure received signals	±5 V input voltage range. 11 bit vertical resolution. 15 parts per million accuracy of time measurement. 1.5% of measurement accuracy of DC gain.
UTEX UT 340 Pulser/Receiver	Generate and receive ultrasonic signals	250 MHz receiver bandwidth.
Type-S Thermo-couple	Monitor furnace tem-perature	Tabulated in Table A-2. NIST Traceable, uncertainty varies with temperature range.
Fluke 54 Series ii Themometer	Display Type-S mea-sured temperature	0.1 $^{\mathrm{o}}$C resolution for temperatures below 1000 $^{\mathrm{o}}$C. 1.0 $^{\mathrm{o}}$C resolution for temperatures above 1000 $^{\mathrm{o}}$C. 0.05% accuracy for Type-S thermocouple.

Error components were calculated as defined below.

$$u_r\% = \frac{0.5 \cdot R_r}{L} \cdot 100\% \tag{A-1}$$

where $u_r\%$ is the uncertainty generated by the limited resolution of the ruler used to measure gage lengths of the acoustic waveguide, 0.5 is a factor accounting for estimation of a measurement to 1/2 the resolution for a confidence level of 95%, R_r is the resolution of the ruler, 0.5 mm, L is the nominal length of each waveguide segment used in the velocity calculation.

$$u_{TypeS}\% = \frac{\varepsilon_{TypeS}}{\bar{T}_{TypeS}} \cdot 100\% \tag{A-2}$$

where $u_{TypeS}\%$ is the uncertainty of the Type S signal, as documented by NIST [NIST Type-S Thermocouple Data Tables], ε_{TypeS} is the reported error of the Type S for the temperature range measured, $\overline{T}_{TypeS}$ is the average absolute temperature reported by the Type S for the steady state measurement, ε_{TypeS} is tabulated as follows:

Table A-2. Type-S thermocouple tabulated error

Temperature Range, °C	Error Range, °C
-50 to 250	-0.02 to 0.02
250 to 1064	-0.01 to 0.01
1064 to 1664.5	-0.0002 to 0.0002
1664.5 to1768.1	-0.002 to 0.002

$$u_{Therm}\% = \frac{0.5 \cdot R_{Therm}}{\overline{T}_{Therm}} \cdot 100\% + A_{Therm} \qquad \textbf{(A-3)}$$

where $u_{Therm}\%$ is the uncertainty generated by the Fluke thermometer. This uncertainty is due to both resolution limitations and measurement error, both of which are specified in the users manual. 0.5 is a factor accounting for estimation of a measurement to 1/2 the resolution for a confidence level of 95%, R_{Therm} is the resolution of the thermometer, 0.1 °C for temperatures below 1000 °C and 1.0 for temperatures above 1000 °C, $\overline{T}_{Therm}$ is the average absolute temperature reported by the thermometer. A_{Therm} is the specified accuracy of the thermometer, 0.05% of reading for a Type-S thermocouple.

$$u_{Oscope}\% = \frac{Range}{2^M} \cdot 100\% + A_t + A_G \qquad \textbf{(A-4)}$$

where $u_{Oscope}\%$ is the uncertainty generated by the analog to digital conversion of the oscilloscope (quantization error), *Range* is the maximum voltage range the oscilloscope is set to record (±5 V), *M* is the bit size available for data recording (11 bit system with use of coherent waveform averaging), A_t is the accuracy of the time measurement (15 ppm), A_G is the accuracy of the DC gain (1.5%).

$$u_{P-R}\% = \left(1 - \frac{R}{\sqrt{1 + R^2}} \right) \cdot 100\% \qquad \text{(A-5)}$$

where $u_{P-R}\%$ is the uncertainty generated by the pulser/receiver system bandwidth limitations, *R* is the ratio of the system bandwidth (250 MHz for the pulser/receiver) to the highest frequency component of interest in the measured signal (approximately 500 kHz for the recorded data signals). Bandwidth of the oscilloscope is 1 GHz, and the additional uncertainty (calculated in the same manner as for the pulser/receiver) is negligible. Also, as the frequency of the measured signals is on the order of 500 kHz and the sampling rate was set to 250 MHz, aliasing of the signals was not considered a significant source of error (i.e. the sampling rate is approximately 250 times the Nyquist frequency).

$$u_{SNR}\% = 1 / \left(\frac{s_{signal}}{s_{noise}} \right) \cdot 100\% \qquad \text{(A-6)}$$

where $u_{SNR}\%$ is the uncertainty generated by the random signal noise, s_{signal} is the variance of the recorded signal, s_{noise} is the variance of the recorded noise.

The uncertainty components were combined using the RSS method as described below:

$$u\% = \sqrt{u_r\%^2 + u_{TypeS}\%^2 + u_{Therm}\%^2 + u_{P-R}\%^2 + u_{Scope}\%^2 + u_{SNR}\%^2} \quad \textbf{(A-7)}$$

Percent uncertainties for each tested material, as a function of temperature, are shown

in Figure A-1. With the exception of the signal to noise ratio contribution, the measurement

uncertainty had a nearly constant value of approximately 2%. The signal to noise ratio

contribution was seen to vary significantly and produced several trends. This is due to the fact

that the signal to noise ratio is affected by many phenomena, both physical (signal attenuation,

mode conversion, background noise) and within the signal acquisition process (signal

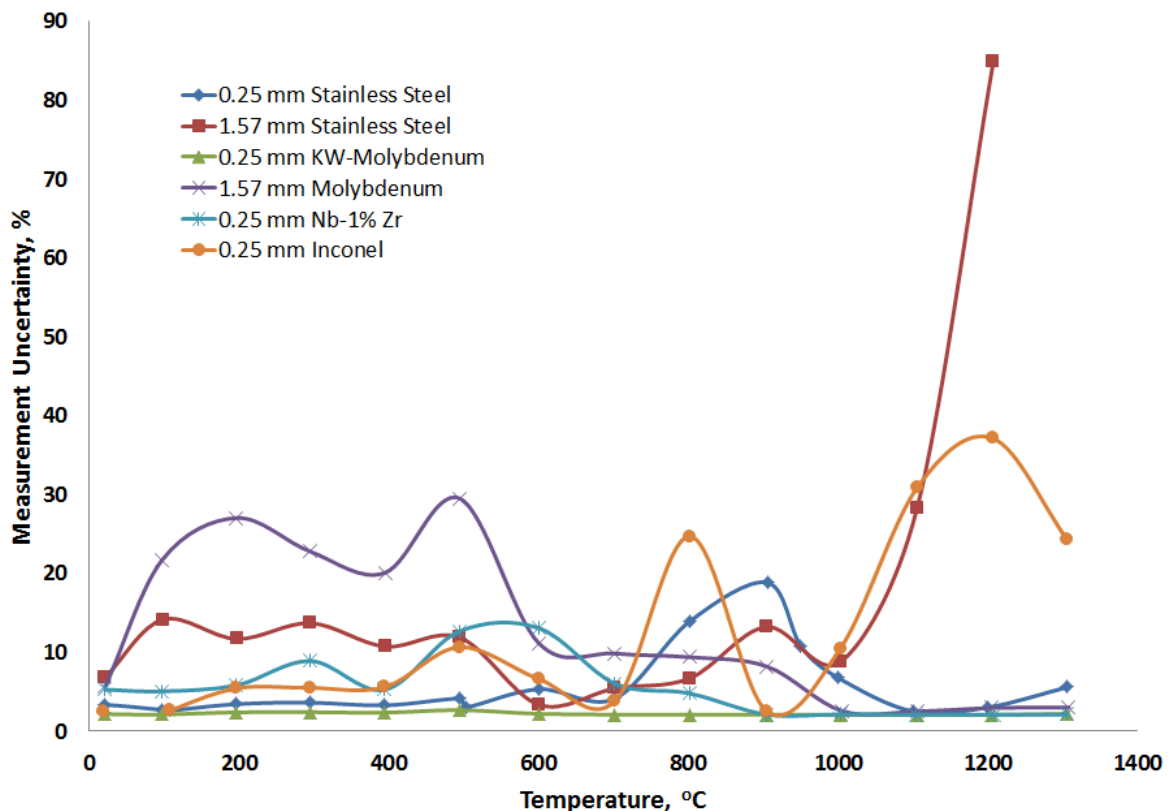amplification, digitization, etc.), many of which are temperature dependant.

Figure A-1. Measurement uncertainty of acoustic velocity measurements.

There are several trends implied by the data. First the measurement uncertainty appears to vary inversely with rod diameter, though the sample size is too small to describe this as a definitive trend. This diameter dependency does make sense as the presence of more modes of propagation are allowed (as predicted by dispersion curves). As the additional modes may travel at different velocities, interference between the primary reflection train used to calculate acoustic velocity and delayed reflections from extra modes could cause the signal to become distorted, which would act like additional noise in the SNR estimate. The drive/sense coils are also a factor. The larger waveguides require a larger coil to achieve the same acoustic power density or signal amplitude. The electrical excitation consisted of 80 ns long square pulses (the maximum of the system used). The constitutive equation for a RL (wire resistance and coil induction) circuit is:

$$E_v = iR_{DC} + L_i\frac{di}{dt} \qquad\qquad \textbf{(A-8)}$$

where E_v is the applied voltage, i is the current, R_{DC} is the DC resistance, L_i is the inductance, $\frac{di}{dt}$ is the time derivative of current. This solution to expression can be written as:

$$i = \frac{E_v}{R_{DC}}\left(1 - e^{-\frac{R_{DC}t}{L_i}}\right) \qquad\qquad \textbf{(A-9)}$$

In this form, the quantity $\frac{L_i}{R_{DC}}$ is the time constant, which describes the amount of time required for the magnetic field of a solenoidal inductor to fully develop. L_i and R_{DC} can be respectively defined as:

$$L_i = \mu_r N A_L n = \mu \frac{N^2}{l_L} A_L \text{ and } R_{DC} = \rho_w \frac{l_R}{A_R} \qquad \textbf{(A-10)} \text{ and } \textbf{(A-11)}$$

where: μ_r is the permeability of the coil core, N is the number of turns of the coil, A_L is the cross sectional area of the coil, n is the number of turns per unit length, l_L is the length of the coil, ρ_w is the resistivity of the coil wire, l_R is the length of wire included in the coil, A_R is the cross sectional area of the coil wire.

So, the ratio of time constants of a larger diameter transducer to a smaller diameter transducer can be written as:

$$\frac{\tau_{Large}}{\tau_{Small}} = \frac{\dfrac{\mu_r \dfrac{N^2_{(Large)}}{l_{L(Large)}} A_{L(Large)}}{\rho_w \dfrac{l_{R(Large)}}{A_{R(Large)}}}}{\dfrac{\mu_r \dfrac{N^2_{(Small)}}{l_{L(Small)}} A_{L(Small)}}{\rho_w \dfrac{l_{R(Small)}}{A_{R(Small)}}}} = \frac{N^2_{(Large)} l_{L(Small)} l_{R(Small)} A_{L(Large)} A_{R(Large)}}{N^2_{(Small)} l_{L(Large)} l_{R(Large)} A_{L(Small)} A_{R(Small)}} \qquad \textbf{(A-12)}$$

The coil wire used for both transducer sizes is identical, and the A_R values cancel. Representing the remaining area values and wire lengths in diameter terms allows reduction to:

$$\frac{\tau_{Large}}{\tau_{Small}} = \frac{N^2_{(Large)} l_{L(Small)} \pi \cdot d_{L(Small)} \dfrac{\pi \cdot d^2_{L(Large)}}{4}}{N^2_{(Small)} l_{L(Large)} \pi \cdot d_{L(Large)} \dfrac{\pi \cdot d^2_{L(Small)}}{4}} \qquad \textbf{(A-13)}$$

The diameter of the large coil was 1.57 times that of the small coil. The length of the large coil was 3 times that of the small coil, meaning the large coil had 3 times the turns of the small coil. This gives a total time constant ratio of approximately 4.7.

The time constant for the small coil is:

$$\tau_{Small} = \frac{L}{R} = \frac{\mu_r \dfrac{N^2_{(Small)}}{l_{L(Small)}}\left(\dfrac{\pi \cdot d^2_{L(Small)}}{4}\right)}{\rho_e \dfrac{N \cdot \pi \cdot d_{L(Small)}}{\pi/4 \cdot d^2_{R(Small)}}} \tag{A-14}$$

Values for the parameters are as follows:

$\mu_r = 20000$ for the relative permeability of Remendur [Wohlfarth, 1980]; total permeability is then $\mu_r {*} \mu_0$ (the permeability of free space), or:

$$\mu = 20000 \cdot 4\pi \cdot 10^{-7}\frac{V \cdot s}{A \cdot m} = 0.025\frac{V \cdot s}{A \cdot m} \tag{A-15}$$

ρ_w is $4.1381{*}10^{-7}$ $\Omega{*}$m (V*m/A) for the electrical resistivity of the silver palladium alloy used in the coils (measured during lab testing), $N_{(small)}$ is 50 turns, $l_{L(small)}$ is 5 mm for the coil length, $d_{L(small)}$ is 1.0 mm for the coil diameter, $d_{R(small)}$ is 0.2 mm for the coil wire diameter. This gives a time constant of approximately 4.77 milliseconds. This is four and a half orders of magnitude greater than the maximum pulse width of the system used for this test. The discrepancy for the larger transducer coil is greater by a factor of nearly five.

The second trend is that uncertainty generally increases with respect to temperature. This is not obvious from the plot, as there are several areas where the total uncertainty appears to decrease as temperature increases. This is due to changes made to the operating parameters

(pulse voltage, pulse duration, magnet position, etc.) made to offset temperature induced attenuation of the received signal. At each temperature, these parameters were adjusted to produce an optimal signal.

Third, uncertainty appears to decrease with increasing melting temperature of the sensor material. This is evident by comparison of the uncertainties of the 0.25 mm diameter samples. This is due to the refractory metals high temperature strength, they do not soften as much over the test temperature range and, so, the signals attenuate less.

These factors are all best represented by the KW-molybdenum sample. This sample shows a nearly constant uncertainty of just over 2%, meaning that the signal to noise ratio was not a significant contributor to uncertainty for this material.

Appendix B: Relevant Publications, Patents, and Awards

Conference Papers

J. Daw, J. Rempe, J. Palmer, P. Ramuhalli, R. Montgomery, H-T Chien, B. Tittmann, B. Reinhardt, G. Kohse, "Ultrasonic Transducer Irradiation Test Results," Accepted abstract for *9th International Topical Meeting on Nuclear Plant Instrumentation, Control, and Human Machine Interface Technologies (NPIC&HMIT 2015)*, Charlotte, NC, Feb. 23-26, 2015.

J. Daw, B. Tittmann, B. Reinhardt, G. Kohse, P. Ramuhalli, R. Montgomery, H-T. Chien, J-F Villard, J. Palmer, and J. Rempe, "Irradiation Testing of Ultrasonic Transducers," *3rd Advancements in Nuclear Instrumentation Measurement Methods and their Applications (ANIMMA)*, Marseille, France, June 23-27, 2013.

J.E. Daw, J.L. Rempe, J.C. Crepeau, "Update On Ultrasonic Thermometry Development At Idaho National Laboratory," *8th International Topical Meeting on Nuclear Plant Instrumentation, Control, and Human Machine Interface Technologies (NPIC&HMIT 2012)*, San Diego, CA, July 22-26, 2012.

J.E. Daw, J.L. Rempe, D.L. Knudson, T.C. Unruh, B.M. Chase, K.L. Davis, and A.J. Palmer, "Temperature Monitoring Options Available at the Idaho National Laboratory Advanced Test Reactor," *9th International Temperature Symposium*, Los Angeles, CA, March 19-23, 2012.

J. Daw, J. Rempe, and S. Curtis Wilkins, "Ultrasonic Thermometry for In-Core Temperature Detection*," 7th International Topical Meeting on Nuclear Plant Instrumentation, Control, and Human Machine Interface Technologies (NPIC&HMIT 2010)*, Las Vegas, NV, November 7-11, 2010.

Reports

J. Daw, J. Rempe, J. Palmer, P. Ramuhalli, P. Keller, R. Montgomery. H.T. Chien, B. Tittmann, B. Reinhardt, "NEET In-Core Ultrasonic Sensor Enablement-Final Repor," INL/EXT-14-32505.

J. Rempe, D. Knudson, J. Daw, T. Unruh, B. Chase, K. Davis, R. Schley, J. Palmer, and K. Condie, "Status Report on Efforts to Enhance Instrumentation to Support Advanced Test Reactor Irradiations,"INL/EXT-13-30427, January 2014.

J. Rempe, J. Daw, R. Schley, K. Davis, T. Unruh, B. Chase, J. Palmer, "In-Core Instrumentation to Support Fuel Cycle Research and Development - FY13 Status Report," INL/LTD-13-29848.

J. Daw, J. Rempe, P. Ramuhalli, R. Montgomery, H.T. Chien, B. Tittmann, B. Reinhardt, "NEET In-Core Ultrasonic Sensor Enablement-FY 2013 Status Report," INL/EXT-13-29144.

J. Rempe, D. Knudson, J. Daw, T. Unruh, B. Chase, K. Davis, R. Schley, J. Palmer, and K. Condie, "2012 Status Report on Efforts to Enhance Instrumentation to Support Advanced Test Reactor Irradiations," INL/EXT-12-27855, December 2012.

J. Daw, J. Rempe, P. Ramuhalli, R. Montgomery, H.T. Chien, B. Tittmann, B. Reinhardt, "NEET In-Core Ultrasonic Sensor Enablement-FY 2012 Status Report," INL/EXT-12-27233.

J. Rempe, J. Daw, D. Knudson, R. Schley, T. Unruh, and B. Chase, "In-pile Instrumentation to Support Fuel Cycle Research and Development -FY12 Status Report," FCRD-FUEL-2012-000282, September 2012.

J. L. Rempe, D. Knudson, J. Daw, T. Unruh, B. Chase, K. Davis, R. Schley, S. Taylor, D. Nigg, and K. Condie, "2011 Status Report on Efforts to Enhance Instrumentation to Support Advanced Test Reactor Irradiations," INL/EXT-11-24233, December 2011.

J. Rempe, J. Daw, D. Knudson, L. Bond, J. Coble, M. Good, R. Meyer, R. Schley, "In-core Instrumentation to Support Fuel Cycle Research and Development - FY11 Status Report," INL/EXT-11-23119.

J.L. Rempe, D.L. Knudson, J.E. Daw, "Status Report on Efforts to Enhance Instrumentation to Support Advanced Test Reactor Irradiations," INL/EXT-11-21231.

J. Rempe, H. MacLean, R. Schley, D. Hurley, J. Daw, S. Taylor, J. Smith, J. Svoboda, D. Kotter, D. Knudson, M. Guers, S. C. Wilkins, "New In-core Instrumentation to Support Fuel Cycle Research and Development," INL/EXT-10-19149.

Presentations

J. Daw, "Enhanced In-Core Instrumentation for Material Test Reactors," INL/MIS-13-30215, Meeting at INL with EDF Representatives.

J. Daw, T. Unruh, "Enhanced Instrumentation Development at INL," INL/MIS-13-29498, Meeting at INL with TerraPower Representatives.

Joshua Daw, "The Purpose, Experimental Design, and Expected Impact of the ATR-NSUF Ultrasonic Transducer Irradiation Experiment," ATR-NSUF User's Week 2013.ATR-NSUF User's Week Presentation

J. Daw, "Irradiation Testing of Ultrasonic Transducers to Enable In-Core Ultrasonic Instrumentation Deployment," Poster presented at National Academies Keck Future Initiative Conference on Advanced Nuclear Technologies, Nov. 15, 2013.

Joshua Daw, Joy Rempe, "In-Core Instrumentation for Irradiation Testing," ANS Student Conference 2013, Massachusetts Institute of Technology.

Joshua Daw, Joy Rempe, "New Sensors for Advanced Test Reactor Irradiations," ANS Student Conference 2011, Georgia Technical Institute.

Joshua E. Daw, Joy L. Rempe, Darrell L. Knudson, Robert S. Schley, Kate B. Boudreau, Steve Taylor, Ben Chase, Troy Unruh, and Gordon Kohse, "Instrumentation to Enhance ATR NSUF Irradiation Testing," Experiment Instrumentation Seminar ATR-NSUF User's Week 2011.

Awards

2014 Idaho National Laboratory Director's Award for Exceptional Engineering Achievement.

Innovations in Fuel Cycle Research Award, 2nd Place Nuclear Fuels Open Competition, 2012.

Patents Pending

"High Frequency Magnetostrictive Transducer for Waveguide Applications, IDR #BA-767, submitted August 8, 2012, Elected by DOE to pursue as a patent, July 2014; Inventors: J. Daw, S. C. Taylor, J. L. Rempe, D. L. Knudson, and S. C. Wilkins.